

Measurement and Scale Analysis of  
Convective Transport over Heterogeneous Terrain

Zur Erlangung des akademischen Grades eines  
DOKTORS DER NATURWISSENSCHAFTEN

von der Fakultät für  
Bauingenieur-, Geo- und Umweltwissenschaften

des Karlsruher Instituts für Technologie (KIT)

genehmigte

DISSERTATION

von

M.Sc. Fabian Eder

aus Neuburg a.d. Donau

Tag der mündlichen

Prüfung: 04.02.2016

Referent: Dr. Matthias Mauder

Korreferentin: Prof. Dr. Almut Arneth

Korreferent: Prof. Dr. Thomas Foken

Karlsruhe (2015)

---

## Summary

The eddy-covariance technique is the most direct and scale-appropriate method for determining fluxes of energy and matter of ecosystems. However, the calculated fluxes often underestimate the ‘true’ fluxes, which causes the energy balance closure problem. It is widely recognized that the non-consideration of flux contributions of meso-scale structures is the major reason for that systematic error, but the current recommendations for the adjustment of the eddy-covariance fluxes lack experimental evidence. Since meso-scale fluxes cannot be captured with point measurements alone, specific measurement strategies are required.

The aim of this thesis is to investigate those scales of convective transport that cannot be captured with the eddy-covariance technique, by using Doppler lidar, tower and aircraft measurements. At first, the principle scales of convective transport in the surface layer are determined, with an emphasis on the role of meso-scale structures for near-surface exchange. Moreover, the meso-scale flux contributions are calculated, and their partitioning between sensible and latent heat is investigated in particular. In addition, potential input variables for future parametrizations ought to be found.

The Doppler lidar measurements provided clear evidence for the presence of meso-scale structures in the surface layer. At least two devices are required and they need to be operated together in dual-Doppler mode, so that the two-dimensional wind field can be detected. The persistent structures that were measured with such a set-up were not directly related to landscape heterogeneities, but they represented turbulent organized structures that extended the entire boundary layer.

The airborne data showed that meso-scale structures significantly contribute to the sensible and latent heat fluxes in the surface layer. Moreover, the issue of the correct energy balance closure adjustment was examined by calculating the meso-scale and small-scale Bowen ratios. The meso-scale Bowen ratios were often found to be smaller than the small-scale ones, which contradicts assumption of scalar similarity.

Regarding the parameterization of the energy balance closure, two approaches from the literature were not applicable to the surface-layer datasets used in this thesis. In particular, the parameterization based on large-eddy simulation suffers from its poor grid resolution close to the surface. Nevertheless, several promising input variables for future parametrization approaches were found. All datasets confirmed that the energy balance closure improves with increasing friction velocity. It can be interpreted as a measure of the relative importance of high-frequency turbulence, as inferred from the surface-layer horizontal wind spectra. The

meso-scale structures become apparent as low-frequency contributions to the horizontal wind spectra, but not to the surface-layer vertical wind spectra. Moreover, the vertical gradients of temperature and moisture were correlated with the energy balance residual. These two variables have much potential for developing a parametrization since they deliver additional information on how to distribute the residual among the sensible and the latent heat flux. In the datasets under investigation, the vertical moisture gradients showed a higher correlation with the residual than the temperature gradient which again suggests that the latent heat flux is more underestimated than the sensible heat flux.

## Zusammenfassung

Die Eddy-Kovarianz Technik ist der direkteste Weg und für die Beobachtungsskala passendste Methode, Energie- und Stoffflüsse von Ökosystemen zu bestimmen. Die hiermit berechneten Flüsse unterschätzen jedoch oft die ‚wahren‘ Flüsse, was im sogenannten Energiebilanzschließungsproblem deutlich wird. Die Nicht-Berücksichtigung der Flussbeiträge mesoskaliger Strukturen wird im Allgemeinen als Hauptgrund für diesen systematischen Fehler angeführt. Die gegenwärtigen Vorschläge zur Korrektur der Eddy-Kovarianz Flüsse sind jedoch noch nicht experimentell bestätigt. Weil die mesoskaligen Flüsse nicht mit Punktmessungen alleine erfasst werden können, sind hierzu besondere Messstrategien erforderlich.

Die vorliegende Arbeit möchte, aufbauend auf Doppler-Lidar-, Turm-, und Flugzeugmessungen, jene Skalen des konvektiven Transports untersuchen, welche mit der Eddy-Kovarianz Methode nicht erfasst werden können. Zuerst sollen die Hauptskalen des konvektiven Transports in der bodennahen atmosphärischen Grenzschicht bestimmt werden. Ein Schwerpunkt wird hierbei auf die Rolle mesoskaliger Strukturen für den bodennahen atmosphärischen Austausch gelegt. Außerdem werden die mesoskaligen Flüsse bestimmt und dabei insbesondere das Verhältnis von fühlbarem zu latentem Wärmestrom untersucht. Des Weiteren sollen potentielle Eingangsvariablen für zukünftige Parametrisierungen gefunden werden.

Die Doppler-Lidare lieferten eindeutige Beweise dafür, dass mesoskalige Strukturen in der Bodenschicht vorhanden sind. Mindestens zwei Geräte sind hierzu nötig und müssen zusammen im dual-Doppler Modus betrieben werden, damit das zweidimensionale Windfeld erfasst werden kann. Die mit diesem Aufbau gemessenen langlebigen Strukturen waren jedoch nicht direkt an Heterogenitäten in der Landschaft gebunden, sondern es waren aus der Selbstorganisation der Turbulenz entstandene Strukturen, die sich über die gesamte Grenzschicht erstrecken.

Die Flugzeugmessungen zeigten, dass die mesoskaligen Strukturen signifikant zu den fühlbaren und latenten Wärmeströmen in der Bodenschicht beitragen. Außerdem wurden die mesoskaligen und kleinskaligen Bowen-Verhältnisse berechnet und somit die Frage untersucht, wie man die ungeschlossene Energiebilanz korrigieren sollte. Das mesoskalige Bowen-Verhältnis war oft niedriger als jenes der kleinen Skalen, was der Annahme von skalarer Ähnlichkeit widerspricht.

Bei der Parametrisierung der Energiebilanzschließung erwiesen sich zwei Ansätze aus der Fachliteratur als nicht anwendbar für die in dieser Arbeit verwendeten Datensätze aus der Bodenschicht. Insbesondere mangelt es jener Parametrisierung, die auf Large-Eddy-Simulation beruht, an einer ausreichenden Gitterauflösung des Modells nahe dem Boden. Nichtsdestotrotz wurden einige vielversprechende Eingangsgrößen für zukünftige Parametrisierungsansätze gefunden. Alle Datensätze bestätigten eine bessere Schließung der Energiebilanz mit zunehmender Schubspannungsgeschwindigkeit. Diese kann als Maß für die relative Bedeutung hochfrequenter Turbulenz interpretiert werden, was sich aus den Horizontalwindspektren der Bodenschicht folgern lässt. Dort rufen mesoskalige Zirkulationen erhebliche niederfrequente Beiträge hervor, jedoch nicht in den Vertikalwindspektren der Bodenschicht. Des Weiteren wurden die vertikalen Gradienten der Temperatur und Luftfeuchte mit dem Energiebilanzresiduum korreliert. Diese zwei Größen weisen ein besonderes Potenzial für die Entwicklung einer Parametrisierung auf, weil sie zusätzlich einen Hinweis dafür liefern, wie das Residuum auf den fühlbaren und latenten Wärmestrom aufgeteilt werden soll. In den untersuchten Datensätzen wiesen die vertikalen Feuchtegradienten eine stärkere Korrelation mit dem Residuum auf als der Temperaturgradient, was erneut nahelegt, dass der latente Wärmestrom stärker unterschätzt wird als der fühlbare Wärmestrom.

---

**Contents**

Summary .....	i
Zusammenfassung .....	iii
Acknowledgements .....	vii
List of manuscripts .....	viii
List of symbols .....	ix
<b>1. Introduction .....</b>	<b>1</b>
1.1 Turbulence in the homogeneous convective boundary layer .....	1
1.2 The eddy-covariance technique .....	2
1.3 Heterogeneous terrain and the energy balance closure problem .....	4
1.4 Measurement approaches for detecting meso-scale structures .....	5
1.5 Objectives of the thesis .....	5
<b>2. Experiments and Datasets .....</b>	<b>7</b>
2.1 TERENO Alpine/Pre-Alps Observatory, southern Germany .....	7
2.2 BOREAS and BERMS, Canada .....	8
2.3 HOPE, western Germany .....	9
2.4 Yatir forest, Israel .....	10
<b>3. Results and Discussion .....</b>	<b>11</b>
3.1 Detection of meso-scale structures with scanning Doppler lidars .....	11
3.1.1 <i>Single Doppler lidar</i> .....	11
3.1.2 <i>Dual-Doppler lidar</i> .....	13
3.2 Meso-scale flux contributions .....	14
3.3 Parameters related to the energy balance closure .....	16
3.3.1 <i>Evaluation of existing parametrizations</i> .....	16
3.3.2 <i>Friction velocity and low-frequency contributions to horizontal wind spectra</i> .	18
3.3.3 <i>Vertical gradients of temperature and humidity</i> .....	22
<b>4. Conclusions .....</b>	<b>26</b>

References ..... 28

List of Appendices ..... 40

Appendix A: Individual contributions to the joint publications..... 41

Appendix B: Evaluation of two energy balance closure parametrizations ..... 44

Appendix C: Meso-scale eddies affect near-surface turbulent exchange: evidence from lidar and tower measurements ..... 69

Appendix D: Secondary circulations at a solitary forest surrounded by semi-arid shrubland and their impact on eddy-covariance measurements..... 87

Selbstständigkeitserklärung.....**Fehler! Textmarke nicht definiert.**

## Acknowledgements

First of all, I would like to thank all the people that supported me during the last years and contributed to the success of this work. In particular, I would like to thank

- my supervisor Matthias Mauder for his outstanding support and his valuable advice that helped me to advance my work, for integrating me into the various projects that were essential for this thesis, and for being always available if any questions or problems arose. I especially appreciated that he encouraged me to develop my own hypotheses and ideas.
- Almut Arneith and HaPe Schmid for reviewing this thesis. Special thanks to HaPe Schmid for his support for the Helmholtz Young Investigator research group, for his critical comments that often brought me into rumination, and especially for the opportunity to conduct a measurement campaign in Israel.
- my co-authors Thomas Damian, Ray Desjardins, Frederik De Roo, Katrin Kohnert, Eyal Rotenberg, HaPe Schmid, Marius Schmidt, Katja Träumner and Dan Yakir for sharing data, thoughts and ideas, and for the critical comments that helped me to successfully publish the manuscripts.
- Baltasar Trancon y Widemann for providing the Wavelet routine and the help with its implementation. It ran smoothly, so that I used it for all datasets.
- my colleagues from the Helmholtz Young Investigator Team, Frederik de Roo, Sha Zhang and Sadiq Abdul Huq. Although I did not understand every single detail of your modelling work, it was a great pleasure to work with you together.
- my colleagues from the TABLE working group and all people from IMK-IFU for the pleasant atmosphere and any support I profited from. Special thanks to my officemates Matthias Zeeman and Frederik De Roo and to all those folks for the comfortable time during our informal coffee meetings, football evenings or any other activities.
- my family and friends who always supported me during the last years and encouraged me to continue this work.

## List of manuscripts

This dissertation is presented in cumulative form. It consists of three individual manuscripts. All manuscripts have already been published in the peer-reviewed journals *Boundary-Layer Meteorology*, the *Journal of Applied Meteorology and Climatology*, and in *Agricultural and Forest Meteorology*.

### *Manuscripts included in this thesis*

Eder F, De Roo F, Kohnert K, Desjardins RL, Schmid HP, Mauder M (2014) Evaluation of two energy balance closure parametrizations. *Boundary-Layer Meteorol* 151:195-219, doi: 10.1007/s10546-013-9904-0

Eder F, Schmidt M, Damian T, Träumner K, Mauder M (2015) Meso-scale eddies affect near-surface turbulent exchange: evidence from lidar and tower measurements. *J Appl Meteorol Climatol* 54:189-206, doi: 10.1175/JAMC-D-14-0140.1

Eder F, De Roo F, Rotenberg E, Yakir D, Schmid HP, Mauder M (2015) Secondary circulations at a solitary forest surrounded by semi-arid shrubland and their impact on eddy-covariance measurements. *Agric For Meteorol* 211:115-127, doi: 10.1016/j.agrformet.2015.06.001

### *Peer-reviewed publication not included in this thesis*

Eder F, Serafimovich A, Foken T (2013) Coherent structures at a forest edge: properties, coupling and impact of secondary circulations. *Boundary-Layer Meteorol* 148: 285-308, doi:10.1007/s10546-013-9815-0

---

**List of symbols**

$c_p$	specific heat capacity of air at constant pressure [ $\text{m K}^{-1} \text{s}^{-2}$ ]
$F$	flux in kinematic units [*]
$g$	gravitational acceleration [ $\text{m s}^{-2}$ ]
$L_{eff}$	effective horizontal scale of landscape heterogeneities [m]
$Q$	flux in energy units [ $\text{W m}^{-2}$ ]
$Q_E$	latent heat flux [ $\text{W m}^{-2}$ ]
$Q_G$	ground heat flux [ $\text{W m}^{-2}$ ]
$Q_H$	sensible heat flux [ $\text{W m}^{-2}$ ]
$Q_R$	residual of the energy balance [ $\text{W m}^{-2}$ ]
$Q_S^*$	net radiation [ $\text{W m}^{-2}$ ]
$R$	energy balance ratio [-]
$R^2$	coefficient of determination [-]
$t$	time [s]
$u$	horizontal wind component, in along-wind direction [ $\text{m s}^{-1}$ ]
$u_*$	friction velocity [ $\text{m s}^{-1}$ ]
$v$	horizontal wind component, in cross-wind direction [ $\text{m s}^{-1}$ ]
$v_r$	radial velocity component, line-of-sight velocity component [ $\text{m s}^{-1}$ ]
$w$	vertical wind component [ $\text{m s}^{-1}$ ]
$w_*$	convective velocity scale after Deardorff (1972) [ $\text{m s}^{-1}$ ]
$x$	Cartesian coordinate, horizontal, in along-wind direction [m]
$y$	Cartesian coordinate, horizontal, in cross-wind direction [m]
$z$	Cartesian coordinate, vertical [m]
$z_i$	boundary-layer height [m]
$z_m$	measurement height [m]
$z_0$	roughness length [m]
$z_{0eff}$	effective roughness length [m]
$\zeta$	scalar quantity [*]
$\zeta'$	fluctuation of scalar quantity [*]
$\bar{\zeta}$	temporal average of scalar quantity [*]
$\zeta_0$	surface value of scalar quantity [*]

## List of symbols

---

$\theta$	potential temperature [K]
$\theta_0$	potential temperature at the surface [K]
$\lambda$	heat of vaporization [m s <sup>-2</sup> ]

\* dimension depends on quantity

## 1. Introduction

The atmospheric boundary layer (ABL) is the lowest part of the atmosphere that responds to surface forcings within a timescale of several tens of minutes (Stull 1988). Since the solar energy that reaches the surface of the earth is the primary energy source for terrestrial ecosystems and the atmosphere, near-surface atmospheric transport processes are of major importance for weather, hydrology and biogeochemistry. In particular, global change has drawn much attention to the investigation of ecosystem-atmosphere interactions. Surface fluxes of energy and trace gases are subject of process-oriented ecosystem research and they are key input variables for atmospheric models. However, for conducting accurate atmospheric flux measurements, a thorough understanding of the structure and the dynamics of the near-surface ABL is required.

### *1.1 Turbulence in the homogeneous convective boundary layer*

In this thesis, the convective ABL is considered. It is conceptually divided into three layers (Stull 1988; Wyngaard 2010): the surface layer, the mixed layer and the entrainment zone or interfacial layer. The surface layer represents approximately the lowest 10% of the boundary layer, where vertical turbulent fluxes do not change with height. The mixed layer is the well-mixed bulk of the convective boundary layer, where wind speed and conserved variables are constant with height. Finally, the entrainment zone constitutes the transition zone from the ABL to the free atmosphere.

The flow in the ABL, unlike in the free troposphere, is turbulent and characterized by irregular local motions, so-called eddies (Batchelor 1950). Since the set of equations describing turbulent flow is not closed, it has to be investigated using phenomenological classifications, stochastic approaches and similarity theories (Stull 1988). Above homogeneous and flat terrain, turbulence in the stationary surface layer follows Monin-Obukhov similarity theory (Monin and Obukhov 1954), with the friction velocity  $u_*$ , the surface heat flux  $\overline{w'\theta'_0}$ , the buoyancy parameter  $g/\theta_0$  and the height  $z$  as governing parameters (Wyngaard 2010).

Under these idealized conditions, the surface-layer spectra exhibit a well-defined shape. The frequency range around the spectral peak at about 100 s denotes the energy-containing eddies, where turbulence receives its energy from shear and buoyancy forces (Tennekes and Lumley 1972; Stull 1988). The turbulent energy is transferred to smaller eddies until energy is dissipated

into heat on the molecular scale, which becomes apparent as an  $-5/3$ -power law in the high-frequency inertial subrange (Obukhov 1941; Kolmogorov 1941). In the low-frequency range left to the spectral peak, there is little spectral energy, a so-called spectral gap, which separates the turbulent motions from the diurnal and synoptic motions (Fig. 1).

However, in contradiction to Fig.1, the horizontal wind components often exhibit significant contributions from convective coherent structures (Kaimal et al. 1972, 1976; Panofsky et al. 1977; Kaimal 1978; Højstrup 1981). Those follow mixed-layer similarity with  $\overline{w'\theta'}$ ,  $g/\theta_0$ ,  $z$  and the ABL height  $z_i$  as scaling parameters, if entrainment is negligible (Wyngaard 2010). They are also called turbulent organized structures (Kanda et al. 2004) and exhibit time scales in the order of tens of minutes.

### 1.2 The eddy-covariance technique

During the last decades, networks of eddy-covariance (EC) systems were established (Baldocchi et al. 2001; Zacharias et al. 2011). It is the method of choice for quantifying energy and trace gas fluxes on the ecosystem scale, since it does not disturb the target area and it operates on the appropriate scale (Baldocchi 2003). The measured fluxes are widely used in environmental research, e.g. to validate models (Chen et al. 2005) and remote sensing techniques (Heinsch et al. 2006) or for determining physical constraints on hydrology (Wilson

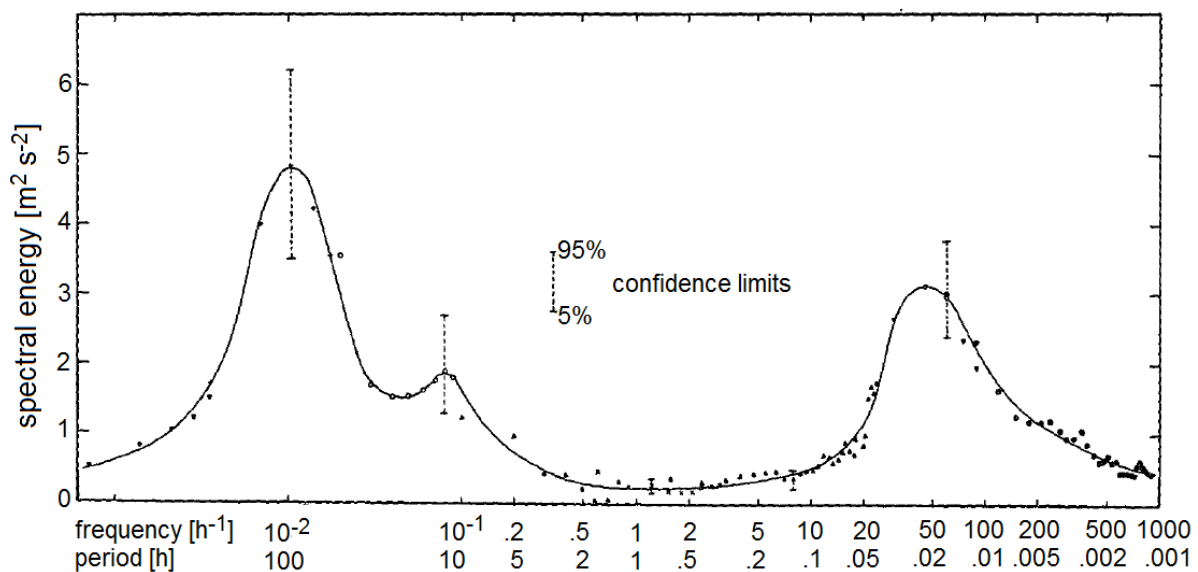


**Fig. 1** Horizontal wind speed spectra at approximately 100 m a.g.l. measured at the meteorological tower of the Brookhaven National Laboratory (Van der Hoven 1957)

et al. 2001) and carbon balance (Reichstein et al. 2007). In the following, a brief description of the EC technique and the underlying assumptions is provided.

Due to the spectral gap that separates turbulence from the mean flow (Fig. 1), atmospheric signals can be decomposed into a mean and a turbulent part, known as Reynolds decomposition (Reynolds 1894). After applying some first simplifications (Businger 1982; Foken 2008a), the kinematic flux  $F_\zeta$  of any scalar quantity  $\zeta$  across the ecosystem-atmosphere interface, measured at a height  $z_m$  is

$$\begin{aligned}
 F_\zeta = & \underbrace{\overline{w'\zeta'}}_{z_m} + \underbrace{\int_0^{z_m} \frac{\partial \zeta}{\partial t} dz}_{II} + \underbrace{\int_0^{z_m} \left( \overline{u} \frac{\partial \zeta}{\partial x} + \overline{v} \frac{\partial \zeta}{\partial y} \right) dz}_{III} + \underbrace{\int_0^{z_m} \overline{w} \frac{\partial \zeta}{\partial z} dz}_{IV} + \\
 & + \underbrace{\int_0^{z_m} \left( \frac{\partial \overline{u'\zeta'}}{\partial x} + \frac{\partial \overline{v'\zeta'}}{\partial y} \right) dz}_{V}
 \end{aligned} \tag{1}$$

where overbars indicate temporal means and primes the corresponding turbulent fluctuations (Foken et al. 2012a).

For measurements near the surface, under stationary conditions and without any significant sources or sinks of  $\zeta$  between the measurement height and the surface, storage (term II) can be neglected. Terms III and V represent horizontal advection and horizontal flux divergences that are insignificant for a horizontally homogeneous flow field. Furthermore, large-scale subsidence is neglected, so that vertical advection (term IV) can be disregarded. If all these conditions are satisfied, Eq.1 simplifies to

$$F_\zeta = \overline{w'\zeta'} \Big|_{z_m} . \tag{2}$$

Thus, the flux of  $\zeta$  between the surface and the atmosphere is equal to the covariance of  $w$  and  $\zeta$  at the measurement height. The averaging timescale is usually 30 min (Foken et al. 2012b) and according to Eq. 2, only the turbulent fluctuations contribute to the flux. Moreover, the ergodic hypothesis is assumed, i.e. the temporal average from a single point in space is representative of the ensemble average (Wyngaard 2010).

### ***1.3 Heterogeneous terrain and the energy balance closure problem***

A series of assumptions are invoked so that the turbulent flux at a certain measurement height above ground is identical to the flux at the surface. However, it was found that the EC technique systematically underestimates the true surface fluxes. This became evident as the energy balance closure problem, meaning that the energy balance ratio  $R$ ,

$$R = \frac{Q_H + Q_E}{-Q_S^* - Q_G} \quad (3)$$

is usually smaller than unity (Desjardins 1985; Tsvang et al. 1991; Kanemasu et al. 1992; Twine et al. 2000; Wilson et al. 2002; Hendricks-Franssen et al. 2010; Stoy et al. 2013).

Instrumental issues (Nakai et al. 2006; Kochendorfer et al. 2012; Horst et al. 2015) or the violation of the underlying assumptions (Finnigan et al. 2003; Aubinet et al. 2003; Foken 2008b; Foken et al. 2011; Leuning et al. 2012) were discussed as potential causes for the non-closure of the energy balance. In particular, the condition of horizontal homogeneity is hardly ever satisfied under field conditions. Differences in surface properties, such as surface roughness, albedo, surface moisture, surface temperature and topography, induce secondary circulations that do not move in space (Mahfouf et al. 1987; Dalu and Pielke 1993; Shen and Leclerc 1995; Patton et al. 2005; Sühling and Raasch 2013; Kang and Lenschow 2014). Accordingly, advection and horizontal flux divergences (terms III – VI in Eq.1) become significant, but these terms cannot be captured with an EC system. Consequently, the missing flux contributions from secondary circulations cause a systematic underestimation of the turbulent fluxes (Lee and Black 1993; Mahrt 1998; Foken 2008b). Similarly, turbulent organized structures with timescales larger than the averaging time of the EC method could be a reason for the non-closure of the energy balance (Laubach and Teichmann 1999; Sakai et al. 2001; Finnigan et al. 2003; Foken et al. 2006; Charuchittipan et al. 2014). Since secondary circulations or turbulent organized structures usually have spatial scales of the meso- $\gamma$  regime (Orlanski 1975), they are often simply called “meso-scale structures”.

As a consequence, the measured EC fluxes need to be adjusted. The current recommendation is to distribute the missing energy among sensible and latent heat according to the measured Bowen ratio (Twine et al. 2000; Foken et al. 2012b). However, other studies found that it should be completely added to the latent heat flux (Falge et al. 2005; Wohlfahrt et al. 2010), or to the sensible heat flux (Ingwersen et al. 2011), or it should be distributed according to ratio of the

sensible heat flux to the buoyancy flux (Brötz et al. 2014; Charuchittipan et al. 2014). Thus, there is still no conclusive finding about how to adjust the EC fluxes.

#### ***1.4 Measurement approaches for detecting meso-scale structures***

This thesis investigates the hypothesis that meso-scale structures are a major reason for the unclosed energy balance. This requires showing their existence in the surface layer and evaluating their flux contributions. Point measurements, even using multiple-tower setups, are not suitable for detecting advection (Aubinet et al. 2010) or meso-scale circulations. Instead, the turbulent flow field needs to be resolved in space.

This can be achieved with a scanning Doppler lidar. A Doppler lidar emits pulsed laser light in the near-infrared range, and detects its frequency shift caused by the movement of air particles (Werner 2005). From this frequency shift, the velocity component along the line-of-sight of the lidar beam is calculated, the so-called radial velocity. The Doppler lidars applied in this thesis allowed scanning the whole half-sphere above the devices. The turbulent wind field of the ABL was resolved at a spatial resolution in the order of tens of metres and at a temporal resolution of seconds to tens of seconds.

Moreover, airborne platforms offer the possibility to sample atmospheric variables along their flight track. Hence, an airplane can fly “through” secondary circulations and coherent structures and deliver their spatial extent and their flux contributions. This can be achieved with spectral analysis tools, e.g. the wavelet technique (Mauder et al. 2007). With respect to point measurements, it is also possible to detect low-frequency motions with timescales  $> 30$  min with spectral analysis, but only if these structures move in space.

#### ***1.5 Objectives of the thesis***

The main objective of this thesis is to extract those scales of convective transport that cannot be captured with the eddy-covariance technique and to investigate their role for ecosystem-atmosphere exchange. In particular, the following three specific objectives were pursued:

- (i) investigate whether turbulent organized structures with time scales  $> 30$  min and heterogeneity-induced secondary circulations reach down into the surface layer;

- (ii) quantify the flux contributions of these structures in order to show how the missing energy of the EC method should be distributed between sensible and latent heat;
- (iii) find parameters that could be suitable for developing a parameterization of the energy balance closure.

All these objectives are addressed by three individual publications presented in Appendices B-D of this thesis.

Eder et al. (2014, Appendix B) test two existing parameterizations of the energy balance closure by Huang et al. (2008) and Panin and Bernhofer (2008) using airborne and tower measurements. Primarily, this study is concerned with objective (iii) by evaluating which of the proposed parameters are applicable to the surface-layer datasets. Moreover, the work of Mauder et al. (2007) is revisited, where meso-scale flux contributions using the same airborne dataset were already calculated. Eder et al. (2014) now focus on the ratio of sensible heat to latent heat carried by meso-scale structures. Assuming that these fluxes are not captured by EC systems, this analysis ought to show how the missing energy is distributed among the sensible and the latent heat flux, which addresses objective (ii).

Eder et al. (2015a, Appendix C) present a comprehensive dataset from single- and dual-Doppler lidars, towers and a microwave radiometer. The Doppler lidar data are analyzed with regard to objective (i), by searching for temporarily persistent patterns in the horizontal and vertical wind components. Objective (ii) is addressed with measurements from a passive microwave radiometer. Vertical temperature and moisture gradients in the atmospheric boundary layer derived from this instrument serve as indicators for the partitioning of the meso-scale flux contributions. This is closely connected to a correlation analysis that refers to objective (iii): Eder et al. (2015a) investigate the relation of the energy balance residual to atmospheric parameters that could be useful for parameterizing the energy fluxes that are not captured with EC systems.

Finally, Eder et al. (2015b, Appendix D) show the results of a measurement campaign at the Yatir forest in Israel, a planted pine forest that is surrounded by semi-arid shrubland. Due to the strong differences in surface buoyancy fluxes, this site is ideal for investigating heterogeneity-induced circulations. According to objective (i), it is attempted to detect a stationary secondary circulation between the forest and the semi-arid shrubland using lidar measurements and large-eddy simulation (LES). Moreover, Eder et al. (2015b) compare the different energy balance ratios in the forest and the desert with the low-frequency contributions to the wind spectra of the sonic anemometers, which is related to objective (iii).

## 2. Experiments and Datasets

The three individual papers of this thesis (Appendices B, C, D) use data from four different datasets that were collected above the Canadian boreal forest, in a flat agricultural area in the West of Germany, in pre-alpine grasslands in southern Germany and in a semi-arid forest region in Israel. The predominant part of these measurements were conducted during the research activities of the Helmholtz Young Investigator Group led by M. Mauder “Capturing all relevant scales of biosphere-atmosphere exchange – the enigmatic energy balance closure problem”, which is funded by the Helmholtz-Association through the President’s Initiative and Networking Fund, and by the Karlsruhe Institute of Technology (KIT). The paper presented in Appendix B uses data from the German Terrestrial Environmental Observatories (TERENO) programme that were collected at the Institute of Atmospheric Environmental Research (IMK-IFU) of the KIT, and aircraft data from the Boreal Ecosystem-Atmosphere Study (BOREAS) project and the Boreal Ecosystem Research and Monitoring Sites (BERMS) programme that were provided by R.L. Desjardins from Agriculture and Agri-Food Canada and Ian MacPherson from the National Research Council of Canada. The paper in Appendix C contains an analysis of an extensive Doppler lidar-, radiometer- and tower-based dataset that was obtained in the framework of the High Definition Clouds and Precipitation (HD(CP)<sup>2</sup>) project, during the “HD(CP)<sup>2</sup> Observational Prototype Experiment” (HOPE) in close collaboration with T. Damian and K. Trümner from the Institute of Troposphere Research (IMK-TRO) of the KIT and M. Schmidt and A. Graf from the Agrosphere Department (IBG-3) of the Jülich Research Centre. Finally, the paper in Appendix D uses a lidar and tower-based dataset that was collected during a measurement campaign initiated by H. P. Schmid and D. Yakir as a cooperation of the KIT/IMK-IFU and the Department of Earth and Planetary Sciences (EPS) of the Weizmann Institute of Science at the Yatir forest in Israel. In the following, a short description of the respective datasets will be given.

### *2.1 TERENO Alpine/Pre-Alps Observatory, southern Germany*

The TERENO programme (Zacharias et al. 2011) that is funded by the Helmholtz Association and the Federal Ministry of Education and Research (BMBF) is designed to observe the effects of global change on terrestrial environmental ecosystems on the regional level. For this purpose, three research stations were established in the Bavarian Alps/pre-Alps Observatory at

Graswang (47.57°N, 11.03°E), Rottenbuch (47.72°N, 10.97°E) and Fendt (47.82°N, 11.06°E), along an altitudinal gradient in the Ammer catchment in southern Germany. The landuse types of the Ammer catchment comprise settlements, grassland, arable land and forests and the terrain is hilly up to mountainous (Eder et al. 2014, Appendix B). At these three sites, the KIT/IMK-IFU operates three surface energy balance stations above managed grassland. For calculating the surface energy balance, data from a CNR 4 net radiometer (Kipp & Zonen, The Netherlands), a CSAT-3 sonic anemometer-thermometer (Campbell Scientific Inc., USA) and LI-7500 or LI-7200 infrared gas analyzers (LI-COR Biogeosciences, USA) were used. The ground heat fluxes were determined from HFP01SC soil heat flux plates (Hukseflux Thermal Sensors B.V, The Netherlands), from M-107 soil temperature probes (Campbell Scientific Inc., USA) and from soil water content measured with CS616-L time domain reflectometers (Campbell Scientific Inc., USA) according to a calorimetric approach (Liebethal et al. 2005). A more detailed description of the measurement setup can be found in Zacharias et al. (2011). The sensible and latent heat fluxes were calculated using the EC technique with the software package TK3.1 (Mauder and Foken 2011) according to the post-processing strategy presented in Mauder et al. (2013). Moreover, CL51 ceilometers (Vaisala Ovj., Finland) are installed next to the EC towers. A ceilometer is a lidar that continuously measures profiles of the attenuated atmospheric backscatter intensity. From the backscatter profiles, the ABL height was determined with the gradient method (Emeis et al. 2007, 2008), which was done with the software ‘BL\_Matlab’ provided by C. Münkler from Vaisala.

### ***2.2 BOREAS and BERMS, Canada***

During the BOREAS project (Sellers et al. 1997) from May to September 1994 and the BERMS programme (Barr et al. 2002) in April 2002, the Twin Otter Research Aircraft of the Canadian National Research Council (NRC) conducted 20 flights in the Candle Lake area in Saskatchewan, Canada. The flight track was located along a transect between 53.57°N, 106.40°W and 53.98°N, 104.29°W. The aircraft overflew the boreal forest and three major lakes in flat terrain, at approximately 30 m a.g.l. at a ground speed of 60 m s<sup>-1</sup>. Aboard the aircraft, the wind vector was determined from a 858AJ28 5-hole probe (Rosemount Inc., USA) in combination with a LTN-90-100 inertial reference system (Litton Industries, USA), the air temperature with a 102DJ1CG heated probe (Rosemount Inc., USA) and the water vapour mixing ratio with a LI-6262 infrared gas analyzer (LI-COR Biogeosciences, USA) at a

frequency of 16 Hz during BOREAS and 32 Hz during BERMS. This high measurement frequency allows calculating the turbulent fluxes of sensible and latent heat using the EC technique. For the study presented in Appendix B, the turbulent heat fluxes were determined using the wavelet transform based on the algorithm of Torrence and Compo (1998). The applied wavelet package was developed by B. Trancón y Widemann. Short introductions to the wavelet transform are given in Mauder et al. (2007) and Eder et al. (2014, Appendix B).

### ***2.3 HOPE, western Germany***

The HD(CP)<sup>2</sup> research initiative that is funded by the German Federal Ministry of Education and Research (BMBF) aims to improve the understanding about cloud and precipitation processes and to build a high-resolution atmospheric model for Germany. For providing a comprehensive dataset, especially for delivering information on sub-grid variability on clouds and precipitation in the convective ABL, the HOPE project was conducted in the west of Germany, in the catchment of the river Rur and close to the Jülich Research Centre, in April and May 2013. The topography is flat, except for the intensive surface mining areas, and the landuse types mainly comprise settlements and agricultural land. During the measurement campaign, a large number of ground-based remote sensing measurements and surface energy balance stations were installed in the area, including the KIT-Cube facility of KIT/IMK-TRO. For the paper presented in Appendix C, data from three scanning Doppler lidars, one radiometer and two surface energy balance stations were used. Two Doppler lidars (Wind Tracer, Lockheed Martin, USA) were operated in dual-Doppler mode using a scan strategy optimized for detecting coherent structures (Stawiarski et al. 2013; Stawiarski 2014; Träumner et al. 2014). The third Doppler lidar (Streamline, Halo Photonics, UK) performed range-height indicator (RHI) scans, i.e. the lidar measured at different elevation angles, but at the same azimuth angle. Moreover, a HATPRO radiometer (RPG Radiometer Physics GmbH, Germany) was operated next to one Wind Tracer system and recorded vertical profiles of potential temperature and relative humidity. The two surface energy balance stations at Merzenhausen (50.93°N, 6.30°E) and Selhausen (50.87°N, 6.45°E) were located above winter wheat and their instrumentation was very similar to the TERENO stations of the Bavarian Alps / Pre-Alps Observatory (Sect. 2.1). The post-processing of the EC data was done with TK3.1. Further information on the research site, the measurement setup, the measurement strategy and the post-processing can be found in Eder et al. (2015, Appendix C).

## *2.4 Yatir forest, Israel*

From 21 August to 10 September 2013, ground-based lidar and EC measurements were carried out by KIT/IMK-IFU and the Weizmann Institute of Science (Eder et al. 2015b, Appendix D). The measurements took place in the Yatir forest (31.35°N, 35.05°E) and the surrounding semi-arid shrub land (31.32°N, 34.98°E). The Yatir forest is a planted pine forest dominated by *Pinus halepensis* and covers an area of about 2800 ha (Grünzweig et al. 2003; Rotenberg and Yakir 2011). Since the campaign took place more than 6 months after the last rain event in the area, the site in the semi-arid shrub land was almost free of vegetation and will be called the “desert” site for simplicity. The campaign aimed at quantifying the surface heat flux differences between the forest and the desert, investigating the effects on the local ABL height, and clarifying whether the differences in surface heat flux induce a secondary circulation. For this purpose, a Streamline Doppler lidar was deployed next to a meteorological tower in the Yatir forest that was equipped with a R3-50 sonic anemometer-thermometer (Gill Instruments, UK), a LI-7000 infrared gas analyzer (LI-COR Biogeosciences, USA), two CM21 pyranometers (Kipp & Zonen, The Netherlands) and two PIR pyrgeometers (The Eppley Laboratory Inc., USA). The sonic anemometer and the inlet of the gas analyzer were mounted at a height of 8 m above the canopy top, the radiation sensors at 5 m above the canopy top (Rotenberg and Yakir 2011). The Doppler lidar was located at the forest floor. It was continuously pointing vertically except for the velocity-azimuth display (VAD) scans that were performed every 30 minutes in order to measure the horizontal wind profile. Moreover, a CL51 ceilometer and a mobile meteorological tower system with similar equipment like the forest tower were deployed at the desert site. The measurement height of the EC system at the desert site was 6 m a.g.l. Further information on the measurement campaign can be found in Eder et al. (2015b).

### 3. Results and Discussion

#### *3.1 Detection of meso-scale structures with scanning Doppler lidars*

EC measurements on meteorological towers are point measurements that rely on the condition that turbulent structures are brought by the mean wind during the observation period, assuming Taylor's frozen turbulence hypothesis (Taylor 1938). As a result, stationary or slowly-moving meso-scale circulations cannot be captured completely. In order to detect such structures, the turbulent flow field in the atmospheric boundary layer needs to be resolved in space and time. This can be achieved with scanning Doppler lidars (Sect. 1.4).

The wind components measured with Doppler lidars contain information about the mean wind, meso-scale circulations and small-scale turbulence. The small-scale turbulence causes high-frequency fluctuations, and the meso-scale circulations cause persistent spatial deviations from the mean wind (Kanda et al. 2004). Accordingly, to extract the meso-scale structures, the retrieved velocity fields were averaged in time in order to eliminate the high-frequency modes. Afterwards, the mean component was removed from the averaged velocity field, e.g. by subtraction. This approach that corresponds to the rationale of the triple decomposition (Wilczak 1984) and was applied to the single- and dual-Doppler measurements.

##### *3.1.1 Single Doppler lidar*

The simplest way to operate a Doppler lidar is to make it point vertically, which yields profiles of the vertical wind component with the maximum temporal resolution. Stationary meso-scale circulations should appear as persistent up- or downdrafts above the device. This approach was tested by Eder et al. (2015b, Appendix D) during the measurement campaign at the Yatir forest in Israel (Sect. 2.4). There, the forest surface creates about 220-290  $\text{W m}^{-2}$  higher surface buoyancy fluxes than the adjacent desert due to its low albedo and its increased surface roughness, which Rotenberg and Yakir (2010) called the 'canopy convective effect'. These flux differences are supposed to create a quasi-stationary secondary circulation between the forest and the desert. Above the forest centre, where the Streamline Doppler lidar was installed, a persistent updraft was expected. It was defined as a mean vertical wind component  $> 0.5 \text{ m s}^{-1}$  for a time period of at least 3 h over a height range  $> 500 \text{ m}$ . However, a persistent updraft was found only on 5 of the 16 measurement days. In order to clarify why no clear evidence for a

secondary circulation was found on every day, a LES of the area (Fig. 2) was performed using the PARallelized Large-eddy simulation Model for atmospheric and oceanic flows (PALM), version 3.9 (Raasch and Schröter 2001; Maronga et al. 2015). The Yatir forest was represented by a rectangular triangle, the difference between forest and desert was encoded in different surface fluxes and roughness lengths, and the topography was neglected (Eder et al. 2015b, Appendix D). Without background wind, the simulation shows a strong persistent vertical updraft above the forest centre (Fig. 2a). With realistic background wind ( $6 \text{ m s}^{-1}$ ), only weak updrafts appear (Fig. 2b). In particular, the strongest updrafts occur approximately 5 km downwind of the forest centre, i.e. the lidar measurements were probably conducted at the wrong location in order to capture these motions. Moreover, the spatial structure of the vertical wind component is dominated by turbulent organized structures that are not related to the surface heat flux heterogeneities. Without background wind, cell-like structures with updrafts at the border lines, so-called Bénard cells (Rayleigh 1916) appear, that are typical for open-cell convection (Schmidt and Schumann 1989; Träumner et al. 2014). With background wind, parallel bands of up- and downdrafts can be recognized, that are traces of horizontal roll structures (Etling and Brown 1993; Maronga and Raasch 2013). As a result, simple vertical measurements with a Doppler lidar are not ideal for detecting secondary circulations, since the device has to be located at the exact location of the up- or downdrafts. Moreover, a vertical profile is still a one-dimensional measurement, and the lidar does not deliver reliable data within the first 80 m, so that near-surface measurements are not possible.

However, scanning lidars offer a variety of measurement strategies. During the HOPE campaign (Sect. 2.3), RHI scans were performed in order to get vertical cross-sections of the lower part of the ABL. A complete scan took about 40 seconds and the obtained radial velocity fields were averaged over 30 min. Then, the spatial deviations of the radial velocities from the space-time averaged wind speed were calculated. Fig. 3 shows an example from 28 April, 1230-1300 UTC. A convergence zone is located at a distance of 750 m from the lidar. Thus, a stationary circulation was detected that reached deep into the surface layer, at least down to 15 m a.g.l., and there is no indication that the circulation got less intense in the surface layer. In contrast, the largest amplitude of the radial velocities occurred close to the surface. However, such strong persistent patterns were not frequently observed, probably to the limited field-of-view of the lidar and because the RHI-scan has to be exactly orientated relative to the mean wind direction. Moreover, the radial velocity component contains information about both the vertical and the horizontal wind components which complicates the interpretation. For disentangling at least two wind components, an additional lidar is needed.

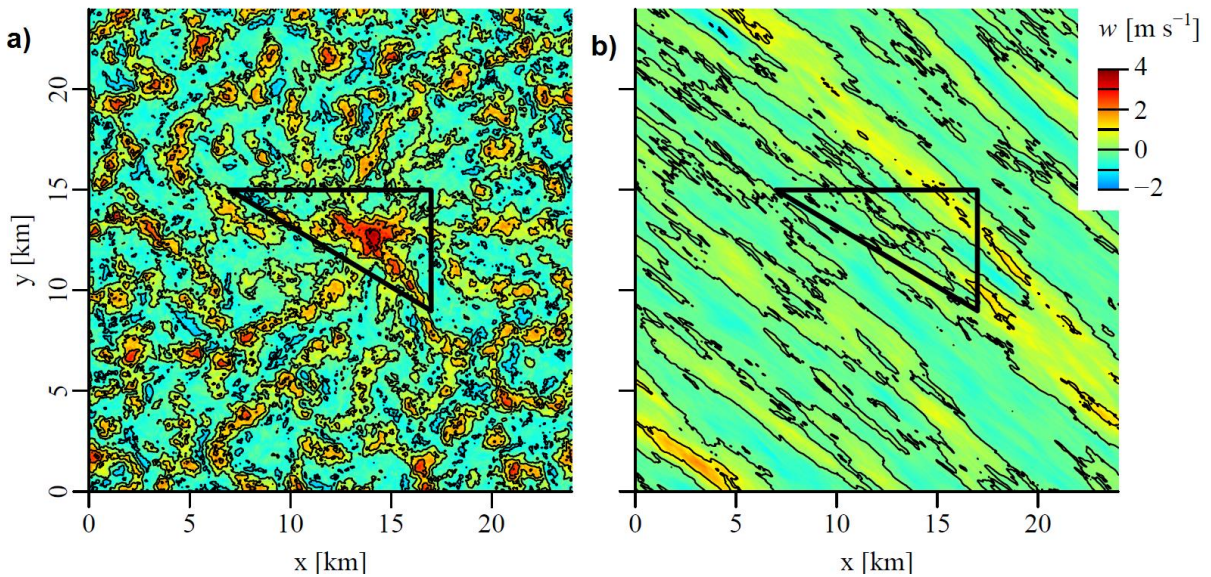


**Fig. 2** Large-eddy simulation of the atmospheric boundary layer above the Yatir forest area: 30-min average of the vertical wind component  $w$  at  $0.6 z_i$  with a prescribed background wind of  $0 \text{ m s}^{-1}$  (a) and  $6 \text{ m s}^{-1}$  (b) from North-West after 3 h of simulation; the thick black triangle indicates the Yatir forest, i.e. the area with increased surface roughness and increased surface heat flux (Eder et al. 2015b, modified)

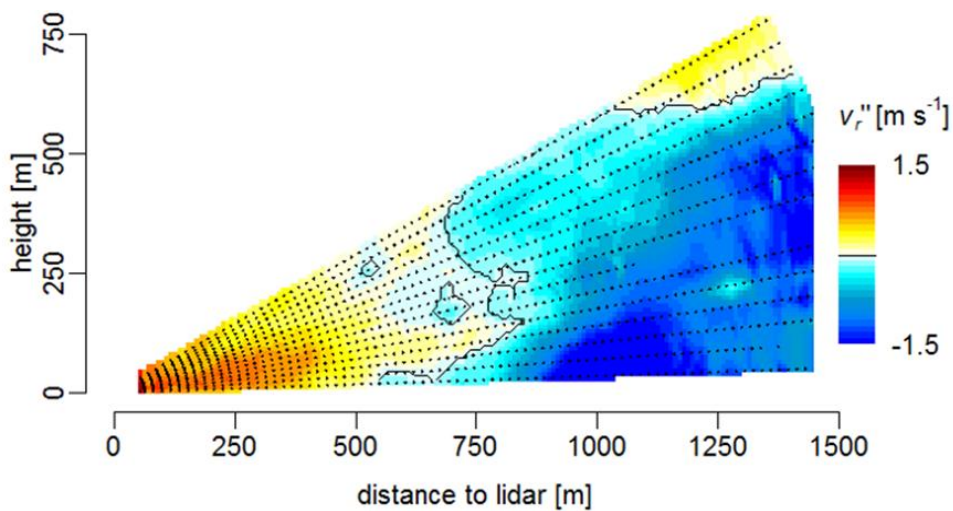


**Fig. 3** 30-min averages of the deviations of the radial velocity  $v_r''$  from the space-time averaged wind, measured with the Streamline Doppler lidar during HOPE on 28 April 2013, 1230 – 1300 UTC; the black dots indicate the respective centres of the range gates, i.e. the measurement points (Eder et al. 2015a, modified)

### 3.1.2 Dual-Doppler lidar

In order to overcome the problems regarding the interpretation of radial velocities, two lidars can be combined in order to measure the two-dimensional wind field in a plane. During HOPE, the IMK-TRO operated two Doppler lidars in Dual-Doppler mode and resolved the horizontal wind field in a slightly tilted horizontal plane at 40-120 m a.g.l, i.e. in the surface layer. The flow fields were averaged over 30 min and from the averaged patterns, the convergence of the horizontal wind field,

$$-\nabla(u v) = -\left(\frac{du}{dx} + \frac{dv}{dy}\right) \quad (4)$$

was calculated (Eder et al. 2015a, Appendix C). On 7 April 2013, 1130-1200 UTC, a low-wind case, thin convergence lines and wide divergence zones were found (Fig. 4a). Above the convergence lines, the vertically-pointing Streamline lidar detected a persistent updraft (Fig. 4b) which indicates that these stationary circulations extended up to ABL top. The observed pattern is known as open-cell convection (Sect. 3.1.1) that is typical for free-convection conditions.

However, pure open-cell convection was only observed on 7 April 2013. Usually, in the presence of background wind, parallel bands of high and low wind speed were found in the surface layer (Eder et al. 2015a, Appendix C) that could be traces of horizontal roll structures similar to those displayed in Fig. 2b. In Eder et al. (2015a, Appendix C), an example from 16 April 2013 is presented. The roll structures and the convective cells were not bound to heterogeneities of the surrounding landscape, since they did not predominantly appear at specific locations. Accordingly, the persistent surface-layer patterns that were observed during the HOPE campaign were most likely turbulent organized structures generated by the self-organizing tendency of geophysical flows (Holmes et al. 1996), but not heterogeneity-induced circulations.

### ***3.2 Meso-scale flux contributions***

As already mentioned (Sects. 1.3 and 1.4), the energy fluxes that are carried with the meso-scale motions cannot be captured with point measurements. However, an airborne platform moves in space and is able to sample meso-scale fluxes along its flight track. But, the flight track needs to be at least 10 times longer than the largest eddies in order to deliver robust flux

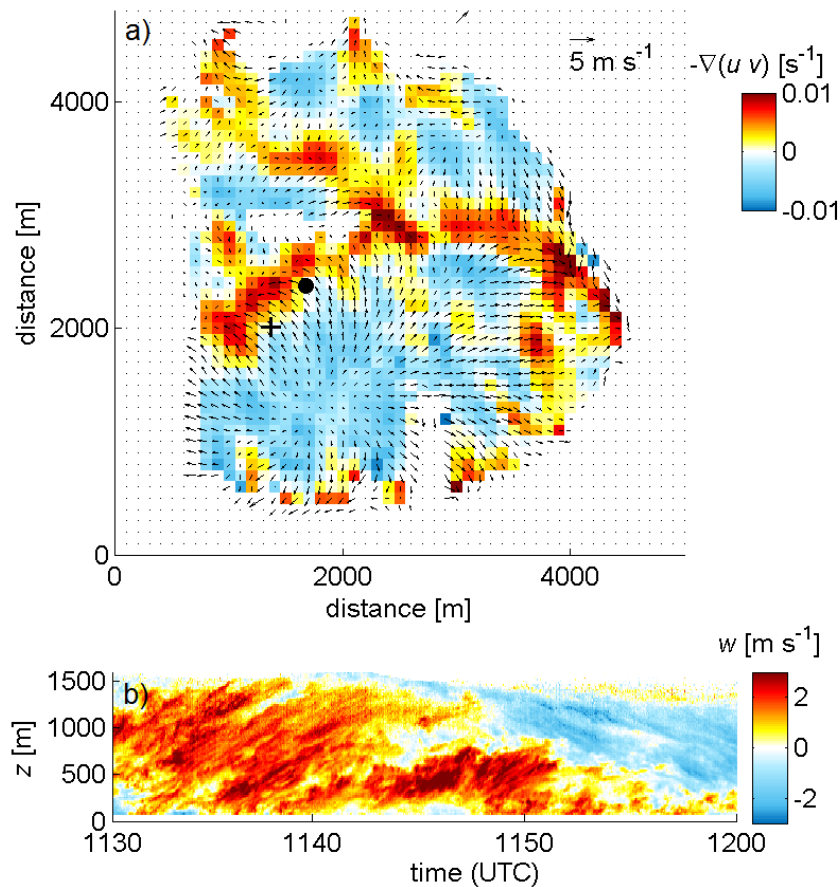


**Fig. 4** (a) 30-min averages of convergence in the horizontal flow field around Selhausen measured with two Doppler lidars in dual-Doppler mode on 7 April 2013, 1130-1200 UTC; the arrows show the horizontal wind vector, the colors show convergences and divergences, the black dot indicates the location of the additional Streamline lidar and the black cross indicates the location of the eddy-covariance station of Selhausen; (b) the vertical wind component  $w$  measured with the Streamline wind lidar during the same 30-min period (Eder et al 2015a, modified)

estimates (Lenschow and Stankov 1986; Lothon et al. 2007). The Candle Lake runs of the Twin Otter research aircraft (Sect. 2.2) were about 115 km long, which is sufficient for this purpose. Mauder et al. (2007) calculated the turbulent fluxes from the airborne data of BOREAS and BERMS using the wavelet technique. Pursuing this approach, Eder et al. (2014, Appendix B) determined the meso-scale flux contributions by integrating over those wavelet coefficients that were associated with scales  $> 2$  km. This cut-off wavelength was suggested by Williams (1996) and Strunin and Hiyama (2005), and Mauder et al. (2007) confirmed a spectral gap (cf. Fig. 1) in the wavelet cospectra around a wavelength of 2 km. In this manner, considerable low-frequency transport could be detected with the airborne measurements. For 15 of the 20 aircraft flights, the meso-scale flux contribution was between 9% and 14%, which corresponds well to the mean non-closure of the energy balance of the EC sites in the area (Barr et al. 2012).

Then, the meso-scale flux partitioning among sensible and latent heat was compared to the small-scale (< 2 km) flux partitioning. If the Bowen-ratio was around unity, the Bowen-ratio of the meso-scale structures was similar to the Bowen-ratio of the small-scale turbulence (Fig. 5). However, for many cases with Bowen-ratios further away from unity, different small-scale and meso-scale Bowen ratios were found and the meso-scale Bowen-ratio was often smaller. In these cases, the meso-scale structures transported relatively more latent heat than the small-scale structures. Let us assume that these meso-scale fluxes were not captured by an EC station, and the energy balance would be corrected with the measured small-scale Bowen-ratio according to Twine et al. (2000). Then, the corrected latent heat fluxes would underestimate the ‘true’ latent heat fluxes, and the corrected sensible heat fluxes would be overestimated. However, under the assumption that the energy balance closure is about 90%, the resulting relative error of the flux estimates for all flights would be less than 6% (Fig. 5).

Studies above rural landscapes in central Europe reported that the sensible heat flux might be more sensitive to an underestimation (Ingwersen et al. 2011; Charuchittipan et al. 2014; Brötz et al. 2014), which contradicts the findings from the BOREAS and BERMS dataset. This can be probably explained by the properties of the research area. The airborne measurements were conducted above a boreal forest with the lake-land boundaries as dominant heterogeneities. As a consequence, the meso-scale surface moisture differences are stronger than the meso-scale surface temperature differences which implicates stronger meso-scale latent heat fluxes.

During the HOPE campaign (Sect 2.3), the meso-scale flux partitioning was evaluated indirectly using the vertical gradients of potential temperature and specific humidity (Eder et al. 2015a, Appendix C), which will be discussed in Sect. 3.3.3.

### ***3.3 Parameters related to the energy balance closure***

#### ***3.3.1 Evaluation of existing parametrizations***

The third goal of this thesis is to find variables that are suitable for developing a parameterization of the energy balance closure. At first, Eder et al. (2014, Appendix B) tested two approaches from the literature using the airborne measurements during BOREAS and BERMS (Sect. 2.2) and the EC data from the TERENO sites of the Alpine/Pre-Alps Observatory (Sect. 2.1). The goal of this analysis was to find out whether the existing approaches could help to develop a robust parametrization.

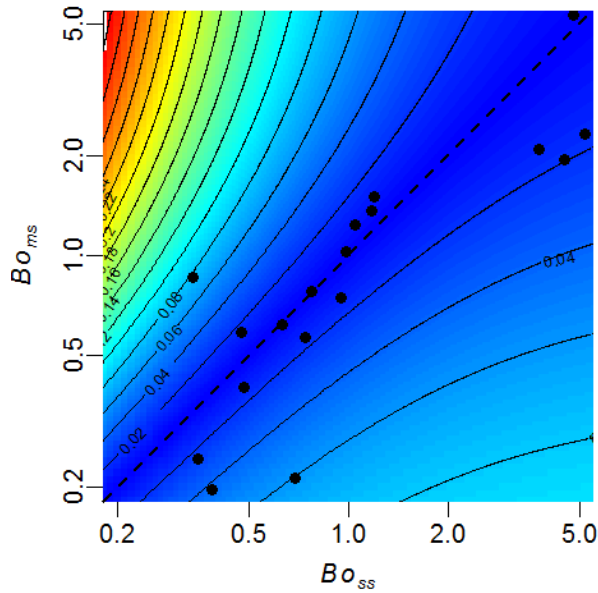


**Fig. 5** Bowen ratio of the small-scale turbulence ( $< 2\text{km}$ ,  $Bo_{ss}$ ), that is supposed to be measurable with EC towers, versus the respective Bowen ratio of the meso-scale range ( $> 2\text{km}$ ,  $Bo_{ms}$ ) for the Twin Otter aircraft flights during BOREAS and BERMS; the colours and solid contour lines indicate the relative error of the sensible heat flux if it was corrected according to the method of Twine et al. (2000) and if an energy balance closure of 90% was assumed; the dashed line indicates the assumption of scalar similarity, i.e.  $Bo_{ss} = Bo_{ms}$  (Eder et al. 2014, modified)

According to the approach of Huang et al. (2008), the non-closure of the surface energy balance is caused by turbulent organized structures, which is in accordance with the dual-Doppler lidar measurements (Sect. 3.1.2). Huang et al. (2008) argue that the energy imbalance can be parameterized with ‘universal functions’ of  $u_*'/w_*$  and  $z_m/z_i$ . Thus, for convective conditions, it should be possible to parameterize the energy balance closure for every 30-min period. However, this approach was neither applicable to the airborne nor to the tower-based dataset. No significant correlation was found with the suggested parameters except for  $u_*$  alone, for which a weak negative dependence was confirmed for the TERENO sites Graswang and Fendt (data not shown). The failure of this approach is probably due to the fact that this parametrization was developed using LES runs of the homogeneous convective boundary layer with a grid resolution ( $50 \times 50 \times 20 \text{ m}$ ) that is not sufficient to represent turbulence in the surface layer realistically. Moreover, Monin-Obukhov similarity theory is used for the first grid layer of the model grid, which is based on horizontal homogeneity and explicitly does not consider turbulent organized structures that obey mixed-layer scaling (Sect. 1.1). In contrast, the lidar measurements (e.g. Fig. 3) clearly demonstrated that turbulent organized structures extend down into the surface layer. This questions the applicability of current LES models for

investigating the energy balance closure problem, unless the simulations are run at a very high resolution.

As an alternative, Panin and Bernhofer (2008) developed an empirical approach that considers quasi-stationary heterogeneity-induced secondary circulations as the major reason for the energy balance closure problem. Thus, the energy balance closure is supposed to be related to the heterogeneity of the surrounding landscape. As heterogeneity index, Panin and Bernhofer (2008) suggested the ratio of the effective surface roughness length  $z_{0eff}$  to the dominant horizontal length scale  $L_{eff}$  of the surface roughness patches (Fig. 6). This length scale was determined with Fourier analysis from surface roughness maps. Details about this approach and its implementation can be found in Panin and Bernhofer (2008) and Eder et al. (2014, Appendix B). This parametrization only characterizes the mean energy balance closure of a site. Only the data from the Candle lake site (Sect. 2.2) corresponded well with the data that are presented in Panin and Bernhofer (2008). For the TERENO sites, this method underestimates the energy imbalance, probably because solely the surface roughness heterogeneities were considered. In the Candle lake area, the lake-land boundaries are the dominant heterogeneities and they are easily captured with the surface roughness, but this approach is not sufficient for the highly complex sites in the pre-alpine area. Differences in surface temperature (Maronga and Raasch 2013; Kang and Lenschow 2014), surface moisture (Higgins et al. 2013; Dixon et al. 2013) and topography (Brötz et al. 2014; Wagner et al. 2015) also induce stationary meso-scale structures. Unfortunately, the lidar measurements from the HOPE campaign did not give clear evidence for strong heterogeneity-induced meso-scale circulations in the ABL. However, at the Yatir forest site, the lidar data showed evidence for a heterogeneity-induced circulation on 5 of the 16 measurement days (Sect 3.1).

### 3.3.2 *Friction velocity and low-frequency contributions to wind spectra*

The friction velocity  $u_*$  is the square root of the shear stress divided by the density of the fluid (Foken 2008a). It is a very common quality criterion to filter out stable, low-wind conditions during night when turbulence is not well developed (Goulden et al. 1996; Barr et al. 2006).

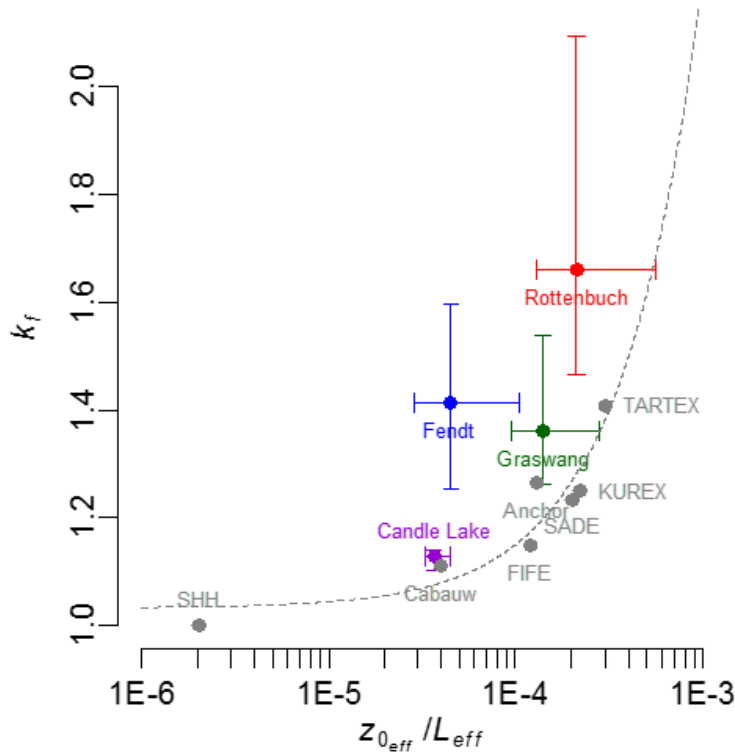


**Fig. 6** Energy balance correction factor  $k_f$ , which is the inverse of the energy balance ratio (Eq.3), for the airborne measurements during BOREAS and BERMS („Candle Lake“) and the EC masts at the TERENO sites Graswang, Rottenbuch and Fendt versus heterogeneity index  $z_{0,eff}/L_{eff}$ ; median values and interquartile ranges are displayed; the data shown in Panin and Bernhofer (2008) are indicated as grey dots and a fit through these data is displayed as a grey dotted line (Eder et al. 2014)

Moreover, many studies (Blanken et al. 1997; Wilson et al. 2002; Falge et al. 2005; Hendricks-Franssen et al. 2010; Stoy et al. 2013; Anderson and Wang 2014) found a negative correlation between the energy balance residual  $Q_R$ ,

$$Q_R = -Q_S^* - Q_G - Q_H - Q_E, \quad (5)$$

and  $u_*$ .

For the HOPE campaign (Sect. 2.3), this dependence was confirmed for the energy balance station at Selhausen (Fig. 7a), but only a very weak correlation was found for the Merzenhausen site ( $R^2 = 0.11$ ). This dependence became also evident in the data from the Yatir area in Israel. For this dataset, since the ground heat fluxes were not measured,  $R$  (Eq. 3) was calculated by integrating  $-Q_S^*$ ,  $Q_H$  and  $Q_E$  over the whole measurement campaign, assuming that the long-term averages of  $Q_G$  and the heat storage terms are insignificant for this 20-day time period (Leuning et al., 2012). The energy balance at the forest site was closed, but a non-closure of

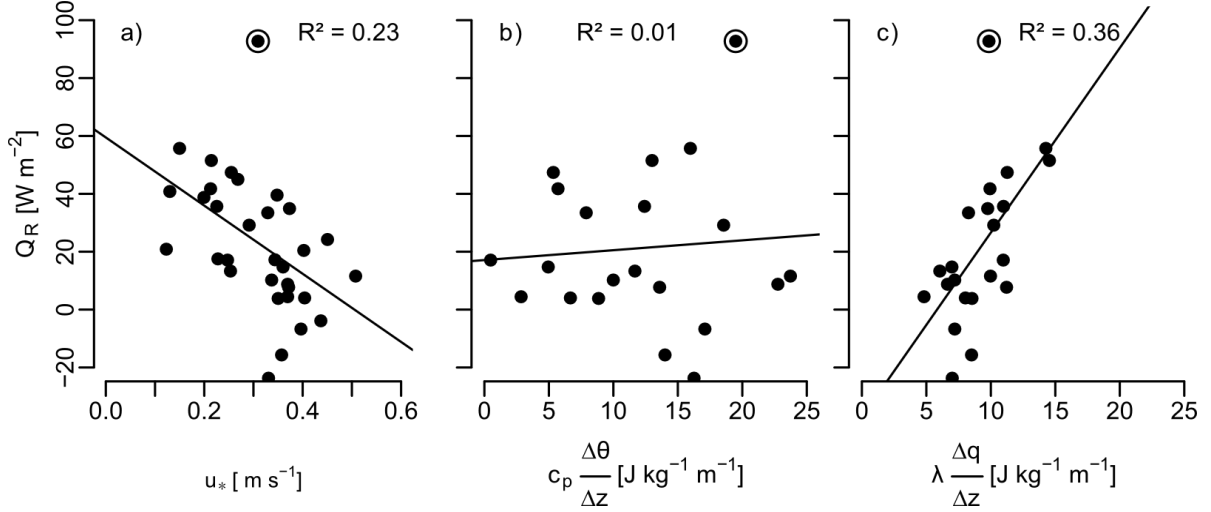


**Fig. 7** Linear regression analysis between the daytime averages of the energy balance residual  $Q_R$  at Selhausen and (a) friction velocity  $u_*$ , (b) the vertical gradients of potential temperature  $\Delta\theta/\Delta z$  multiplied by  $c_p$  and (c) specific humidity  $\Delta q/\Delta z$  multiplied by  $\lambda$ , determined from the HATPRO profiles (0 – 250 m a.g.l.); days with a mean wind direction from 0° - 135° and less than 50% data availability were excluded from the analysis; the specific heat capacity of air at constant pressure  $c_p$  and the heat of vaporization  $\lambda$  were needed for the conversion into energy units; for each data point, only the daytime data (0800-1700 UTC) were used and the circle denotes an outlier (Eder et al. 2015a).

19% was found at the desert site (Eder et al. 2015b, Appendix D). The mean friction velocity at the forest site was significantly higher (0.78 m s<sup>-1</sup>) than at the desert site (0.24 m s<sup>-1</sup>).

The dependence on friction velocity illustrates that the energy balance closure improves with the intensity of mechanically-induced turbulent mixing. If mixing is strong, the high-frequency turbulence that is generated from the wind shear near the surface contributes more to near-surface exchange, whereas meso-scale structures are less relevant. In order to test this hypothesis, wavelet spectra of the three wind components were calculated. Point measurements are not able to detect secondary circulations that do not move in space. However, slowly moving turbulent organized structures with timescales > 30 min are detectable if the time series is long enough.

For the Yatir measurement campaign, wavelet spectra were calculated from the  $u$ ,  $v$  and  $w$  time series measured with the sonic anemometers in the desert (Fig. 8a) and the forest (Fig. 8b). From the wavelet spectra, the ratio of the low-frequency spectral energy (period > 30 min) to the total spectral energy was calculated (Eder et al. 2015b, Appendix D). For the  $u$  and  $v$  spectra, it was found that about 30% of the spectral energy at the desert site originated from low-frequency fluctuations, but only about 11-12% at the forest site. The low-frequency contributions to the  $w$  spectra were negligible at both sites. As previously mentioned, the energy

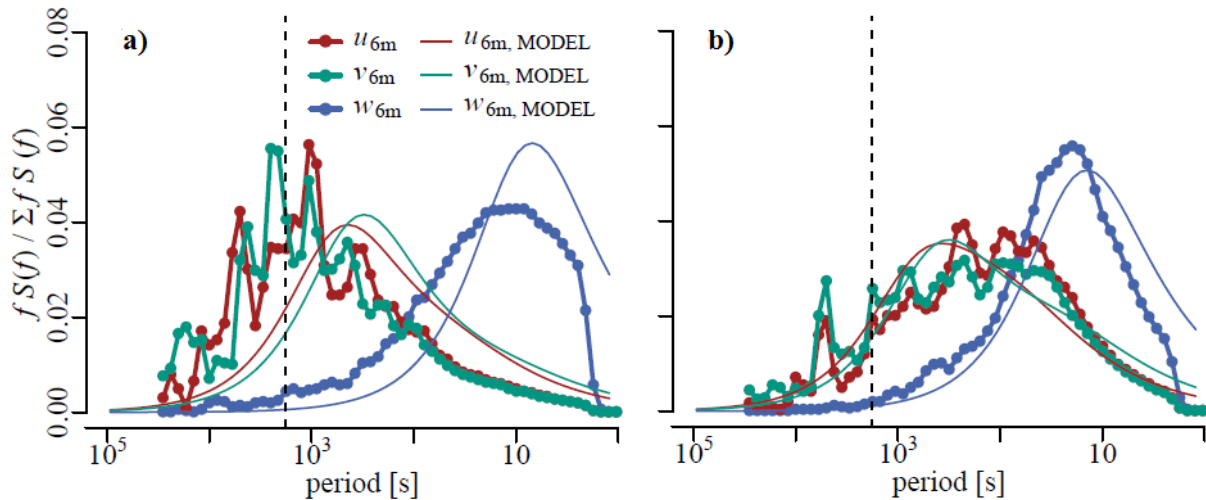


**Fig. 8** Normalized wavelet spectra of the surface-layer wind components  $u$ ,  $v$  and  $w$  from 25 August at (a) the desert site and (b) the forest site. The spectra were compared with the spectral model of Højstrup (1981), indicated as thin solid lines. The vertical dashed line indicates a period of 30 minutes, i.e. the averaging time for the EC measurements (Eder et al. 2015b).

balance was closed at the forest site, and an imbalance of 19% was found at the desert site. Consequently, the poor closure at the desert site is probably due to low-frequency motions that are not captured within the 30-minute averaging period of the eddy-covariance method. In the roughness sublayer above the forest, however, mixing is very intense and the friction velocities are significantly higher. There, the large structures are either (i) broken up into smaller eddies or (ii) additional high-frequency turbulence is generated according to the mixing-layer analogy (Raupach et al. 1996). As a consequence, the low-frequency contributions are less significant, and the energy balance is closed.

The measured spectra were also compared with the spectral model of Højstrup (1981) that explicitly considers the low-frequency contributions of turbulent organized structures to the surface-layer horizontal wind components (Fig. 8). The data from the forest site show a good agreement, but the measured low-frequency contributions at the desert site were larger than predicted by the model. These additional contributions probably originate from secondary circulations induced by the forest-desert heterogeneity or by the topography. However, this cannot be verified with the present dataset, since no Doppler lidar measurements were conducted at the desert site.

Thus, investigating the  $u$  and  $v$  spectra may help to identify the presence of meso-scale structures. For this reason, a similar analysis was performed for the Selhausen site of the HOPE dataset. It was possible to characterize the different energy balance ratios on specific days, e.g.

7 April and 16 April 2013 (Eder et al. 2015a, Appendix C), but for the whole dataset, a correlation analysis between the relative low-frequency contribution to the  $u$  spectra and the mean daytime energy balance ratio was not conclusive ( $R^2 = 0.05$ ). The synoptic weather conditions in Central Europe are highly variable, and the veering wind causes low-frequency fluctuations that are probably not related to meso-scale circulations. As a consequence, this approach is only applicable to sites with constant mean wind and constant weather conditions, such as the Yatir forest.

Commonly, low-frequency contributions to surface-layer measurements are assessed with the ogive function (Desjardins et al. 1989; Foken et al. 1995), which is the cumulative integral of the co-spectrum starting at the highest frequencies. If the normalized ogive function converges to unity within the averaging interval of the EC method, all relevant turbulent motions are captured. This test was performed with the Yatir dataset (Eder et al., 2015b, Appendix D). At the forest site, the ogive functions converged for all fluxes within a period of 30 min (Fig. 9c, d). At the desert site, the ogive functions converged for the sensible heat flux (Fig. 9b), but not for the momentum flux (Fig. 9a). Thus, low-frequency contributions can be found in the co-spectrum of  $u$  and  $w$ , but not in the co-spectrum of  $w$  and  $T$ . As a consequence, the ogive test cannot be applied to the vertical turbulent heat fluxes in order to test for low-frequency contributions, because only the momentum flux contains meso-scale flux contributions. A virtual control volume approach based on LES (Eder et al. 2015b, Appendix D) confirmed that the meso-scale structures do not affect the vertical turbulent heat fluxes in the surface layer. The meso-scale structures induce horizontal advection and horizontal flux divergences.

### *3.3.3 Vertical gradients of temperature and humidity*

The flux contribution of meso-scale structures could be successfully estimated using an airborne platform (Sect. 3.2). However, aircraft data are usually not available for every research site. As an alternative, meso-scale fluxes could also be estimated from ground-based remote sensing measurements, but only if the instruments are able to measure the instantaneous wind, temperature and humidity field over a sufficient large area, i.e. several km, and at a sufficient temporal resolution, i.e. at least in the order of tens of seconds. However, such systems are not available yet.

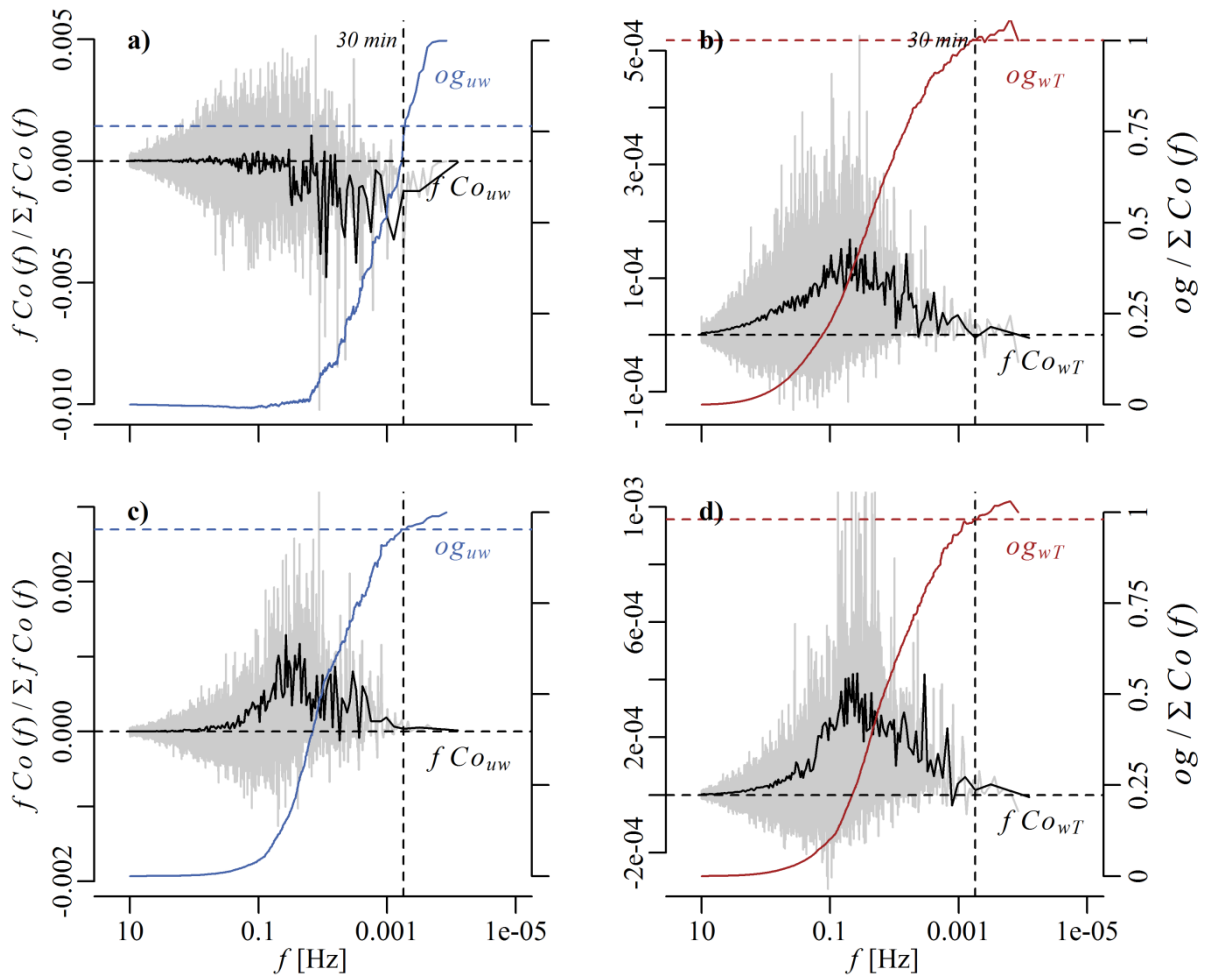


**Fig. 9** Ogive analysis for the Yatir measurement campaign. Fourier co-spectra and ogive functions normalized by the co-spectrum for momentum flux (a, c) and sensible heat flux (b, d) at the desert site (a, b) and the forest site (c, d) on 25 August 2013. The grey line indicates the original co-spectrum, the black line the smoothed co-spectrum, the solid coloured lines the normalized ogive function, and the horizontal dashed line the respective value of the ogive function at a period of 30 min (Eder et al., 2015b).

Nevertheless, Eder et al. (2015a, Appendix C) developed a simple method to indirectly estimate the meso-scale flux partitioning, but this requires several assumptions. First, only the daytime convective boundary layer above terrestrial ecosystems is considered. Accordingly, the air in the surface layer is expected to be warmer and moister than in the overlying mixed layer (Fig. 10), if no internal boundary layers (Garratt 1990) disturb the local profiles. As a consequence, regardless of whether relatively cool and dry air is brought downward or warm and moist air is lifted upward, the resulting vertical heat fluxes are always positive. Meso-scale structures are supposed to extend over the entire atmospheric boundary layer (Sect. 3.1.2) which means that they directly transport air from the surface layer to the mixed layer and vice versa. This leads

to the hypothesis that large differences in potential temperature and specific humidity between the surface layer and the mixed layer entail large meso-scale fluxes. If meso-scale fluxes are large, eddy-covariance systems should exhibit a poor closure of the surface energy balance.

This hypothesis was tested with the HOPE dataset (Eder et al. 2015a, Appendix C) by performing a correlation analysis between the energy balance residual  $Q_R$  and the vertical gradients of temperature and humidity. In a first step, data from problematic wind sectors were discarded, since it was found that backwind deficiencies of the CSAT-3 sonic anemometer and flow distortion effects due to the tower mountings considerably reduce the energy balance ratio  $R$ . Moreover, days with precipitation and days with less than 50% data availability were excluded from the analysis. Then, the mean daytime  $Q_R$  of Selhausen was compared to the mean daytime vertical gradients of temperature and humidity measured with a HATPRO radiometer (Fig. 7b, c). A positive correlation with the humidity gradient was found ( $R^2 = 0.36$ ), but no correlation with the potential temperature gradient ( $R^2 = 0.01$ ). Thus, a poor energy balance closure predominantly occurred on days with strong differences in humidity between the surface layer and the mixed layer, i.e. when the meso-scale latent heat fluxes were large. Since no relation between  $Q_R$  and the potential temperature gradient was found, the energy balance residual at the Selhausen site should be completely added to the latent heat flux. This finding conflicts with the approach of Twine et al. (2000) that assumes scalar similarity, and with the suggestion of Brötz et al. (2014) and Charuchittipan et al. (2014) who distribute the residual according to the ratio of sensible heat flux to buoyancy flux. The results from the airborne measurements during BOREAS and BERMS (Sect. 3.2) also suggest that the majority of the energy balance residual should be assigned to the latent heat flux, or it should be distributed according to the Bowen ratio. The latter was confirmed for the Merzenhausen site, where Eder et al. (2015a, Appendix C) calculated the vertical gradients from the measured turbulent fluxes using the universal functions, and found a correlation with both temperature ( $R^2 = 0.35$ ) and moisture gradients ( $R^2 = 0.38$ ). Apparently, the distribution of the meso-scale energy among sensible and latent heat seems to be highly dependent on the measurement site. However, at least for the data presented in this thesis, it seems likely that the relative underestimation of the latent heat flux is either larger than or equal to the underestimation of the sensible heat flux.

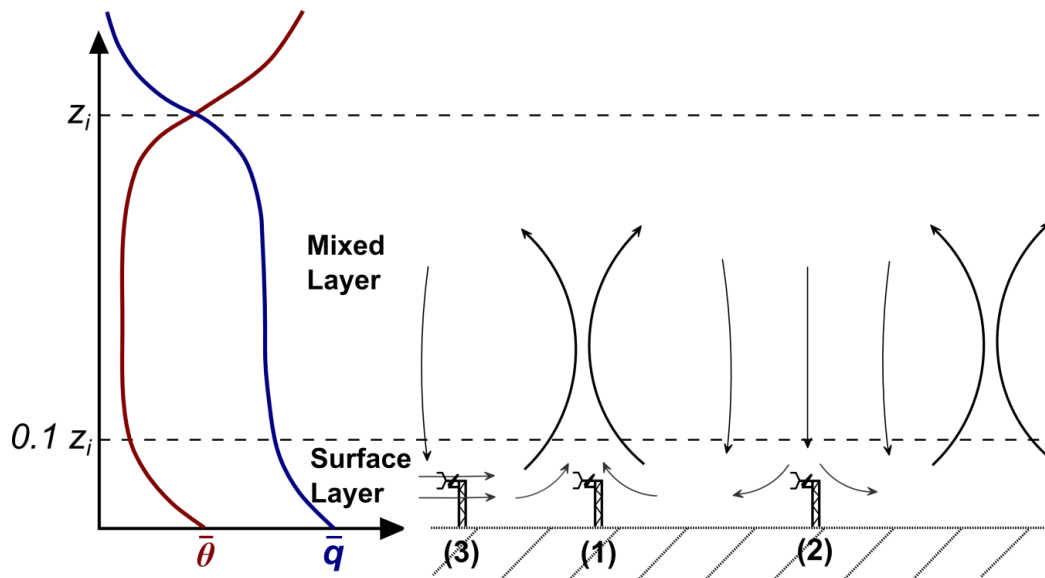


**Fig. 10** Scheme illustrating the meso-scale structures in the atmospheric boundary layer and the mean daytime vertical gradients of potential temperature  $\theta$  and specific humidity  $q$ . The meso-scale structures either transport warm and moist air upward (1) or cool and dry air downward (2) or cause horizontal advection (3), i.e. the sensible ( $Q_H$ ) and latent heat fluxes ( $Q_E$ ) are always underestimated by the EC technique – independent of the measurement location. Strong vertical gradients of  $\theta$  and  $q$  cause large meso-scale fluxes of  $Q_H$  and  $Q_E$  (M. Mauder, pers. comm., concept is based on Stull 1988 and Mahrt 1998)

#### 4. Conclusions

For detecting meso-scale structures, the velocity field of the atmospheric boundary layer has to be resolved in space and time. Eder et al. (2015a, Appendix C) achieved this with scanning Doppler lidars. Using one single device, only a few stationary circulations were detectable, and only during periods when the measurement plane was orientated parallel to the mean wind direction. The dual-Doppler technique makes it possible to continuously measure the two-dimensional velocity field in the surface layer. This method proved to deliver robust evidence for turbulent organized structures with timescales  $> 30$  min. However, for the HOPE dataset (Eder et al. 2015a, Appendix C), these structures were obviously not induced by surface heterogeneities, but rather the result of the self-organizing tendency of atmospheric flows. At the Yatir site (Eder et al. 2015b, Appendix D), which is characterized by strong surface heat flux differences, the lidar measurements provided solid evidence for a heterogeneity-induced secondary circulation on 5 of 16 measurement days. Consequently, this work clearly shows that turbulence in the surface layer does not purely consist of high-frequency modes, which partially invalidates Monin-Obukhov similarity theory. Mixed-layer structures reach close to the surface and cause convergences, divergences, and low-frequency motions in the horizontal wind components.

The flux contributions of meso-scale structures to surface sensible and latent heat fluxes were successfully estimated from the aircraft measurements of BOREAS and BERMS using wavelet analysis (Eder et al. 2014, Appendix B). In particular, it was found that the meso-scale Bowen-ratio is not necessarily identical to the Bowen ratio of the high-frequency turbulence. During the HOPE campaign (Eder et al. 2014, Appendix C), the meso-scale fluxes were indirectly estimated from the vertical temperature and humidity gradients in the lower atmospheric boundary layer. Both studies show that the flux partitioning in the meso-scale range is highly dependent on the measurement site and the meso-scale fluxes tend to have lower Bowen ratios than the small scales. Therefore, the universal use of the scalar similarity approach or the recently published approach based on the ratio of buoyancy flux to sensible heat flux for closing the energy balance cannot be recommended in general. Both methods tend to underestimate the latent heat fluxes for the datasets used in thesis.

No reliable parametrization of the energy balance closure is available at the moment (Eder et al. 2014, Appendix B). To provide recommendations for future approaches, atmospheric variables and turbulence parameters were compared with the energy balance closure. For the datasets collected during HOPE (Eder et al. 2015a, Appendix C), in the Yatir area (Eder et al.

2015b, Appendix D) and at the TERENO sites the energy balance closure improved with increasing friction velocity, which characterizes the relative importance of the high-frequency turbulence for the exchange process. For sites with constant synoptic weather conditions, e.g. the Yatir site (Eder et al. 2015b, Appendix D), the energy balance closure is even directly inferable from the low-frequency contributions to the surface-layer horizontal wind spectra or from the co-spectrum of  $u$  and  $w$ . However, the surface-layer vertical wind spectra did not show considerable energy in the low-frequency range for the HOPE and the Yatir dataset, which questions the rationale of the ogive test for detecting low-frequency contributions to turbulent heat fluxes. Finally, the vertical gradients of temperature and moisture between the surface layer and the mixed layer turned out to be very promising variables for developing a parametrization. They correlate with the energy balance closure (Eder et al. 2015a, Appendix C), and in particular, the gradients also give hints about how to distribute the energy balance residual among sensible and latent heat.

Thus, further progress is made when surface energy balance measurements are combined with a ground-based remote sensing instrument that is able to conduct temperature and moisture profile measurements close to the surface and in the mixed layer. Ideally, the remote sensing instrument could also measure horizontal gradients over at least a few km, since these gradients may also be associated with significant meso-scale fluxes, similar to the vertical gradients. For an improved understanding of the underlying processes, high-resolution LES models should be consulted that are able to resolve atmospheric turbulence down to a few metres or even decimetres above ground. Only under the controlled conditions in a model simulation, the different factors affecting the EC flux measurement could be disentangled.

**References**

- Anderson RG, Wang D (2014) Energy budget closure observed in paired eddy covariance towers with increased and continuous daily turbulence. *Agric For Meteorol* 184:204-209
- Aubinet M, Feigenwinter C, Heinesch B, Bernhofer C, Canepa E, Lindroth A, Montagnani L, Rebmann C, Sedlak P, Van Gorsel E (2010) Direct advection measurements do not help to solve the night-time CO<sub>2</sub> closure problem: evidence from three different forests. *Agric For Meteorol* 150:655-664
- Aubinet M, Heinesch B, Yernaux M (2003) Horizontal and vertical CO<sub>2</sub> advection in a sloping forest. *Boundary-Layer Meteorol* 108:397-417
- Baldocchi D, Falge E, Gu LH, Olson R, Hollinger D, Running S, Anthoni P, Bernhofer C, Davis K, Evans R, Fuentes J, Goldstein A, Katul G, Law B, Lee XH, Malhi Y, Meyers T, Munger W, Oechel W, Paw KT, Pilegaard K, Schmid HP, Valentini R, Verma S, Vesala T, Wilson K, Wofsy S (2001) FLUXNET: A new tool to study the temporal and spatial variability of ecosystem-scale carbon dioxide, water vapor, and energy flux densities. *Bull Amer Meteorol Soc* 82:2415-2434
- Baldocchi DD (2003) Assessing the eddy covariance technique for evaluating carbon dioxide exchange rates of ecosystems: past, present and future. *Global Change Biol* 9:479-492
- Barr AG, Griffis TJ, Black TA, Lee X, Staebler RM, Fuentes JD, Chen Z, Morgenstern K (2002) Comparing the carbon budgets of boreal and temperate deciduous forest stands. *Can J For Res* 32:813-822
- Barr AG, Morgenstern K, Black TA, McCaughey JH, Nesic Z (2006) Surface energy balance closure by the eddy-covariance method above three boreal forest stands and implications for the measurement of the CO<sub>2</sub> flux. *Agric For Meteorol* 140:322-337
- Barr AG, van der Kamp G, Black TA, McCaughey JH, Nesic Z (2012) Energy balance closure at the BERMS flux towers in relation to the water balance of the White Gull Creek watershed 1999-2009. *Agric For Meteorol* 153:3-13

- Batchelor GK (1950) The application of the similarity of turbulence to atmospheric diffusion. *Q J R Meteorol Soc* 76:133-146
- Blanken PD, Black TA, Yang PC, Neumann HH, Nesic Z, Staebler R, den Hartog G, Novak MD, Lee X (1997) Energy balance and canopy conductance of a boreal aspen forest: partitioning overstory and understory components. *J Geophys Res Atmos* 102:28915-28927
- Brötz B, Eigenmann R, Dörnbrack A, Foken T, Wirth V (2014) Early-morning flow transition in a valley in low-mountain terrain under clear-sky conditions. *Bound -Layer Meteor* 152:45-63
- Businger JA (1982) Equations and concepts. in: Nieuwstadt FTM, Van Dop H (ed) *Atmospheric turbulence and air pollution modeling: a course held in The Hague, 21-25 September 1981*. Reidel Publ. Co., Dordrecht. pp. 1-36
- Charuchittipan D, Babel W, Mauder M, Leps JP, Foken T (2014) Extension of the averaging time in eddy-covariance measurements and its effect on the energy balance closure. *Boundary-Layer Meteorol* 152:303-327
- Chen JM, Chen X, Ju W, Geng X (2005) Distributed hydrological model for mapping evapotranspiration using remote sensing inputs. *J Hydrol* 305:15-39
- Dalu GA, Pielke RA (1993) Vertical heat fluxes generated by mesoscale atmospheric flow induced by thermal inhomogeneities in the PBL. *J Atmos Sci* 50:919-926
- Deardorff JW (1972) Numerical investigation of neutral and unstable planetary boundary layers. *J Atmos Sci* 29:91-115
- Desjardins RL (1985) Carbon dioxide budget of maize. *Agric For Meteorol* 36:29-41
- Desjardins RL, MacPherson JJ, Schuepp PH, Karanja F (1989) An evaluation of aircraft flux measurements of CO<sub>2</sub>, water vapor and sensible heat. *Boundary-Layer Meteorol* 47:55-69

- Dixon NS, Parker DJ, Taylor CM, Garcia-Carreras L, Harris PP, Marsham JH, Polcher J, Woolley A (2013) The effect of background wind on mesoscale circulations above variable soil moisture in the Sahel. *Q J R Meteorol Soc* 139:1009-1024
- Eder F, De Roo F, Kohnert K, Desjardins RL, Schmid HP, Mauder M (2014) Evaluation of two energy balance closure parametrizations. *Boundary-Layer Meteorol* 151:195-219
- Eder F, Schmidt M, Damian T, Träumner K, Mauder M (2015a) Meso-scale eddies affect near-surface turbulent exchange: evidence from lidar and tower measurements. *J Appl Meteorol Climatol* 54:189-206
- Eder F, De Roo F, Rotenberg E, Yakir D, Schmid HP, Mauder M (2015b) Secondary circulations at a solitary forest surrounded by semi-arid shrubland and their impact on eddy-covariance measurements. *Agric For Meteorol* 211: 115-127
- Emeis S, Jahn C, Munkel C, Münsterer C, Schäfer K (2007) Multiple atmospheric layering and mixing-layer height in the Inn valley observed by remote sensing. *Meteorol Z* 16:415-424
- Emeis S, Schäfer K, Munkel C (2008) Surface-based remote sensing of the mixing-layer height - a review. *Meteorol Z* 17:621-630
- Etling D, Brown RA (1993) Roll vortices in the planetary boundary layer: a review. *Boundary-Layer Meteorol* 65:215-248
- Falge E, Reth S, Brüggemann N, Butterbach-Bahl K, Goldberg V, Oltchev A, Schaaf S, Spindler G, Stiller B, Queck R, Köstner B, Bernhofer C (2005) Comparison of surface energy exchange models with eddy flux data in forest and grassland ecosystems of Germany. *Ecol Model* 188:174-216
- Finnigan JJ, Clement R, Malhi Y, Leuning R, Cleugh HA (2003) A re-evaluation of long-term flux measurement techniques Part I: averaging and coordinate rotation. *Boundary-Layer Meteorol* 107:1-48

- Foken T, Dlugi R, Kramm G (1995) On the determination of dry deposition and emission of gaseous compounds at the biosphere-atmosphere interface. *Meteorol Z* 4:91-118
- Foken T (2008a) *Micrometeorology*. Springer, Heidelberg. 308 pp
- Foken T (2008b) The energy balance closure problem: an overview. *Ecolog Appl* 18:1351-1367
- Foken T, Aubinet M, Finnigan JJ, Leclerc MY, Mauder M, Paw U KT (2011) Results of a panel discussion about the energy balance closure correction for trace gases. *Bull Amer Meteorol Soc* 92:ES13-ES18
- Foken T, Aubinet M, Leuning R (2012a) The eddy covariance method. in: Aubinet M, Vesala T, Papale D (ed) *Eddy Covariance - a practical guide to measurement and data analysis*. Springer, Dordrecht. pp. 1-19
- Foken T, Leuning R, Oncley SR, Mauder M, Aubinet M (2012b) Corrections and data quality control. in: Aubinet M, Vesala T, Papale D (ed) *Eddy covariance: A practical guide to measurement and data analysis*. Springer, Dordrecht, Heidelberg, London, New York. pp. 85-131
- Foken T, Wimmer F, Mauder M, Thomas C, Liebethal C (2006) Some aspects of the energy balance closure problem. *Atmos Chem Phys* 6. pp 4395-4402
- Garratt JR (1990) The internal boundary layer - a review. *Bound -Layer Meteor* 50:171-203
- Goulden ML, Munger JW, Fan SM, Daube BC, Wofsy SC (1996) Measurements of carbon sequestration by long-term eddy covariance: methods and a critical evaluation of accuracy. *Global Change Biol* 2:169-182
- Grünzweig JM, Lin T, Rotenberg E, Schwartz A, Yakir D (2003) Carbon sequestration in arid-land forest. *Global Change Biol* 9:791-799
- Heinsch FA, Zhao M, Running SW, Kimball JS, Nemani RR, Davis KJ, Bolstad PV, Cook BD, Desai AR, Ricciuto DM, Law BE, Oechel WC, Kwon H, Luo H, Wofsky SC, Dunn AL, MUNGER JW, Baldocchi DD, Xu L, Hollinger DY, Richardson AD, Stoy PC, Siqueira

- MBS, Monson RK, Burns SP, Flanagan LB (2006) Evaluation of remote sensing based terrestrial productivity from MODIS using regional tower eddy flux network observations. *IEEE Trans Geosci Remote Sens* 44:1908-1925
- Hendricks-Franssen HJ, Stöckli R, Lehner I, Rotenberg E, Seneviratne SI (2010) Energy balance closure of eddy-covariance data: a multisite analysis for European FLUXNET stations. *Agric For Meteorol* 150:1553-1567
- Higgins CW, Pardyak E, Froidevaux M, Simeonov V, Parlange MB (2013) Measured and estimated water vapor advection in the atmospheric surface layer. *J Hydrometeorol* 14:1966-1972
- Højstrup J (1981) A simple model for the adjustment of velocity spectra in unstable conditions downstream of an abrupt change in roughness and heat flux. *Boundary-Layer Meteorol* 21:341-356
- Holmes P, Lumley JL, Berkooz G (1996) *Turbulence, coherent structures, dynamical systems and symmetry*. Cambridge University Press, New York. 420 pp
- Horst TW, Semmer SR, Maclean G (2015) Correction of a non-orthogonal, three-component sonic anemometer for flow distortion by transducer shadowing. *Boundary-Layer Meteorol* 1-25
- Huang J, Lee X, Patton E (2008) A modelling study of flux imbalance and the influence of entrainment in the convective boundary layer. *Boundary-Layer Meteorol* 127:273-292
- Ingwersen J, Steffens K, Högy P, Warrach-Sagi K, Zhunusbayeva D, Poltoradnev M, Gäbler R, Wizemann HD, Fangmeier A, Wulfmeyer V, Streck T (2011) Comparison of Noah simulations with eddy covariance and soil water measurements at a winter wheat stand. *Agric For Meteorol* 151:345-355
- Kaimal JC (1978) Horizontal velocity spectra in an unstable surface layer. *J Atmos Sci* 35:18-24

- Kaimal JC, Wyngaard JC, Haugen DA, Coté OR, Izumi Y, Caughey SJ, Readings CJ (1976) Turbulence structure in the convective boundary layer. *J Atmos Sci* 33:2152-2169
- Kaimal JC, Wyngaard JC, Izumi Y, Coté OR (1972) Spectral characteristics of surface-layer turbulence. *Q J R Meteorol Soc* 98:563-589
- Kanda M, Inagaki A, Letzel MO, Raasch S, Watanabe T (2004) LES Study of the energy imbalance problem with eddy covariance fluxes. *Boundary-Layer Meteorol* 110:381-404
- Kanemasu ET, Verma SB, Smith EA, Fritschen LJ, Wesely M, Field RT, Kustas WP, Weaver H, Stewart JB, Gurney R, Panin G, Moncrieff JB (1992) Surface flux measurements in FIFE: An overview. *J Geophys Res Atmos* 97:18547-18555
- Kang SL, Lenschow DH (2014) Temporal evolution of low-level winds induced by two-dimensional mesoscale surface heat-flux heterogeneity. *Boundary-Layer Meteorol* 151:501-529
- Kochendorfer J, Meyers TP, Frank J, Massman WJ, Heuer MW (2012) How well can we measure the vertical wind speed? Implications for fluxes of energy and mass. *Boundary-Layer Meteorol* 145:383-398
- Kolmogorov AN (1941) Dissipation of energy in isotropic turbulence. *Dokl Akad Nauk SSSR* 31:538-541
- Laubach J, Teichmann U (1999) Surface energy budget variability: a case study over grass with special regard to minor inhomogeneities in the source area. *Theor Appl Climatol* 62:9-24
- Lee X, Black TA (1993) Atmospheric turbulence within and above a douglas-fir stand. Part II: eddy fluxes of sensible heat and water vapour. *Boundary-Layer Meteorol* 64:369-389
- Lenschow DH, Stankov BB (1986) Length scales in the convective boundary layer. *J Atmos Sci* 43:1198-1209

- Leuning R, van Gorsel E, Massman WJ, Isaac PR (2012) Reflections on the surface energy imbalance problem. *Agric For Meteorol* 156:65-74
- Liebenthal C, Huwe B, Foken T (2005) Sensivity analysis for two ground heat flux calculation approaches. *Agric For Meteorol* 132:253-262
- Lothon M, Couvreux F, Donier S, Guichard F, Lacarrère P, Lenschow D, Noilhan J, Saïd F (2007) Impact of coherent eddies on airborne measurements of vertical turbulent fluxes. *Boundary-Layer Meteorol* 124:425-447
- Mahfouf JF, Richard E, Mascart P (1987) The influence of soil and vegetation on the development of mesoscale circulations. *J Climate Appl Meteorol* 26:1483-1495
- Mahrt L (1998) Flux sampling errors for aircraft and towers. *J Atmos Oceanic Technol* 15:416-429
- Maronga B, Gryschka M, Heinze R, Hoffmann F, Kanani-Sühring F, Keck M, Ketelsen K, Letzel MO, Sühring M, Raasch S (2015) The Parallelized Large-Eddy Simulation Model (PALM) version 4.0 for atmospheric and oceanic flows: model formulation, recent developments, and future perspectives. *Geosci Model Dev Discuss* 8:1539-1637
- Maronga B, Raasch S (2013) Large-eddy simulations of surface heterogeneity effects on the convective boundary layer during the LITFASS-2003 experiment. *Boundary-Layer Meteorol* 146:17-44
- Mauder M, Cuntz M, Drüe C, Graf A, Rebmann C, Schmid HP, Schmidt M, Steinbrecher R (2013) A strategy for quality and uncertainty assessment of long-term eddy-covariance measurements. *Agric For Meteorol* 169:122-135
- Mauder M, Desjardins RL, MacPherson I (2007) Scale analysis of airborne flux measurements over heterogeneous terrain in a boreal ecosystem. *J Geophys Res* 112:D13112
- Mauder M, Foken T (2011) Documentation and instruction manual of the Eddy-Covariance software package TK3. *Arbeitsergebnisse*. Bayreuth, Germany. ISSN:1614-8916. 60 pp

- 
- Monin AS, Obukhov AM (1954) Basic laws of turbulent mixing in the surface layer of the atmosphere near the ground. *Tr Akad Nauk SSSR Geophys Inst* 24:163-187
- Nakai T, Van der Molen MK, Gash JHC, Kodama Y (2006) Correction of sonic anemometer angle of attack errors. *Agric For Meteorol* 136:19-30
- Obukhov AM (1941) On the energy distribution in the spectrum of a turbulent flow. *Izvestiya Akad Nauk SSSR, Ser Geogra Geofiz* 5:453-466
- Orlanski I (1975) A rational subdivision of scales for atmospheric processes. *Bull Amer Meteorol Soc* 56:527-530
- Panin GN, Bernhofer Ch (2008) Parametrization of turbulent fluxes over inhomogeneous landscapes. *Izvestiya Atmos Oceanic Phys* 44:701-716
- Panofsky HA, Tennekes H, Lenschow DH, Wyngaard JC (1977) The characteristics of turbulent velocity components in the surface layer under convective conditions. *Boundary-Layer Meteorol* 11:355-361
- Patton EG, Sullivan PP, Moeng CH (2005) The influence of idealized heterogeneity on wet and dry planetary boundary layers coupled to the land surface. *J Atmos Sci* 62:2078-2097
- Raasch S, Schröter M (2001) PALM - A large-eddy simulation model performing on massively parallel computers. *Meteorol Z* 10:363-372
- Raupach MR, Finnigan JJ, Brunet Y (1996) Coherent eddies and turbulence in vegetation canopies: The mixing-layer analogy. *Boundary-Layer Meteorol* 78:351-382
- Rayleigh L (1916) On convection currents in a horizontal layer of fluid, when the higher temperature is on the under side. *Philos Mag Ser* 32:529-546
- Reichstein M, Papale D, Valentini R, Aubinet M, Bernhofer C, Knohl A, Laurila T, Lindroth A, Moors E, Pilegaard K, Seufert G (2007) Determinants of terrestrial ecosystem carbon balance inferred from European eddy covariance flux sites. *Geophys Res Lett* 34:L01402

- Reynolds O (1894) On the dynamical theory of incompressible fluids and the determination of the criterion. *Philos Trans R Soc London A* 186:123-164
- Rotenberg E, Yakir D (2010) Contribution of semi-arid forests to the climate system. *Science* 327:451-454
- Rotenberg E, Yakir D (2011) Distinct patterns of changes in surface energy budget associated with forestation in the semiarid region. *Global Change Biol* 17:1536-1548
- Sakai RK, Fitzjarrald DR, Moore KE (2001) Importance of low-frequency contributions to eddy fluxes observed over rough surfaces. *J Appl Meteorol* 40:2178-2192
- Schmidt H, Schumann U (1989) Coherent structure of the convective boundary layer derived from large-eddy simulations. *J Fluid Mech* 200:511-562
- Sellers PJ, Hall FG, Kelly RD, Black A, Baldocchi D, Berry J, Ryan M, Ranson KJ, Crill PM, Lettenmaier DP, Margolis H, Cihlar J, Newcomer J, Fitzjarrald D, Jarvis PG, Gower ST, Halliwell D, Williams D, Goodison B, Wickland DE, Guertin FE (1997) BOREAS in 1997: Experiment overview, scientific results, and future directions. *J Geophys Res* 102:28731-28769
- Shen S, Leclerc MY (1995) How large must surface inhomogeneities be before they influence the convective boundary layer structure? A case study. *Q J R Meteorol Soc* 121:1209-1228
- Stawiarski C (2014) Optimizing dual-Doppler lidar measurements of surface layer coherent structures with large-eddy simulations. Dissertation, Karlsruhe Institute of Technology, Karlsruhe. 197 pp
- Stawiarski C, Träumner K, Knigge C, Calhoun R (2013) Scopes and challenges of dual-Doppler lidar wind measurements - an error analysis. *J Atmos Oceanic Technol* 30:2044-2062
- Stoy PC, Mauder M, Foken T, Marcolla B, Boegh E, Ibrom A, Arain MA, Arneth A, Aurela M, Bernhofer C, Cescatti A, Dellwik E, Duce P, Gianelle D, van Gorsel E, Kiely G, Knohl A, Margolis H, McCaughey H, Merbold L, Montagnani L, Papale D, Reichstein

- M, Saunders M, Serrano-Ortiz P, Sottocornola M, Spano D, Vaccari F, Varlagin A (2013) A data-driven analysis of energy balance closure across FLUXNET research sites: the role of landscape scale heterogeneity. *Agric For Meteorol* 171–172:137-152
- Strunin MA, Hiyama T (2005) Spectral structure of small-scale turbulent and mesoscale fluxes in the atmospheric boundary layer over a thermally inhomogeneous land surface. *Boundary-Layer Meteorol* 117:479-510
- Stull RB (1988) An introduction to boundary layer meteorology. Kluwer Academic Publishers, Dordrecht. 666 pp
- Sührling M, Raasch S (2013) Heterogeneity-induced heat flux patterns in the convective boundary layer: can they be detected from observations and is there a blending height? - A large-eddy simulation study for the LITFASS-2003 experiment. *Boundary-Layer Meteorol* 148:309-331
- Taylor GI (1938) The spectrum of turbulence. *Proc R Soc London A: Math Phys Eng Sci* 164:476-490
- Tennekes H, Lumley JL (1972) A first course in turbulence. MIT Press, Cambridge. 300 pp
- Torrence C, Compo GP (1998) A practical guide to wavelet analysis. *Bull Amer Meteorol Soc* 79:61-78
- Träumner K, Damian T, Stawiarski C, Wieser A (2014) Turbulent structures and coherence in the atmospheric surface layer. *Boundary-Layer Meteorol* 154:1-25
- Tsvang LR, Fedorov MM, Kader BA, Zubkovskii SL, Foken T, Richter SH, Zeleny Y (1991) Turbulent exchange over a surface with chessboard-type inhomogeneities. *Boundary-Layer Meteorol* 55:141-160
- Twine TE, Kustas WP, Norman JM, Cook DR, Houser PR, Meyers TP, Prueger JH, Starks PJ, Wesley ML (2000) Correcting eddy-covariance flux underestimates over a grassland. *Agric For Meteorol* 103:279-300

- Van der Hoven I (1957) Power spectrum of horizontal wind speed in the frequency range from 0.0007 to 900 cycles per hour. *J Meteorol* 14:160-164
- Wagner JS, Gohm A, Rotach MW (2015) The impact of valley geometry on daytime thermally driven flows and vertical transport processes. *Q J R Meteorol Soc* 141:1780-1794
- Werner C (2005) Doppler wind lidar. in: Weitkamp C (ed) *Lidar: Range-Resolved Optical Remote Sensing of the Atmosphere*. Springer, New York. pp. 325-354
- Wilczak JM (1984) Large-scale eddies in the unstably stratified atmospheric surface layer. Part I: velocity and temperature structure. *J Atmos Sci* 41:3537-3550
- Williams AG, Kraus H, Hacker JM (1996) Transport processes in the tropical warm pool boundary layer. Part I: spectral composition of fluxes. *J Atmos Sci* 53:1187-1202
- Wilson K, Goldstein A, Falge E, Aubinet M, Baldocchi D, Berbigier P, Bernhofer C, Ceulemans R, Dolman H, Field C, Grelle A, Ibrom A, Law BE, Kowalski A, Meyers T, Moncrieff J, Monson R, Oechel W, Tenhunen J, Valentini R, Verma S (2002) Energy balance closure at FLUXNET sites. *Agric For Meteorol* 113:223-243
- Wilson KB, Hanson PJ, Mulholland PJ, Baldocchi DD, Wullschlegel SD (2001) A comparison of methods for determining forest evapotranspiration and its components: sap-flow, soil water budget, eddy covariance and catchment water balance. *Agric For Meteorol* 106:153-168
- Wohlfahrt G, Irschick C, Thalinger B, Hörtnagl L, Obojes N, Hammerle A (2010) Insights from independent evapotranspiration estimates for closing the energy balance: a grassland study. *Vadose Zone J* 9:1025-1033
- Wyngaard JC (2010) *Turbulence in the atmosphere*. Cambridge University Press, Cambridge. 393 pp
- Zacharias S, Bogenha H, Samaniego L, Mauder M, Fuß R, Pütz T, Frenzel M, Schwank M, Baessler C, Butterbach-Bahl K, Bens O, Borg E, Brauer A, Dietrich P, Hajnsek I, Helle G, Kiese R, Kunstmann H, Klotz S, Munch JC, Papen H, Priesack E, Schmid HP,

Steinbrecher R, Rosenbaum U, Teutsch G, Vereecken H (2011) A network of terrestrial environmental observatories in Germany. *Vadose Zone J* 10:955-973

**List of Appendices**

Appendix A: Individual contributions to the joint publications..... 41

Appendix B: Evaluation of two energy balance closure parametrizations ..... 44

Appendix C: Meso-scale eddies contribute to near-surface exchange: evidence from lidar and tower measurements ..... 69

Appendix D: Secondary circulations at a solitary forest surrounded by semi-arid shrubland and their impact on eddy-covariance measurements..... 87

## **Appendix A : Individual contributions to the joint publications**

This thesis is presented in cumulative form and consists of three individual publications that were composed in cooperation with other researchers. This section specifies the individual contributions to the joint publications, with a special emphasis on my own contributions.

### ***Appendix B***

Eder F\*, De Roo F, Kohnert K, Desjardins RL, Schmid HP, Mauder M (2014) Evaluation of two energy balance closure parametrizations. *Boundary-Layer Meteorol* 151:195-219, doi: 10.1007/s10546-013-9904-0

I was responsible for the entire analysis presented in the manuscript, including an implementation of a software routine in order to perform the Wavelet analysis with the airborne dataset, and making the surface roughness maps based on landuse maps. With respect to the TERENO sites, the eddy-covariance fluxes were already processed automatically. I also was responsible for writing the entire manuscript.

Frederik De Roo assisted at writing the discussion section, especially those parts about the large-eddy simulation models and why they are not able to reproduce atmospheric turbulence correctly close to the surface. Katrin Kohnert was responsible for processing the ceilometer data and provided the data about the boundary-layer height. Raymond L. Desjardins provided the Candle lake data set and gave valuable editorial advice during the writing process. Hans Peter Schmid gave helpful feedback during the analysis, which especially helped to clarify Section 2 in the manuscript. My supervisor Matthias Mauder encouraged me to write this manuscript and guided me through the analysis and the writing process. Furthermore, he was responsible for implementing the automated processing of the eddy-covariance fluxes of the TERENO sites and helped me to get along with the airborne dataset.

### ***Appendix C***

Eder F\*, Schmidt M, Damian T, Träumner K, Mauder M (2015a) Meso-scale eddies affect near-surface turbulent exchange: evidence from lidar and tower measurements. *J Appl Meteorol Climatol* 54:189-206, doi: 10.1175/JAMC-D-14-0140.1

I operated the Streamline Doppler lidar during the HOPE campaign and I conducted the complete analysis after having received the processed eddy-covariance data and 30-minute averaged dual-Doppler measurements. I discovered the dependence of the energy balance closure on wind direction, I processed the Streamline Doppler lidar data, adapted the wavelet routine to the HOPE dataset, performed the regression analysis, and I wrote the entire manuscript.

Marius Schmidt was responsible for the eddy-covariance stations at Selhausen and provided the processed eddy-covariance data, the radiation data and the soil measurements. Thomas Damian and Katja Träumner conducted the Doppler lidar measurements, provided the dual-Doppler dataset and performed the 30-minute averaging. They also made the microwave radiometer measurements available. Moreover, Katja Träumner gave valuable feedback during the writing process, especially about the correct nomenclature of coherent structures in the atmospheric boundary layer. Matthias Mauder raised the hypothesis that vertical gradients of temperature and humidity might be related to the energy balance closure problem. In addition, he suggested to determine the vertical gradients using the universal functions. As my supervisor, he guided me through the measurement, analysis and writing process.

#### ***Appendix D***

Eder F\*, De Roo F, Rotenberg E, Yakir D, Schmid HP, Mauder M (2015b) Secondary circulations at a solitary forest surrounded by semi-arid shrubland and their impact on eddy-covariance measurements. *Agric For Meteorol* 211:115-127

I was responsible for conducting the ground-based remote sensing measurements, i.e. the Doppler lidar, at the Yatir site. I calculated the Wavelet spectra by adapting the software routine to the Yatir dataset, I calculated the Fourier spectra and implemented the ogive analysis. Finally, I was responsible for writing and editing the entire manuscript.

Frederik De Roo performed the large-eddy simulations and wrote the major part in the materials and methods section about the large-eddy simulation model. Moreover, he developed and implemented the virtual control volume approach. Eyal Rotenberg was, together with the staff from the Earth and Planetary Sciences department of the Weizmann Institute of Science, responsible for the eddy-covariance measurements during the campaign and provided the eddy-

covariance raw data and the radiation measurements. Dan Yakir and Hans Peter Schmid initiated the measurement campaign and defined its major goals. My supervisor Matthias Mauder supported me during the beginning of the measurement campaign and we both decided about the measurement strategy, in close collaboration with Eyal Rotenberg, Dan Yakir and Hans Peter Schmid. Matthias Mauder processed the eddy-covariance data using the software TK3.1. Moreover, he advised me during the analysis and gave valuable editorial comments during the writing process.

## Appendix B

Eder F\*, De Roo F, Kohnert K, Desjardins RL, Schmid HP, Mauder M (2014) Evaluation of two energy balance closure parametrizations. *Boundary-Layer Meteorol* 151:195–219, doi: 10.1007/s10546-013-9904-0

© Springer. Used with permission.

Boundary-Layer Meteorol (2014) 151:195–219  
DOI 10.1007/s10546-013-9904-0

---

ARTICLE

### Evaluation of Two Energy Balance Closure Parametrizations

Fabian Eder · Frederik De Roo · Katrin Kohnert ·  
Raymond L. Desjardins · Hans Peter Schmid ·  
Matthias Mauder

Received: 19 April 2013 / Accepted: 31 December 2013 / Published online: 20 January 2014  
© Springer Science+Business Media Dordrecht 2014

**Abstract** A general lack of energy balance closure indicates that tower-based eddy-covariance (EC) measurements underestimate turbulent heat fluxes, which calls for robust correction schemes. Two parametrization approaches that can be found in the literature were tested using data from the Canadian Twin Otter research aircraft and from tower-based measurements of the German Terrestrial Environmental Observatories (TERENO) programme. Our analysis shows that the approach of Huang et al. (*Boundary-Layer Meteorol* 127:273–292, 2008), based on large-eddy simulation, is not applicable to typical near-surface flux measurements because it was developed for heights above the surface layer and over homogeneous terrain. The biggest shortcoming of this parametrization is that the grid resolution of the model was too coarse so that the surface layer, where EC measurements are usually made, is not properly resolved. The empirical approach of Panin and Bernhofer (*Izvestiya Atmos Oceanic Phys* 44:701–716, 2008) considers landscape-level roughness heterogeneities that induce secondary circulations and at least gives a qualitative estimate of the energy balance closure. However, it does not consider any feature of landscape-scale heterogeneity other than surface roughness, such as surface temperature, surface moisture or topography. The failures of both approaches might indicate that the influence of mesoscale structures is not

---

F. Eder (✉) · F. De Roo · K. Kohnert · H. P. Schmid · M. Mauder  
Institute of Meteorology and Climate Research,  
Atmospheric Environmental Research (IMK-IFU), Karlsruhe Institute of Technology (KIT),  
Kreuzackbahnstrasse 19, 82467 Garmisch-Partenkirchen, Germany  
e-mail: fabian.eder@kit.edu

K. Kohnert  
Department of Micrometeorology, University of Bayreuth, Universitätsstrasse 30,  
95444 Bayreuth, Germany

*Present Address*

K. Kohnert  
Helmholtz Centre Potsdam, GFZ German Research Centre for Geosciences, Telegrafenberg,  
14473 Potsdam, Germany

R. L. Desjardins  
Agriculture and Agri-Food Canada, 960 Carling Avenue, Ottawa, ON K1A 0C6, Canada

a sufficient explanation for the energy balance closure problem. However, our analysis of different wind-direction sectors shows that the upwind landscape-scale heterogeneity indeed influences the energy balance closure determined from tower flux data. We also analyzed the aircraft measurements with respect to the partitioning of the “missing energy” between sensible and latent heat fluxes and we could confirm the assumption of scalar similarity only for Bowen ratios  $\approx 1$ .

**Keywords** Airborne measurements · Eddy covariance · Energy balance closure · Surface heterogeneity · TERENO programme

## 1 Introduction

The eddy-covariance (EC) technique is widely used in environmental research to quantify the biosphere-atmosphere exchange of mass and energy. However, in numerous field experiments over the last few decades, it was found that the surface energy balance at the land surface could not be closed. The available energy, which is the sum of net radiation ( $Q_S^*$ ) and ground heat flux ( $Q_G$ ), should be totally balanced by the surface fluxes of sensible ( $Q_H$ ) and latent heat ( $Q_E$ ) except for minor terms, e.g. photosynthesis. In most field experiments and long-term measurements, the sum of turbulent fluxes usually are about 10–30% lower than the available energy, which produces an energy balance residual  $\Delta$  up to more than  $100 \text{ W m}^{-2}$  around noon in summer (Desjardins 1985; Lee and Black 1993; Twine et al. 2000; Wilson et al. 2002; Oncley et al. 2007; Foken et al. 2010; Hendricks-Franssen et al. 2010; Barr et al. 2012; Stoy et al. 2013),

$$-Q_S^* - Q_G = Q_H + Q_E + \Delta. \quad (1)$$

The fluxes are defined to be positive when directed away from the earth’s surface. As an alternative to Eq. 1, an energy balance ratio ( $R$ ) can be defined as the ratio of turbulent energy to available energy (Wilson et al. 2002),

$$R = \frac{Q_H + Q_E}{-Q_S^* - Q_G}. \quad (2)$$

In the literature, various hypotheses for the non-closure of the energy balance can be found. Instrumental issues have always been under discussion, but intercomparison experiments such as Mauder et al. (2007c) could not confirm that instrumental errors are the reason for the systematic underestimation of turbulent fluxes. Currently, the underestimation of vertical wind velocity by non-orthogonal sonic anemometers is considered (Kochendorfer et al. 2012). Furthermore, a considerable amount of energy can be stored in the soil, vegetation and air between the surface and the location of the measurement devices (Leuning et al. 2012). The energy storage in the atmosphere is directly related to the flux divergence (Betts et al. 1992). For measurements above low vegetation, the energy storage in air and biomass is negligible, but not the energy storage in the soil (Oncley et al. 2007). In this study, the latter was determined according to Liebethal et al. (2005) and included into  $Q_G$ .

The aim of our study is to test two parametrizations of the energy balance closure that follow the hypothesis that large-scale circulations are the reason for the non-closure of the energy balance (Sect. 2). Huang et al. (2008) argue that the EC method underestimates turbulent fluxes as compared to spatially-averaged fluxes due to large, organized structures, whereas Panin and Bernhofer (2008) claim that non-closure is correlated with the heterogeneity of the land surface, which can be regarded as an initiator of secondary circulations.

Therefore, the role of large-scale circulations on EC measurements will be explained further in the following paragraphs.

Conventionally, EC flux estimates are based on block averages over time periods of a certain length, usually 30 min. It is assumed that within this time interval, the meteorological conditions are sufficiently stationary and all turbulent scales are captured. However, low-frequency motions with time scales larger than the selected averaging time (Finnigan et al. 2003) and non-propagating eddies that do not move with the mean wind (Lee and Black 1993; Mahrt 1998) are not detected: when calculating the EC flux, a Reynolds decomposition is applied, the flux is calculated from the covariance of the fluctuating parts of two atmospheric entities, but the structures mentioned above only affect the mean components. During daytime, when the absolute values of the fluxes are large, the air close to the ground is usually warmer and moister than above, so that the non-consideration of any turbulent transport mechanism would lead to an underestimation in  $Q_H$  and  $Q_E$ , i.e. to a non-closure of the energy balance (Mauder et al. 2010). In addition, low-frequency motions and non-propagating eddies might also be responsible for the net advection of energy into the control volume of the measurement, which is an alternative explanation for the energy balance closure problem (Aubinet et al. 2003).

Horizontal homogeneity is one condition for the validity of EC theory (Finnigan et al. 2003), and above such surfaces, energy balance ratios  $\approx 1$  have been reported (Heusinkveld et al. 2004; Mauder et al. 2007a; Leuning et al. 2012). However, most sites do not fulfil the condition of horizontal homogeneity, especially at the landscape scale. Secondary circulations that are induced by surface heterogeneities, e.g. differences in surface roughness, temperature and moisture (Segal et al. 1988; Segal and Arritt 1992; Sun et al. 1997; Strunin and Hiyama 2005), transport up to 30% of scalar fluxes (Randow et al. 2002) and were related to the energy balance closure problem (Foken 2008; Foken et al. 2010; Ingwersen et al. 2011). Moreover, Desjardins et al. (1992) showed during the First ISLSCP Field Experiment (FIFE) that heterogeneous topography also induces a lack of energy balance closure.

Secondary circulations are also called ‘mesoscale’ motions because the respective size of the surface patches is crucial: for the mesoscale heterogeneity regime, the established theories developed for the homogenous atmospheric boundary layer (ABL) are not valid (Mahrt 2000). The minimum size that surface patches must have in order to induce mesoscale motions, is considered to be of the size of the ABL height (Shen and Leclerc 1995; Raasch and Harbusch 2001). Patton et al. (2005) found that the wavelength of any surface heterogeneity should be around 4–9 times the ABL height in order to be effective in generating secondary circulations. Simulations above multi-scale landscapes showed that mesoscale motions have a preferred scale  $\approx 10$ –20 km (Baidya Roy et al. 2003) and they are mainly formed due to surface differences in the upstream area (Maronga and Raasch 2013). However, complex topography, small-scale heterogeneities and flow singularities might also be responsible for the non-closure of the energy balance, at least at certain sites in ‘non-ideal’ terrain (Panin et al. 1998; Foken et al. 2010).

To date, however, there is still no clear evidence that surface heterogeneities and secondary circulations cause the non-closure of the energy balance. The arguments presented above should be regarded as hypotheses, not as facts. Nevertheless, because surface fluxes are necessary input parameters for atmospheric models, and the EC method is widely used to determine trace gas budgets on an ecosystem scale, a robust parametrization of the missing turbulent energy is necessary. If the magnitude of underestimation, as well as the partitioning of the missing energy among sensible and latent heat are known, the measured fluxes can be corrected.

Therefore, we tested the two above-mentioned approaches that attempt to parametrize the non-closure of the energy balance, one of [Huang et al. \(2008\)](#) and one of [Panin and Bernhofer \(2008\)](#). Firstly, the two approaches are presented (Sect. 2) and data from aircraft and ground-based tower measurements (Sect. 3) are used to determine the respective value of  $R$  and to test both parametrizations (Sect. 4). The observed energy balance closure is discussed in the light of landscape heterogeneities. Fundamental shortcomings of the existing parametrization approaches are highlighted and potential improvements suggested (Sect. 5). We debate whether the underlying hypothesis, i.e. the existence of mesoscale circulations, can be verified. In addition, a note on the partitioning of the missing energy between  $Q_H$  and  $Q_E$  is made, which is not included in either of the two parametrizations.

## 2 Approaches to Parametrize the Non-Closure of the Energy Balance

### 2.1 Parametrization of [Huang et al. \(2008\)](#)

[Huang et al. \(2008\)](#) used large-eddy simulation (LES) to develop a parametrization scheme, based on earlier LES studies of [Kanda et al. \(2004\)](#) and [Steinfeld et al. \(2007\)](#). They showed that the spatial average of the EC flux of any scalar  $\varphi$  that is based on the temporal covariance  $\overline{\langle w'\varphi' \rangle}$  (the ‘temporal’ EC method) is smaller than the temporarily-averaged spatial covariance  $\overline{\langle w''\varphi'' \rangle}$  (the ‘spatial’ EC method), where  $w$  represents the vertical wind component. Here, the single prime denotes deviations from the temporal mean, the double prime denotes deviations from the spatial mean, angular brackets represent spatial averages, and the overbar represents temporal averages. Under horizontally homogeneous conditions and a negligible spatially-averaged vertical velocity  $\langle w \rangle$ , the spatial EC flux can be regarded as the ‘true’ ensemble flux ([Kanda et al. 2004](#); [Steinfeld et al. 2007](#)), so that the mean imbalance  $\langle I \rangle$  of the temporal EC method can be defined as

$$\langle I \rangle = \frac{\overline{\langle w'\varphi' \rangle} - \overline{\langle w''\varphi'' \rangle}}{\overline{\langle w''\varphi'' \rangle}}. \quad (3)$$

In terms of conventional EC tower measurements, this definition is equivalent to the ratio  $\Delta/(-Q_S^* - Q_G)$ . The underestimation of the ‘true’ flux by the temporal EC method can be explained by the presence of turbulent organized structures, which are a fundamental property of the homogeneous convective ABL. They are characterized by narrow bands of relatively strong thermal updrafts that are surrounded by larger regions of weak subsidence. Under low wind conditions, the thermal updrafts are organized into spoke-like patterns, whereas with a significant background flow, streaky patterns appear near the surface, which merge into roll-like vortices at larger heights ([Schmidt and Schumann 1989](#); [Moeng and Sullivan 1994](#)). It is important to note that these coherent structures remain at the same place even after 1-h averaging ([Kanda et al. 2004](#)). Therefore, they produce low-frequency trends and mean vertical advection, which cannot be reliably captured by point measurements and the use of the temporal EC technique. Consequently, turbulent fluxes are systematically underestimated, resulting in a negative imbalance. [Kanda et al. \(2004\)](#); [Steinfeld et al. \(2007\)](#) and [Huang et al. \(2008\)](#) argued that this imbalance can explain the energy balance residual detected by the EC approach in field measurements.

Following [Huang et al. \(2008\)](#), the magnitude of the underestimation depends on friction velocity  $u_*$ , the Deardorff convective velocity  $w_*$ , and the ratio of measuring height  $z$

to the ABL height  $z_i$ ,

$$\langle I \rangle = -f_1 \left( \frac{u_*}{w_*} \right) f_2 \left( \frac{z}{z_i} \right). \tag{4}$$

The empirical functions  $f_1$  and  $f_2$  capture an exponentially decreasing dependence of  $\langle I \rangle$  on  $u_*/w_*$  and an elliptic relationship to  $z/z_i$  and are further explained in Eqs. 11a, b and Table 2 in Huang et al. (2008). With increasing  $u_*$  the absolute value of the imbalance should decrease (Aubinet et al. 2000; Wilson et al. 2002; Hendricks-Franssen et al. 2010), because the stronger mechanical turbulence increases the probability that large-scale structures are advected past the point measurement and can be captured by the temporal EC method (Kanda et al. 2004). Larger sensible heat fluxes, inducing larger values of  $w_*$ , are supposed to be accompanied by lower flux imbalances (Kanda et al. 2004; Steinfeld et al. 2007). Finally, the imbalance relates to the height within the ABL ( $z/z_i$ ) because turbulent organized structures are strongest in the middle of the ABL and the magnitude of imbalance might also be influenced by entrainment processes at the top of the ABL (Steinfeld et al. 2007; Huang et al. 2008).

### 2.2 Parametrization of Panin and Bernhofer (2008)

Besides the parametrization of Huang et al. (2008) an alternative approach was proposed by Panin and Bernhofer (2008). Whereas the former concentrates on the large-scale structure of turbulence in a homogeneously heated ABL, the latter explicitly focuses on the role of surface heterogeneities by advancing the concept of Panin et al. (1998). Moreover, Panin and Bernhofer (2008) only propose a parameter that describes the mean closure of a site, whereas the approach of Huang et al. (2008) is designed to parametrize the energy balance closure on a 30-min basis.

The presence of surface heterogeneities violates basic assumptions of the EC methodology, so that they can be regarded as a potential reason for the lack of energy balance closure. In heterogeneous landscapes, cospectra of surface fluxes show additional peaks in the low-frequency range, far beyond the typical averaging period of the temporal EC method (Finnigan et al. 2003). Consequently, flux contributions associated with these low-frequency motions are not captured. Therefore, the sum of sensible and latent heat fluxes determined by the EC method under the assumption of horizontal homogeneity  $(Q_H + Q_E)_{HH}$  has to be corrected by a factor  $k_f$ , which is independent of the magnitude of the fluxes, in order to retrieve the ‘true’ sum of the heat fluxes in inhomogeneous terrain  $(Q_H + Q_E)_{INH}$ ,

$$(Q_H + Q_E)_{HH} = k_f (Q_H + Q_E)_{INH}. \tag{5}$$

Here,  $(Q_H + Q_E)_{INH}$  is equivalent to the amount of available energy  $(-Q_S^* - Q_G)$ . Panin and Bernhofer (2008) showed that the magnitude of the correction factor  $k_f$  relates to the heterogeneity of the surrounding landscape. As a measure of non-homogeneity, they primarily focussed on surface roughness expressed by the roughness length  $z_0$ , and suggested a parameter  $z_0^{eff}/L^{eff}$ , where  $z_0^{eff}$  is the effective roughness length of the surrounding area of the measurement location and  $L^{eff}$  is the dominant horizontal scale of landscape inhomogeneities. Following Panin and Bernhofer (2008), there should be a linear dependence between  $k_f$  and  $z_0^{eff}/L^{eff}$ ,

$$k_f = K \frac{z_0^{eff}}{L^{eff}} + C, \tag{6}$$

with  $K$  and  $C$  being empirical constants.

The analysis is restricted to several km around the measuring point because only heterogeneities within that distance have a significant influence on the exchange process.

### 3 Data and Analysis

#### 3.1 Description of Aircraft Data and Tower Measurements

Parts of the dataset for this study were taken from flights of the Twin Otter aircraft of the Canadian National Research Council (NRC). An intercomparison study proved the reliability of the data with respect to spectra, standard deviation of horizontal and vertical wind and flux estimates (Dobosy et al. 1997). In the framework of the Boreal Ecosystem-Atmosphere Study (BOREAS) experiment (Sellers et al. 1997), 16 flights were conducted over the boreal forest at Candle Lake, Saskatchewan, Canada between May and September 1994. These “Candle Lake Runs” always followed the same flight route along an approximately 115 km long transect between 53.57°N, 106.40°W and 53.98°N, 104.29°W at a height of roughly 30 m a.g.l. (MacPherson 1996). The landscape is flat and can be characterized as a homogeneous boreal forest with numerous major or minor lakes distributed within; for details, see Mauder et al. (2007b). Measurements of the wind vector, temperature ( $T$ ) and water vapour mixing ratio ( $q$ ) were conducted on board of the Twin Otter aircraft, with a sampling rate of 16 Hz (MacPherson 1996). In April 2002, four additional flights took place on the same track in the framework of the Boreal Ecosystem Research and Monitoring Sites (BERMS) programme (Barr et al. 2002), when data were recorded at a sampling rate of 32 Hz.

In addition, tower-based measurements were also used to test both parametrizations. These measurements were conducted in the framework of the Terrestrial Environmental Observatories (TERENO) programme (Zacharias et al. 2011), which aims at observing the long-term impact of global change at a regional level. EC masts were mounted at three sites: Graswang (47.57°N, 11.03°E, 865 m a.s.l.), Rottenbuch (47.72°N, 10.97°E, 763 m a.s.l.) and Fendt (47.82°N, 11.06°E, 600 m a.s.l.). They are located in the Ammer catchment in southern Bavaria, Germany and are part of TERENO’s Bavarian Alps/pre-Alps Observatory (Figs. 1, 2). The landscape is a varied mosaic of villages, grassland, some arable land and coniferous and mixed forests. Furthermore, the sites are surrounded by hilly terrain and the southernmost site, Graswang, is already located in the “Ammergebirge” mountains. All three EC stations are located on grassland (Fig. 2b, d, f). The EC stations run continuously and here, data for the period 1 April 2012–30 September 2012 were used. The equipment used for this study is listed in Table 1, and further information on instrumentation and data storage can be found in Zacharias et al. (2011).

#### 3.2 Calculation of Turbulent Fluxes and the Energy Balance Residual

In order to derive estimates of  $Q_H$  and  $Q_E$  from the time series of the Twin Otter aircraft, wavelet analysis (Grossmann and Morlet 1984; Kronland-Martinet et al. 1987; Grossmann et al. 1989) was applied. As compared to the Fourier transform, the wavelet transform has the advantage that it is able to resolve the signal in frequency domain and time domain. Therefore, it especially allows spectral analysis of non-stationary data, e.g. if the dominant transport scales vary along the flight track. Details on the applied wavelet methodology can be found in Torrence and Compo (1998) and Mauder et al. (2007b). Here, only the fundamental steps are given.

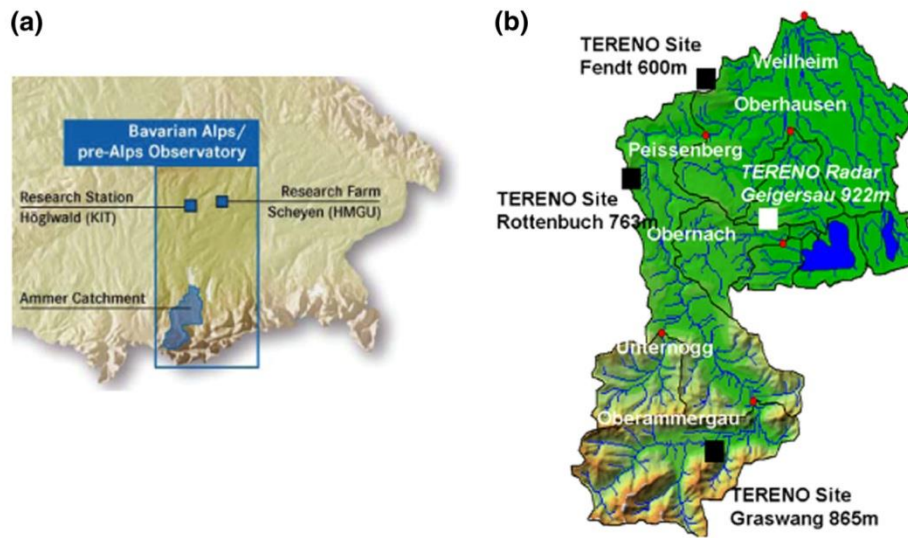


**Fig. 1** Overview of the of the Bavarian Alps/pre-Alps Observatory located in southern Germany (a) and overview of the Ammer catchment (b) with *black squares* showing the locations of the TERENO sites (Zacharias et al. 2011)

In analogy to Mauder et al. (2007b), the Morlet wavelet with frequency parameter  $\omega_0 = 6$  served as mother wavelet because of its better resolution in the frequency domain than other mother wavelets that are frequently used for analyzing atmospheric time series, such as the Haar wavelet or the Mexican Hat wavelet. Let  $T_x(a, b)$  and  $T_y(a, b)$  denote the wavelet coefficients of two time series  $x(n)$  and  $y(n)$ , where  $a$  is the scaling and  $b$  is the translation parameter. The integration over the product  $T_x(a, b)T_y^*(a, b)$  in time and frequency domain, where the asterisk represents the complex conjugate, gives an estimate of the covariance, i.e. an estimate of the turbulent flux. We considered only those wavelet coefficients outside of the cone of influence; accordingly, the cross-spectrum  $W_{xy}(a)$  is defined as

$$W_{xy}(a) = \frac{\delta j}{a} \frac{\delta t}{C_\delta} \frac{1}{N} \sum_{b=0}^{N-1} T_x(a, b) T_y^*(a, b) \quad (7)$$

and gives the spectral contributions to the turbulent flux  $\overline{x'y'}$  (Hudgins et al. 1993). The non-dimensional factor  $\delta j = 0.25$  determines the spacing between the scales  $a$  of the wavelet transform,  $\delta t$  denotes the timestep of the time series,  $C_\delta = 0.776$  is a constant for the Morlet wavelet and  $N$  is the length of the time series. The integration over the cross-spectrum in the frequency domain gives the total flux. When the integration is restricted to distinct scales, their respective contribution to the total turbulent flux can be quantified.

As suggested by Williams et al. (1996) and Strunin and Hiyama (2005), 2 km was chosen as the cut-off wavelength to separate small-scale from mesoscale motions. We claim that the scales larger than 2 km are not captured by typical EC masts, because they represent secondary circulations that do not move with the mean wind. Under the assumption that the neglect of mesoscale fluxes is the major reason for the lack of energy balance closure, their respective flux contributions could be regarded as an estimate of the corresponding value of  $\Delta$  (Eq. 1) and the ratio of small-scale contributions to total turbulent fluxes should be equivalent to  $R$  (Eq. 2). Accordingly, the negative mean energy imbalance  $-\langle I \rangle$  (Eq. 3) is the mesoscale

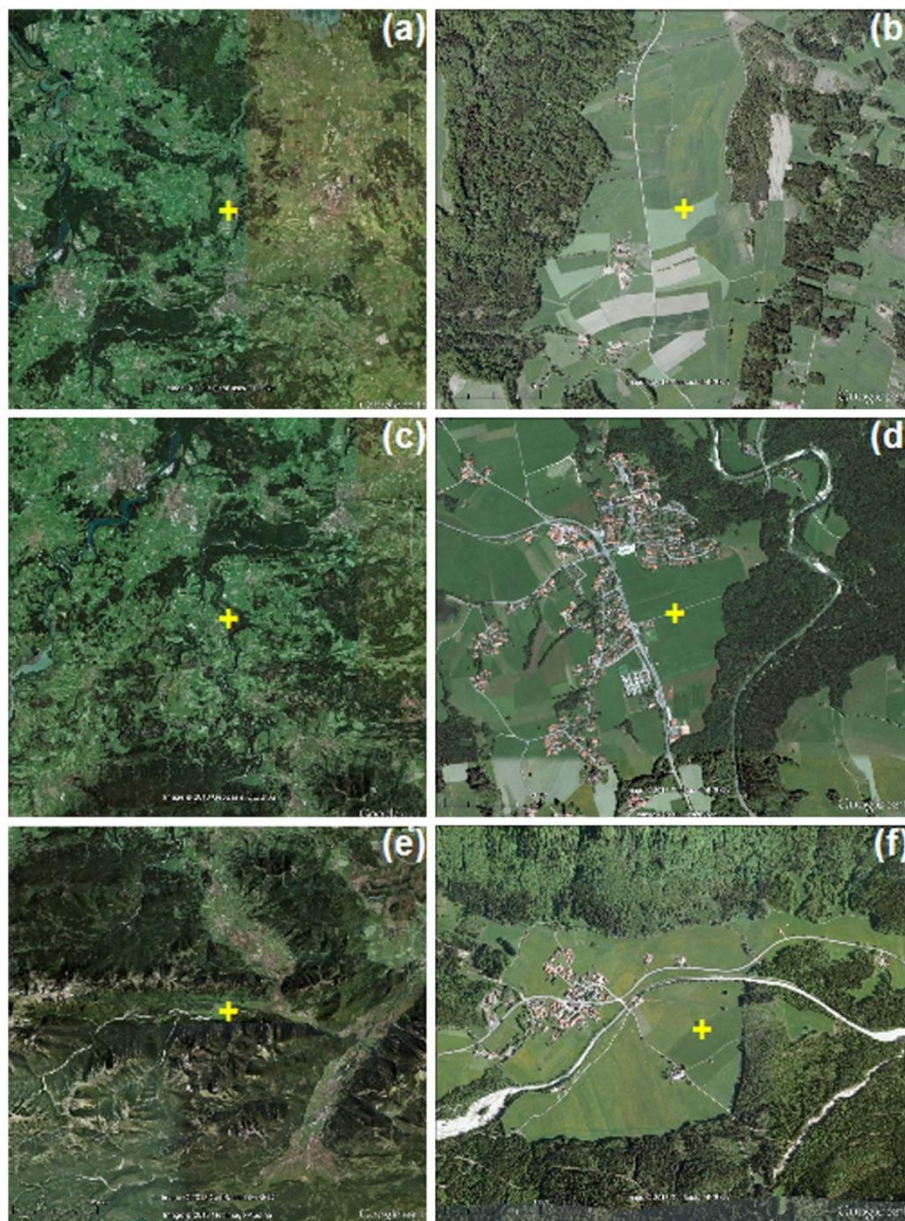


**Fig. 2** Satellite images (area roughly  $25 \text{ km} \times 25 \text{ km}$ , i.e. landscape scale, (a, c, e) and  $2 \text{ km} \times 2 \text{ km}$ , i.e. flux footprint scale (b, d, f), Google 2013) of Fendt (a, b), Rottenbuch (c, d) and Graswang (e, f), where *yellow crosses* indicate the approximate location of the EC masts

contribution divided by the total turbulent flux. Please note that this is a very crucial step, since this method might underestimate  $\Delta$  because other potential reasons for the lack of energy balance closure, such as instrumental problems or horizontal heterogeneity within the footprint of the measurement, are not considered. The method could also overestimate  $\Delta$  if

**Table 1** Part of the equipment of the TERENO stations (Zacharias et al. 2011) of the Bavarian Alps/pre-Alps Observatory used for this study

Variables	Device	Manufacturer
Wind vector, $T_s$	CSAT-3	Campbell Scientific Inc., Utah USA
$q$	LI-7500, LI-7200	LI-COR Biosciences, Nebraska USA
$Q_S^*$	CNR 4	Kipp & Zonen, The Netherlands
$Q_{G,HFP}$	HFP01SC (3x)	Hukseflux Thermal Sensors B.V., The Netherlands
Soil temperature	M-107 (18x)	Campbell Scientific Inc., Utah USA
Soil moisture	CS616-L (18x)	Campbell Scientific Inc., Utah USA
$z_i$	CL51	Vaisala Oyj., Finland

LI-7500: Graswang, Fendt; LI-7200: Rottenbuch

at least some parts of the scales >2 km completely pass by an EC tower within the averaging period of 30 min (Sect. 5.1).

Turbulent fluxes at the EC stations in Graswang, Rottenbuch and Fendt were derived by using the software package TK3.1 (Mauder, Foken 2011); for detailed information on post-processing of the high-frequency tower data, including quality assessment and quality control, see Mauder et al. (2013). The respective EC estimates of  $Q_H$  and  $Q_E$  were derived on a 30-min basis. A considerable amount of energy is stored in the soil layer between the soil heat flux plate at depth  $z_{HFP}$  and the soil surface (Onclay et al. 2007). This storage term was calculated using a calorimetric approach and added to the measured soil heat flux  $Q_{G,HFP}$  (Liebethal et al. 2005), so that the ground heat flux ( $Q_G$ ) is defined as

$$Q_G = Q_{G,HFP} + \int_{z_{HFP}}^0 c_{v,soil} \frac{\delta T}{\delta t} dz. \tag{8}$$

The amount of stored energy equals the vertically integrated temperature change  $\delta T/\delta t$  within the considered time interval multiplied by the volumetric heat capacity of the soil  $c_{v,soil}$ . For testing both parametrizations, only those EC data with the best quality flag of 0 according to the scheme described in Mauder et al. (2013) were used; these high-quality data are characterized as being suitable for fundamental research. For the Huang et al. (2008) parametrization, only daytime data with absolute values of global radiation  $>30 \text{ W m}^{-2}$  were considered. With respect to the approach of Panin and Bernhofer (2008),  $R$  was calculated on a daily basis.

### 3.3 Data Preparation for the Parametrization of Huang et al. (2008)

According to Huang et al. (2008), the energy balance residual is a function of  $u_*$ ,  $w_*$ ,  $z$  and  $z_i$  (Sect. 2). For the calculation of  $u_*$ , high-frequency data of the wind vector are needed,

$$u_* = \left( \overline{u'w'^2} + \overline{v'w'^2} \right)^{\frac{1}{4}}. \tag{9}$$

With respect to the Twin Otter aircraft data, the wind vector was determined from the vector difference between the air velocity relative to aircraft, measured by pressure transducers of a Rosemount 858AJ 5-hole probe, and the aircraft velocity relative to the ground (MacPherson 1996). For the EC tower data from the TERENO sites, the wind vector was measured with

a CSAT3 sonic anemometer (Table 1) and  $u_*$  was automatically calculated with the TK3.1 software.

For the calculation of the convective velocity scale  $w_*$  (Deardorff 1972), the surface sensible heat flux  $\overline{w'\theta'}$ , a reference potential temperature  $\theta$  of the convective ABL, and  $z_i$  are needed,

$$w_* = \left( \frac{g}{\theta} z_i \overline{w'\theta'} \right)^{\frac{1}{3}}, \quad (10)$$

where  $g$  represents the acceleration due to gravity. For the aircraft data,  $\overline{w'\theta'}$  was determined by integration of the cross-spectrum of  $w$  and  $T$  (Sect. 3.2). For  $\theta$ , the mean potential temperature along the flight track was used and, during BOREAS,  $z_i$  was determined every hour by a ground-based 915-MHz wind profiling radar system near the north-eastern edge of the flight track at 104.67°W and 53.91°N (Wilczak et al. 1997). For BERMS, no values of  $z_i$  are available, so that the test of the parametrization of Huang et al. (2008) is restricted to the BOREAS dataset. With respect to the TERENO stations, the surface sensible heat flux was calculated with the TK3.1 software and for  $\theta$ , the 30-min average of the sonic temperature was used. The ABL height was determined by continuously running CL51 ceilometers (Table 1) at all three TERENO sites, which measure profiles of optical backscatter intensities. The height of the mixed layer, which can be regarded as the ABL height during convective conditions, was determined with the software tool 'BL\_Matlab' that was run in Matlab2012a (version 7.14). It uses the algorithm of 'BL-VIEW' (Vaisala Oyj., Finland) that is based on the gradient method (Emeis et al. 2007, 2008). In the mixed layer, particle concentrations are considerably higher than in the free atmosphere, and accordingly,  $z_i$  is the height at which the first derivative of the measured backscatter intensity has a minimum.

### 3.4 Data Preparation for the Parametrization of Panin and Bernhofer (2008)

In order to test the parametrization of Panin and Bernhofer (2008), spatial distributions of  $z_0$  for the surrounding area are necessary, which can be derived from land-use maps. For the Candle Lake area, data from the Landsat Thematic Mapper image at a grid resolution of 30 m are available (Hall et al. 1997). For the TERENO sites, raster data on land use at a grid resolution of 100 m were obtained from the Coordination of Information on the Environment (CORINE) programme of the European Union. Here, raster data from version 16 of the CORINE Land Cover 2006 project (CLC2006) were used (URL: <http://www.eea.europa.eu/data-and-maps/data/corine-land-cover-2006-raster-2>). Afterwards, each land-use class was assigned a  $z_0$  value according to Table 2. The effective surface roughness  $z_0^{\text{eff}}$  was evaluated using

$$\log z_0^{\text{eff}} = \frac{1}{n} \sum_{i=1}^n \log z_{0,i} \quad (11)$$

where  $n$  is the number of pixels of the  $z_0$  raster map of the analyzed terrain. This approach was originally proposed by Taylor (1987) but there would be more sophisticated schemes developed using LES that also consider the effect of horizontal variability, such as the blending-height concept of Bou-Zeid et al. (2007). In addition, the  $z_0$  for water (Table 2) is quite high, especially at low and moderate wind speeds (Smith 1988), but we wish to test the parametrization of Panin and Bernhofer (2008) without serious modification.

**Table 2** Roughness length  $z_0$  for homogenous land-use patches (Wieringa 1993; Jong et al. 1999)

$z_0$ (m)	Land-use type
0.0002	Water
0.0003	Bare rocks
0.0005	Roads
0.0012	Sparse vegetation
0.003	Bare soil
0.019	Grassland, pasture
0.04	Bog, heath
0.08	Fen
0.11	Arable land
0.3	Woodland-shrub transition
0.8	Green urban areas
0.95	Villages, urban area
1.2	Forest (coniferous, deciduous, mixed)

Here,  $L^{\text{eff}}$  was determined from selected transects along the  $z_0$  map. For the Candle Lake area, both in the north–south direction and in the east–west direction, 10 transects of the  $z_0$  pixel map were randomly chosen. For the TERENO sites, the surrounding area was divided into eight wind sectors, and at the centre of each sector—at  $0^\circ, 45^\circ, \dots, 315^\circ$ —one transect of 15-km length and starting at the location of the EC mast was taken. For each transect, a Fourier spectrum was calculated. The dominant horizontal scale  $L$  of one transect is half the wavelength of the maximum of the Fourier spectrum. Generally, values of  $L$  were discarded if no clear maximum could be found for the transect, i.e. the Fourier coefficients increased with wavelength and the maximum of the spectrum appeared at the largest wavelength. Only for the Rottenbuch site, along two of the eight transects ( $135^\circ$  and  $180^\circ$ ), no maximum was found in the Fourier spectrum. The  $L^{\text{eff}}$  value of each area is the arithmetic mean of the  $L$  values of the respective transects. Panin and Bernhofer (2008) used only two transects, but it is assumed that the method applied here delivers a measure that is more representative of the surrounding area.

The CORINE raster data are projected in Lambert azimuthal equal-area projection centred at  $52^\circ\text{N}$  and  $10^\circ\text{E}$ . The projection is not length preserving and as the TERENO sites are located at a considerable distance from the projection centre (Table 1), this introduces an error into the estimation of horizontal length scales. However, in order to keep the regular grid, the original raster data were not re-projected. All calculations, if not stated otherwise, were made with the statistical software R, version 14.2.

## 4 Results

### 4.1 Energy Balance Closure for the Candle Lake Aircraft Flights and the TERENO EC Measurements

For the Twin Otter aircraft flights in the Candle Lake area, the values of  $R$  range from 0.73 to 0.99 and for 15 of the 20 flights during BOREAS and BERMS,  $R$  is between 0.86 and 0.91. The missing energy at all TERENO sites within the period from 1 July 2012 to 31 October 2012 (Table 3) is larger than for the Candle Lake area. Graswang ( $R = 0.75$ ) and Fendt

**Table 3** Observed values of  $R$  at the TERENO sites Graswang, Rottenbuch and Fendt in the period from July to October 2012; due to a malfunction of the LI-7200, no reliable data are available at the Rottenbuch site between 30 August and 12 October 2012

Period	Graswang	Rottenbuch	Fendt
July 2012	0.75	0.61	0.81
August 2012	0.75	0.60	0.74
September 2012	0.77	–	0.77
October 2012	0.74	0.54	0.75
July 2012–October 2012	0.75	0.60	0.77

**Table 4** Height of aircraft above the ground  $z$ , boundary-layer height  $z_i$ , friction velocity  $u_*$ , convective velocity scale  $w_*$ , and mesoscale flux contribution to the sum of the sensible and latent heat fluxes (interpreted as the negative mean energy imbalance along the flight track  $-(I)$ , Sects. 2.1 and 3.3) during the Twin Otter aircraft flights of the BOREAS experiment between May 1994 and September 1994 and the BERMS programme in April 2002

Date	Time (LT)	$z$ (m)	$z_i$ (m)	$u_*$ ( $\text{m s}^{-1}$ )	$w_*$ ( $\text{m s}^{-1}$ )	$-(I)$ (%)
25 May 1994	1041–1116	29.6	1,850	0.16	2.41	9.3
25 May 1994	1118–1152	30.0	2,000	0.14	3.05	12.5
25 May 1994	1154–1228	31.2	2,000	0.30	3.48	13.5
27 May 1994	1328–1403	42.5	1,500	0.84	2.07	1.1
1 Jun 1994	1259–1333	64.7	2,150	0.76	3.82	12.4
6 Jun 1994	1058–1130	34.7	700	0.71	0.71	14.1
6 Jun 1994	1133–1212	34.7	850	0.73	0.99	9.5
21 Jul 1994	1611–1647	36.1	1,700	0.65	1.49	11.7
23 Jul 1994	1056–1126	38.4	1,700	0.69	1.61	10.9
25 Jul 1994	1220–1252	38.8	1,500	0.42	2.04	11.3
25 Jul 1994	1631–1702	38.0	2,250	0.41	1.76	12.5
25 Jul 1994	1515–1547	37.5	2,200	0.38	2.57	19.8
27 Jul 1994	1106–1137	41.4	900	0.36	0.90	10.7
8 Sep 1994	1413–1444	35.5	700	0.38	0.70	6.1
12 Sep 1994	1140–1208	41.6	500	0.55	0.55	27.2
17 Sep 1994	1201–1232	33.7	1,200	0.45	1.04	11.9
20 Apr 2002	1237–1309	33.8	–	0.71	–	12.5
20 Apr 2002	1359–1435	43.6	–	0.69	–	8.7
21 Apr 2002	1234–1304	44.0	–	0.97	–	5.7
21 Apr 2002	1356–1432	43.5	–	0.88	–	9.6

( $R = 0.77$ ) sites are similar, whereas the Rottenbuch site exhibits an exceptionally poor energy balance closure ( $R = 0.60$ ). Thus, it is of interest whether the two parametrization approaches are able to explain these large differences.

#### 4.2 Parametrization of Huang et al. (2008)

Table 4 gives an overview of the data from the Twin Otter aircraft that are necessary for testing the parametrization of Huang et al. (2008). All flights were conducted at heights between 29 m and 65 m a.g.l. during fair weather conditions, i.e. the sky was either cloudless or less than 50% cloud cover. The friction velocities range between 0.14 and  $0.84 \text{ m s}^{-1}$ ; values of  $w_*$

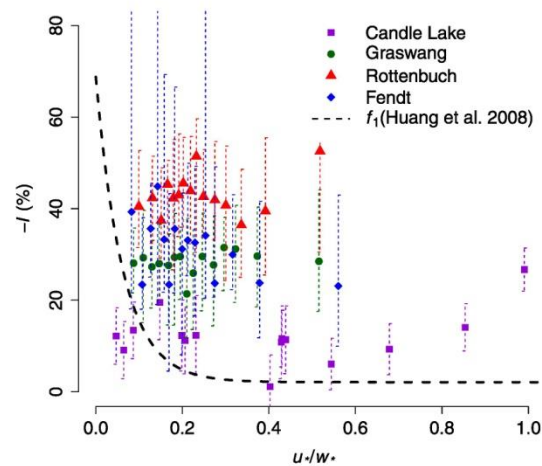


**Fig. 3** Observed energy imbalance  $-I$  for the 16 Candle lake runs during BOREAS and for the TERENO sites Graswang, Rottenbuch and Fendt as a function of the ratio of friction velocity to convection velocity  $u_*/w_*$ . Due to the large amount of data, the respective data from the TERENO sites were binned into 15 groups of equal size according to their value of  $u_*/w_*$ ; for each group, the median and the interquartile range is displayed; for the Candle Lake data, the *error bars* represent the random error of the airborne flux measurements (Lenschow and Stankov 1986). In addition, the suggested function  $f_1$  for  $Q_H$  by Huang et al. (2008) is indicated as a *dashed line*

are highly variable ( $0.55\text{--}3.82\text{ m s}^{-1}$ ), which could be attributed to the large differences in  $z_i$  ( $500\text{--}2,250\text{ m}$ ). Thus, during these convective conditions, buoyant plumes need  $\approx 10\text{--}20$  min for rising from the ground to the top of the ABL. The mesoscale flux contributions determined from the aircraft flights range between 1.1 and 27.2%.

With respect to the EC data from the TERENO sites, only daytime data were analyzed and values of  $u_*$ ,  $w_*$  and  $z_i$  were calculated on a 30-min basis (data not shown). At the Rottenbuch site the values of  $u_*$  (median:  $0.21\text{ m s}^{-1}$ ) and  $w_*$  (median:  $1.01\text{ m s}^{-1}$ ) are larger than at Graswang ( $u_*$ :  $0.20\text{ m s}^{-1}$ ,  $w_*$ :  $0.95\text{ m s}^{-1}$ ) and Fendt ( $u_*$ :  $0.17\text{ m s}^{-1}$ ,  $w_*$ :  $0.87\text{ m s}^{-1}$ ) sites. The mean ABL height is largest at Graswang (median of  $z_i$ :  $997\text{ m}$ ), which is located in the Alps, and smallest at the Fendt site (median of  $z_i$ :  $813\text{ m}$ ), which is located furthest away from the mountains.

Huang et al. (2008) derived the parametrization in the following way: for constant  $z/z_i$ , they attempted to find the function  $f_1$  that describes the dependence of  $-\langle I \rangle$  on  $u_*/w_*$ . Then, they determined  $f_2$  by finding a fit for  $-\langle I \rangle/f_1$  versus  $z/z_i$  for zero background wind, i.e. free convection conditions and constant  $u_*/w_*$ . Neglecting any interaction between both terms, the product of these two functions should be a reliable parametrization of  $-\langle I \rangle$ . Figure 3 shows the attempt to find the function  $f_1$  for the BOREAS aircraft data and for the EC data from the TERENO sites. The data do not follow the exponential relation suggested by Huang et al. (2008) and no correlation was found between  $-\langle I \rangle$  and  $u_*/w_*$ . This implies that  $u_*/w_*$  cannot explain the observed variability of  $-\langle I \rangle$ , but the suggested universal function of Huang et al. (2008) might serve as a lower bounds for the data. The function  $f_2$  also cannot be confirmed, simply because it does not make sense to calculate  $-\langle I \rangle/f_1$ , since  $f_1$  is already false. Furthermore, we could not find a significant correlation between  $-\langle I \rangle$  and  $z/z_i$ . It should be noted that close to the surface ( $z/z_i < 0.08$ ), the function  $f_2$  becomes imaginary and the parametrization becomes invalid. All in all, the parametrization did not work for our near-surface measurements.

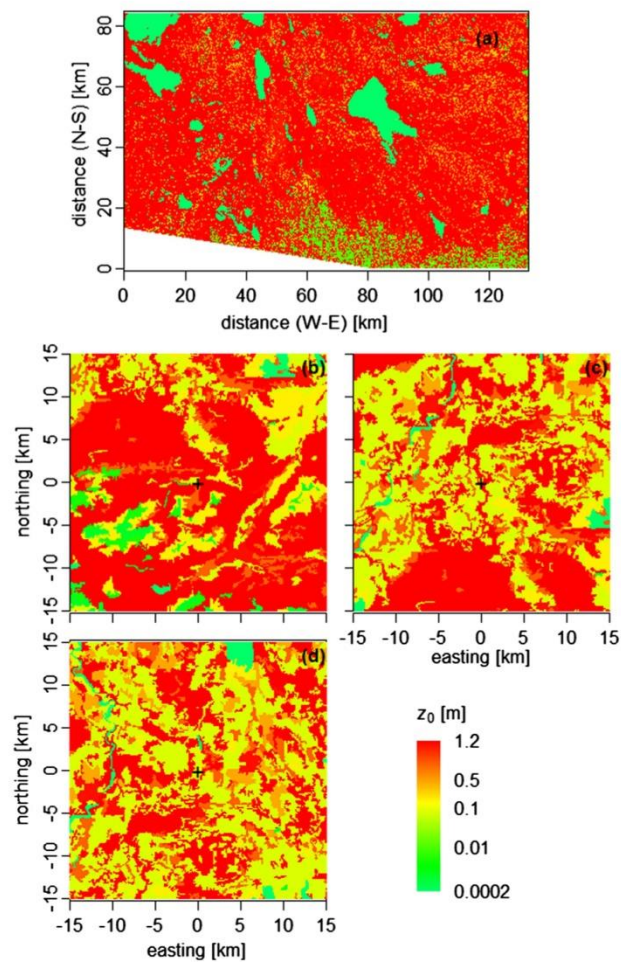


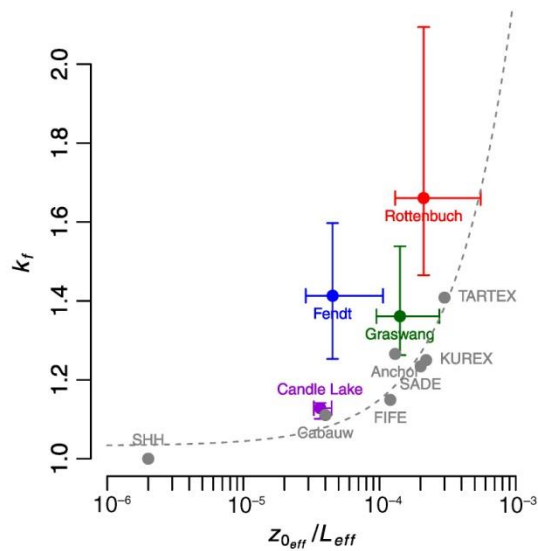
**Fig. 4** Surface roughness maps of the Candle Lake area (a) and the TERENO sites at Graswang (b), Rottenbuch (c) and Fendt (d); in (b)–(d), black crosses mark the approximate location of the EC masts; please note that the colour scale is logarithmic

#### 4.3 Parametrization of Panin and Bernhofer (2008)

The maps of the Candle Lake area and the TERENO sites that show the spatial distribution of the roughness length  $z_0$  are displayed in Fig. 4. Lakes and rocky areas are green, grassland and agricultural land is yellow and villages and forests are red. The values of the heterogeneity index  $z_0^{\text{eff}}/L^{\text{eff}}$  are  $3.66 \times 10^{-5}$  for the Candle Lake area,  $1.4 \times 10^{-4}$  for the Graswang,  $2.11 \times 10^{-4}$  for the Rottenbuch and  $4.52 \times 10^{-5}$  for the Fendt sites. Thus, according to Panin and Bernhofer (2008), the Candle Lake area represents the least heterogeneous landscape.

As shown in Fig. 5, only the data from Candle Lake and Graswang are in accordance with the results of Panin and Bernhofer (2008) and all sites lie above a linear fit ( $R^2 = 0.87$ ,  $p = 0.002$ ) through the data of Panin and Bernhofer (2008). Please note that in Fig. 5, the regression line does not appear as a straight line due to the logarithmic y-axis. The non-closure of the energy balance, especially at the TERENO stations Fendt and Graswang,

**Fig. 5** Energy balance correction factor  $k_f$  for the Candle Lake area and the EC masts at Graswang, Rottenbuch and Fendt versus heterogeneity index  $z_0^{\text{eff}}/L^{\text{eff}}$ ; median values and interquartile ranges are displayed; data shown in Panin and Bernhofer (2008) are indicated as grey dots and a fit through these data is displayed as a grey dotted line; please note that the abscissa is logarithmic



is poorer than this parametrization suggests. However, at least the order of the  $k_f$  values can roughly be explained by the heterogeneity index, e.g. the Rottenbuch site has the poorest closure of all sites and the largest value of  $z_0^{\text{eff}}/L^{\text{eff}}$ . To summarize, the parametrized imbalance using the approach of Panin and Bernhofer (2008) is lower than the measured imbalance, especially for the sites in the pre-alpine region.

## 5 Discussion

### 5.1 Short Note on the Aircraft-Based Estimate of the Energy Balance Closure

An aircraft is able to detect mesoscale structures that EC towers are not able to capture due to its motion in space (Mauder et al. 2007b). Consequently, we assumed that the energy balance residual measured with EC towers can be estimated with the aircraft by determining the flux contribution of eddies of scales  $>2$  km (Sect. 3.2). However, several conditions need to be fulfilled in order to apply this method.

First, the flight track should be sufficiently long in order to capture the complete longwave fraction of the flux, e.g. it should be  $>50z_i$  (Lothon et al. 2007). This condition is fulfilled, because the largest value of  $z_i$  during the BOREAS flights (Table 4) would require a track length of 112.5 km. The long flight track of 115 km also ensures that the random error of the flux measurement is below 10% (Lenschow and Stankov 1986). Moreover, the aircraft-based fluxes are a good estimate of the surface fluxes, because all flights were conducted within the surface layer whose height is approximately  $0.1z_i$  (Stull 1988). Finally, the selection of the cut-off wavelength is a crucial step, because it is assumed that atmospheric motions with wavelengths longer than the cut-off wavelength are not detected with an EC tower. Here, a scale of 2 km serves as a cut-off wavelength that was suggested by Williams et al. (1996) and Strunin and Hiyama (2005). Mauder et al. (2007b) also used this threshold and showed, for the Twin Otter aircraft flights, that the flux contribution from scales  $>2$  km is approximately equal to the missing energy measured at EC stations in the Candle Lake area.

Moreover, eddies of scale  $>2$  km usually exceed the ABL height, and there is a spectral gap in the wavelet cospectra at a wavelength of 2 km (Mauder et al. 2007b) that separates the small-scale region from the mesoscale region (Vickers and Mahrt 2003).

The mean yearly values of  $R$  in the Candle Lake area, based on long-term EC measurements, vary between 0.76 and 0.95 with a mean  $R$  of 0.85 for all sites and years (Barr et al. 2012), which is close to the estimated value of  $R$  from the Twin Otter runs (Sect. 4.1). Consequently, the chosen cut-off wavelength delivers reliable results and it is assumed that the energy balance closure of near-surface EC masts can be assessed with airborne flux measurements in the surface layer.

## 5.2 Energy Balance Closure at the TERENO Sites

This study is the first to present the energy balance closure at all three sites of the TERENO Bavarian Alps/pre-Alps Observatory. With respect to the Fendt and Graswang sites, Mauder et al. (2013) already reported estimates on systematic errors, which were based on monthly-averaged energy balance ratios of 0.81 and 0.72, respectively. Thus, the energy balance at the Fendt site is usually closer to balance than at the Graswang site, although the data used in this study only show a minor difference (Table 3). The observed non-closure is in accordance with similar studies conducted over short vegetation (Wilson et al. 2002; Hendricks-Franssen et al. 2010; Stoy et al. 2013). The  $R$  value from 32 grassland sites from the FLUXNET database is  $0.86 \pm 0.20$ , and for the crop sites, it is  $0.78 \pm 0.16$  (Stoy et al. 2013). Above agricultural land near Ottawa, Canada, a mean  $R$  of 0.77 was found (Mauder et al. 2010). During the LITFASS-2003 (Lindenberg Inhomogeneous Terrain – Fluxes between Atmosphere and Surface: a long term Study) experiment, a mean  $R$  of 0.75 was measured at a grassland site during daytime (Mauder et al. 2006; Foken et al. 2010). With respect to the patchiness of the land use, the last two experiments were conducted in landscapes that are similar to the TERENO area, but the topography around the TERENO sites is more complex. Nevertheless, the values of  $R$  are comparable, which suggests that surface heterogeneities due to fragmented land use might play a key role for the energy balance closure problem (Sect. 5.4).

Sites with a comparably poor non-closure such as at Rottenbuch ( $R = 0.60$ ) can rarely be found in the literature. We can exclude serious measurement errors because the measurement set-up as well as the post-processing is identical at the other two sites except for the enclosed-path gas analyzer used at Rottenbuch (Table 1). In the FLUXNET database, there are several sites with a comparable or even poorer non-closure: Stoy et al. (2013) report values of  $R$  down to 0.26, even after excluding severe outliers because of quality control concerns. In addition, Hendricks-Franssen et al. (2010) mention two EC stations above short vegetation with a comparably poor non-closure. The site of ‘East Saltoun’ is located east of Edinburgh, United Kingdom, approximately 10 km from the coastline, and has a mean  $R$  of 0.49. The site ‘Grignon’ lies west of Paris, France, within a densely populated area and has a mean  $R$  of 0.68. These two EC stations might be influenced by local circulations, due to sea-breeze effects or due to an urban heat-island circulation. The measurements at Rottenbuch might be influenced by similar circulations because of its proximity to a village and to the steep Ammer valley (Fig. 2d).

## 5.3 Parametrization of Huang et al. (2008)

No correlation was found between  $-\langle I \rangle$  and  $u_*$ ,  $w_*$  or  $z_i$ , which firstly could be attributed to problems in determining  $z_i$ , which also affects the values of  $w_*$  (Eq. 10). The  $z_i$  values at the Candle Lake site vary considerably (Table 4), which causes most of the variability in  $u_*/w_*$ .

At the TERENO sites, the mixed-layer height  $z_i$  was determined with ceilometers by detecting the sharp decrease of particle concentration at the top of the ABL (Emeis et al. 2008). This requires, (a) a significant particle source at the surface, and (b) good vertical mixing up to ABL top. Aerosol layers in the free atmosphere might cause unrealistically high estimates of  $z_i$ , whereas weak turbulent mixing results in an underestimation of  $z_i$ . Nevertheless, single daily cycles measured at the TERENO sites show the well-known pattern with increasing values of  $z_i$  during the morning hours and the highest values in the late afternoon. Thus, at least during daytime convective conditions, ceilometers produce reliable results.

Furthermore, Huang et al. (2008) derived the functions  $f_1$  and  $f_2$  in a different way than used here. They first derived  $f_1$  by restricting their LES analysis to the heights between 0.3 and  $0.5z/z_i$ , where they found the maximum imbalance in the model, and afterwards, they determined  $f_2$  for zero background wind. In contrast, the measurements at Candle Lake and at the TERENO sites were conducted in the surface layer, as with most experiments focusing on air-land interactions. Furthermore, all daytime data with sufficient data quality (Sect. 3.2) were used, including wind speeds up to  $10 \text{ m s}^{-1}$ .

In addition, it should be mentioned that this parametrization is based on LES above homogeneous terrain. However, according to Inagaki et al. (2006) and Steinfeld et al. (2007), turbulent organized structures are not the only transport mechanism that the temporal EC method is not able to capture. Thermally-driven mesoscale circulations also play a significant role, especially in the lower half of the ABL above heterogeneous terrain (Strunin and Hiyama 2005). Maronga and Raasch (2013) confirm the formation of secondary circulations due to surface differences in the upstream area. According to Hiyama et al. (2007), low values of  $u_*/w_*$  serve as a good indicator for the presence of such heterogeneity-induced local circulations, but we could not confirm that (Fig. 3).

The usual dimensionless scaling parameter for universal functions in the surface layer is  $z/L$ , with  $L$  being the Obukhov length (Stull 1988), which differs mainly from  $u_*/w_*$  (Eqs. 8, 9) by the height scaling. For  $z/L$ , the measurement height is an important parameter, but the term  $u_*/w_*$  is height-invariant due to the use of  $z_i$  instead of  $z$ . Attempts to explain the observed energy imbalance by  $z/L$  have shown that  $R$  is lowest for very unstable conditions (Stoy et al. 2013). We did not find a comparable dependence on  $u_*/w_*$  (Fig. 3), so that the use of  $w_*$  for parametrizing the energy imbalance in the surface layer does not appear to be a promising approach.

Finally, a shortcoming of the configuration of current LES models should be mentioned. If the boundary conditions at the ground surface are prescribed by the heat fluxes and the model correctly captures the physics, the energy balance near the surface has to be closed. In LES models, the strength of turbulent organized structures, as well as the simulated energy imbalance, are negligible within the entire surface layer ( $z/z_i < 0.1$ , Kanda et al. 2004; Inagaki et al. 2006; Steinfeld et al. 2007; Huang et al. 2008; Maronga and Raasch 2013). The latter contradicts almost all EC tower measurements so that we conclude that either (a) mesoscale motions are not the major reason of the unclosed energy balance of near-surface measurements, or (b) that the grid resolution of LES models is too coarse near the surface. The simulations of Huang et al. (2008) were obviously not able to resolve all turbulent motions due to the limited grid resolution, so that the major part of the turbulent energy had to be parametrized. Furthermore, many subgrid parametrization schemes work better away from wall regions, and Monin-Obukhov similarity theory, which was used for the first grid layer of the LES grid, is based on horizontal homogeneity. In other words, heterogeneity-induced secondary circulations might also have a high impact on transport processes near the surface and might even make contact with the ground (Foken 2008), but this can neither be justified nor falsified with current LES models.

#### 5.4 Parametrization of Panin and Bernhofer (2008)

In contrast to the functions suggested by Huang et al. (2008), which consider boundary-layer dynamics, the empirical approach of Panin and Bernhofer (2008) focuses on the role of roughness heterogeneities for the non-closure of near-surface EC measurements. Following a similar hypothesis, Stoy et al. (2013) recently demonstrated for 180 FLUXNET sites across the world that the energy imbalance can be related to the variability of the vegetation within an area of 20 km by 20 km surrounding the measurement site.

The parametrization of Panin and Bernhofer (2008) does not explain the entire missing energy (Fig. 5). This finding suggests that heterogeneity-induced mesoscale motions are not the only reason for the unclosed energy balance, and other effects that are not included in the parametrization, such as instrumental issues, also play a role. Moreover, there might be factors other than  $z_0^{\text{eff}}/L^{\text{eff}}$ , such as topography, differences in surface temperature or surface moisture, that induce mesoscale circulations, see below.

For the Candle Lake area, the observed imbalance is quite close to that derived from the data used by Panin and Bernhofer (2008), but for the TERENO sites, especially for Rottenbuch and Fendt, the imbalance is larger than expected (Fig. 5). One reason for the poor closure at the TERENO sites might be the use of non-orthogonal sonic anemometers that are suspected to underestimate sensible heat fluxes (Kochendorfer et al. 2012; Frank et al. 2013). However, this problem is still under debate (Mauder 2013) and it also cannot explain the different magnitudes of underestimation at the different sites. Probably the observed deviations from the data of Panin and Bernhofer (2008) can be better explained by the fact that not all surface heterogeneities are represented in a  $z_0$  map. It should be noted that the experiments on which they developed their parametrization were mainly conducted over flat terrain and in remote areas. So, surface heterogeneities are mainly caused by differences in vegetation and, therefore, calculating  $L^{\text{eff}}$  based on a  $z_0$  map is sufficient to determine the heterogeneity of the landscape. The topography of the Candle Lake area is also flat and the lake-forest boundaries, which are clearly visible in the  $z_0$  maps (Fig. 4a), are the dominant heterogeneities. The data from Graswang are also close to the data from Panin and Bernhofer (2008), although the topography is very complex. However, the mountains can be recognised in the  $z_0$  map, because the mountain slopes are usually covered with forest and mountain tops are rocky areas. Thus, at Graswang,  $L^{\text{eff}}$  determined on the basis of  $z_0$  is a good estimate for the dominant horizontal scale. Regarding the  $z_0$  maps of the Rottenbuch and Fendt sites (Fig. 4c, d), not all surface heterogeneities are clearly visible. Forests and villages, for example, have a similar roughness length, but usually a different surface temperature. However, a re-analysis of the data with an unrealistic high surface roughness for villages ( $z_0 = 30$  m) did not improve the results (data not shown).

If we plot the values of  $R$  from the Fendt (Fig. 6a) and Rottenbuch (Fig. 6b) sites for different wind directions ( $\varphi$ ) it can be seen that the surrounding landscape affects the EC measurements. For southerly winds ( $157.5^\circ < \varphi < 247.5^\circ$  for Fendt,  $112.5^\circ < \varphi < 202.5^\circ$  for Rottenbuch), the energy balance closure is significantly lower than for all other directions (one-sided Wilcoxon rank sum test,  $p < 0.05$ ). Due to the foehn effect of the Alpine mountains, warm and dry air is brought from southern directions, but the EC method does not account for horizontal advection. The secondary minimum at the Fendt site for the northern wind sector ( $-22.5^\circ < \varphi < 22.5^\circ$ ) might be caused by the advection of moist air, because there is a small lake surrounded by swampy terrain approximately 3 km north of the site (visible in Fig. 4d as a small bluish spot). As explained Sect. 5.2, small-scale

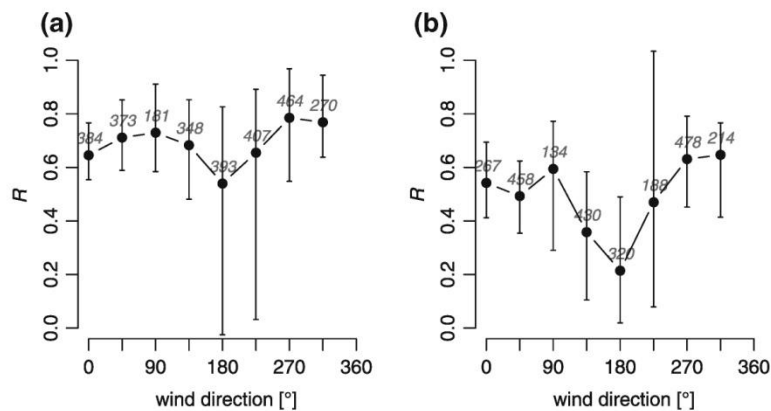


**Fig. 6** 30-min  $R$  values for different wind directions at Fendt (a) and Rottenbuch (b) sites; the data were grouped into wind sectors of  $45^\circ$  size and the respective sample sizes are indicated as *grey italic numbers*. The *black dots* indicate the sample median and the *error bars* represent the interquartile range

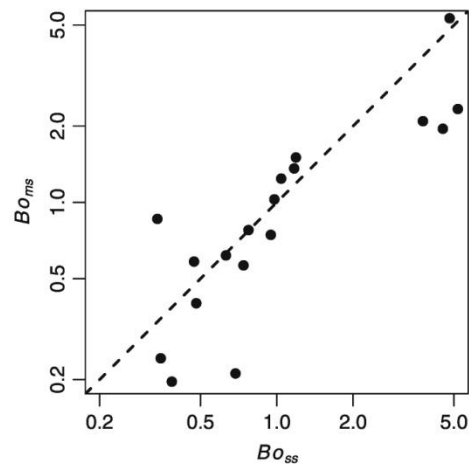
effects might also play a role at the Rottenbuch site that exhibits an extraordinarily poor closure.

Besides our main criticism that Panin and Bernhofer (2008) only consider roughness heterogeneities, we also argue that the suggested heterogeneity index  $z_0^{\text{eff}}/L^{\text{eff}}$  is not well chosen. There is no evidence that the magnitude of  $z_0^{\text{eff}}$  has any influence on the energy balance closure because large imbalances were found above various land-use types (Hendricks-Franssen et al. 2010; Stoy et al. 2013). For constant  $z_0^{\text{eff}}$ , the heterogeneity index increases with decreasing  $L^{\text{eff}}$ . Thus, the shorter  $L^{\text{eff}}$ , the larger should be the energy balance residual. However, this contradicts theoretical considerations (Dalu et al. 1996), scaling approaches (Mahrt 2000) and LES results (Raasch and Harbusch 2001; Patton et al. 2005) on heterogeneity-induced mesoscale transport, which found that there is an optimal surface length scale with respect to the strength of mesoscale motions. Particularly, the heterogeneities should be at least as large as  $z_i$ , so that there should be a minimum threshold for  $L^{\text{eff}}$ , below which no considerable imbalance occurs. However, the estimated  $L^{\text{eff}}$  of the TERENO sites and the Candle Lake area are larger than the corresponding values of  $z_i$ , so that we could not identify a decrease of the imbalance for small horizontal length scales.

Finally, a short methodological note should be made: when calculating the Fourier spectrum along a transect on a  $z_0$  map, multiple local maxima can occur in the spectrum, implying that the landscape is not dominated by one single heterogeneity scale, but is a superposition of multiple scales. Here, we followed Panin and Bernhofer (2008) and only considered the global maximum, although we might have neglected additional heterogeneity scales that also have an impact on the exchange process.

All in all, the parametrization approach of Panin and Bernhofer (2008) appears to work only if  $L^{\text{eff}}$  captures, through  $z_0$ , the dominant landscape-scale heterogeneities. In our study, this is only the case for the Candle Lake area and, to a minor extent, for the Graswang site. Consequently, future parametrizations should not neglect the influences of surface temperature, surface moisture and complex topography, which might also be responsible for the generation of secondary circulations. A thorough assessment of the importance of all surface heterogeneities for the energy balance closure problem is beyond the scope of the present paper.

**Fig. 7** Bowen ratio of the small-scale turbulence range ( $Bo_{ss}$ , eddy scale  $<2$  km), that is supposed to be measurable by standard EC techniques, versus the respective Bowen ratio of the mesoscale range ( $Bo_{ms}$ , eddy scale  $>2$  km) from the Twin Otter aircraft flights during BOREAS and BERMS. For comparison, the *dashed line* indicates the assumption of scalar similarity for closing the energy balance



### 5.5 Partitioning of the Missing Energy Between $Q_H$ and $Q_E$

A parametrization suitable for correcting the measured turbulent heat fluxes also has to consider the partitioning of the missing energy between  $Q_H$  and  $Q_E$ . Foken et al. (2012) recommend correcting both energy fluxes using the measured Bowen ratio. This implies the assumption of scalar similarity, which is justified for the high-frequency range of turbulence (Pearson et al. 1998), but cannot be taken for granted at longer wavelengths (Ruppert et al. 2006). Therefore, the Bowen ratios of the small-scale ( $Bo_{ss}$ ) and the mesoscale range ( $Bo_{ms}$ ) were determined from the flux contributions of the Twin Otter aircraft flights (Fig. 7). In accordance with Lamaud and Irvine (2006), the mean Bowen ratio itself influences the partitioning of  $T$  and  $q$  in the mesoscale range. For  $Bo_{ss} \approx 1$ , the assumption of scalar similarity could be confirmed, but if  $Bo_{ss}$  largely differs from unity,  $Bo_{ms}$  is mostly smaller than the respective  $Bo_{ss}$ . This implies that assigning the missing energy to  $Q_H$  and  $Q_E$  according to the measured Bowen ratio would result in an underestimation in  $Q_E$ .

This finding is in accordance with Barr et al. (2006), who found a larger flux deficit for  $Q_E$  in the Candle Lake area. This can be explained by the fact that the dominating surface heterogeneities are the lakes that are distributed within the boreal forest. These lakes can be regarded as small, wet patches within a relatively homogeneous ‘matrix’ and, following Moene and Schüttemeyer (2008), these wet patches of mesoscale size mainly affect the mesoscale fluxes of  $Q_E$ . Consequently, the finding that  $Q_E$  is more sensitive to an underestimation seems to be a site-specific effect and cannot be transferred to other areas. Studies above forests or agricultural sites, where differences in surface temperature are larger, found that the residual should be mainly added to  $Q_H$  (Stoy et al. 2006; Ingwersen et al. 2011). In summary, we hypothesize that the partitioning of the missing energy between  $Q_H$  and  $Q_E$  depends on the surface properties of the surrounding landscape: if surface moisture differences are more important than surface temperature differences, the EC method underestimates  $Q_E$  to a greater extent than  $Q_H$ .

## 6 Conclusions

We investigated the energy balance closure of tower-based measurements from the Bavarian Alps/pre-Alps observatory of the German TERENO network. In addition, we also estimated

the closure from aircraft data obtained in Canada: the flux contribution of atmospheric motions with wavelengths longer than 2 km served as an estimate of the missing energy of near-surface tower measurements. The energy balance ratios of the aircraft flights (0.86–0.91) are larger than at the TERENO sites (0.60–0.77). The main focus was on testing two energy balance closure parametrization schemes of Huang et al. (2008) and of Panin and Bernhofer (2008). However, both approaches are not able to predict the closure, but the latter leads at least to qualitatively correct results.

The approach of Huang et al. (2008) was not suitable for our measurements in the surface layer and the proposed dependencies of the imbalance on  $u_*/w_*$  and  $z/z_i$  could not be confirmed. The main problem of this approach is that it is only based on LES studies, which have insufficient grid resolution near the surface, so that the relevant transport processes are not resolved. Additionally, this parametrization only considers the homogeneous ABL and neglects the influence of an underlying heterogeneous surface. This is the main asset of the approach of Panin and Bernhofer (2008), which focuses on surface roughness heterogeneities. The non-closure at the Candle Lake site is in good agreement with the data analyzed by Panin and Bernhofer (2008), but the observed non-closure at the TERENO sites in the pre-alpine region is worse than expected using this approach. This might be due to neglecting additional surface heterogeneities, e.g. complex topography or differences in surface temperature and moisture. We are not able to state which type of surface heterogeneity is the most important for parametrizing the energy balance closure, but our wind-direction dependent analysis indicates that there is indeed an influence of the upwind surface characteristics on the landscape scale. Particularly, the advection of warm air through foehn winds from the south strongly contributes to the non-closure of the energy balance.

In addition, we have analyzed the aircraft data from the Candle Lake area with regard to the partitioning of the mesoscale flux between  $Q_H$  and  $Q_E$ . For Bowen ratios around unity, we could confirm the recommendation of Foken et al. (2012) to correct the fluxes with the Bowen ratio. But for Bowen ratios different from unity, the mesoscale structures mostly transport more latent heat than sensible heat.

Therefore, we suggest that an analysis of tower and aircraft data for the same area might give more insights into the role of large-scale structures on point measurements. With respect to the tower measurements, special attention should be addressed to longer wavelengths, i.e. time scales  $>30$  min. Such investigations should go in hand with LES models that have a fine grid resolution close to the surface. Future parametrization approaches should probably also include the effects of topography and surface temperature besides surface roughness. Appropriate parameters for characterizing the relevant meteorological conditions that control the energy balance closure remain to be found.

**Acknowledgments** The authors would like to thank Baltasar Trancón y Widemann for providing the wavelet routine. Some aspects of this manuscript are part of the master's thesis of Katrin Kohnert at the University of Bayreuth, which was supervised by Thomas Foken. Funding for TERENO & TERENO-ICOS was provided by BMBF. The support by the land owners of the TERENO sites and technical staff of KIT/IMK-IFU is appreciated. This work was conducted within the Helmholtz Young Investigator Group "Capturing all relevant scales of biosphere-atmosphere exchange—the enigmatic energy balance closure problem", which is funded by the Helmholtz-Association through the President's Initiative and Networking Fund, and by KIT.

## References

Aubinet M, Grelle A, Ibrom A, Rannik Ü, Moncrieff J, Foken T, Kowalski AS, Martin PH, Berbigier P, Bernhofer C, Clement R, Elbers J, Granier A, Grünwald T, Morgenstern K, Pilegaard K, Rebmann C,

- Snijders W, Valentini R, Vesala T (2000) Estimates of the annual net carbon and water exchange of forests: the EUROFLUX methodology. *Adv Ecol Res* 30:113–175
- Aubinet M, Heinesch B, Yernaux M (2003) Horizontal and vertical CO<sub>2</sub> advection in a sloping forest. *Boundary-Layer Meteorol* 108:397–417
- Baidya Roy S, Weaver CP, Nolan DS, Avissar R (2003) A preferred scale for landscape forced mesoscale circulations? *J Geophys Res* 108:8854
- Barr AG, Griffis TJ, Black TA, Lee X, Staebler RM, Fuentes JD, Chen Z, Morgenstern K (2002) Comparing the carbon budgets of boreal and temperate deciduous forest stands. *Can J For Res* 32:813–822
- Barr AG, Morgenstern K, Black TA, McCaughey JH, Nesic Z (2006) Surface energy balance closure by the eddy-covariance method above three boreal forest stands and implications for the measurement of the CO<sub>2</sub> flux. *Agric For Meteorol* 140:322–337
- Barr AG, van der Kamp G, Black TA, McCaughey JH, Nesic Z (2012) Energy balance closure at the BERMS flux towers in relation to the water balance of the White Gull Creek watershed 1999–2009. *Agric For Meteorol* 153:3–13
- Betts AK, Desjardins RL, MacPherson JI (1992) Budget analysis of the boundary layer grid flights during FIFE 1987. *J Geophys Res* 97:18533–18546
- Bou-Zeid E, Parlange MB, Meneveau C (2007) On the parameterization of surface roughness at regional scales. *J Atmos Sci* 64:216–227
- Dalu GA, Pielke RA, Baldi M, Zeng X (1996) Heat and momentum fluxes induced by thermal inhomogeneities with and without large-scale flow. *J Atmos Sci* 53:3286–3302
- De Jong JJ, De Vries AC, Klaasen W (1999) Influence of obstacles on the aerodynamic roughness of the Netherlands. *Boundary-Layer Meteorol* 91:51–64
- Deardorff JW (1972) Numerical investigation of neutral and unstable planetary boundary layers. *J Atmos Sci* 29:91–115
- Desjardins RL (1985) Carbon dioxide budget of maize. *Agric For Meteorol* 36:29–41
- Desjardins RL, Schuepp PH, MacPherson JI, Buckley DJ (1992) Spatial and temporal variations of the fluxes of carbon dioxide and sensible and latent heat over the FIFE site. *J Geophys Res* 97:18467–18475
- Dobosy RJ, Crawford TL, MacPherson JI, Desjardins RL, Kelly RD, Oncley SP, Lenschow DH (1997) Inter-comparison among four flux aircraft at BOREAS in 1994. *J Geophys Res* 102:29101–29111
- Emeis S, Jahn C, Münkel C, Münsterer C, Schäfer K (2007) Multiple atmospheric layering and mixing-layer height in the Inn valley observed by remote sensing. *Meteorol Z* 16:415–424
- Emeis S, Schäfer K, Münkel C (2008) Surface-based remote sensing of the mixing-layer height—a review. *Meteorol Z* 17:621–630
- Finnigan JJ, Clement R, Malhi Y, Leuning R, Cleugh HA (2003) A re-evaluation of long-term flux measurement techniques, Part I: averaging and coordinate rotation. *Boundary-Layer Meteorol* 107:1–48
- Foken T (2008) The energy balance closure problem: an overview. *Ecol Appl* 18:1351–1367
- Foken T, Mauder M, Liebethal C, Wimmer F, Beyrich F, Leps JP, Raasch S, DeBruin H, Meijninger W, Bange J (2010) Energy balance closure for the LITFASS-2003 experiment. *Theor Appl Climatol* 101:149–160
- Foken T, Leuning R, Oncley SR, Mauder M, Aubinet M (2012) Corrections and data quality control. In: Aubinet M, Vesala T, Papale D (eds) *Eddy covariance: a practical guide to measurement and data analysis*. Springer, Dordrecht, pp 85–131
- Frank JM, Massman WJ, Ewers BE (2013) Underestimates of sensible heat flux due to vertical velocity measurement errors in non-orthogonal sonic anemometers. *Agric For Meteorol* 171–172:72–81
- Grossmann A, Morlet J (1984) Decomposition of hardy functions into square integrable wavelets of constant shape. *SIAM J Math Anal* 15:723–736
- Grossmann A, Kronland-Martinet R, Morlet J (1989) Reading and understanding continuous wavelet transforms. In: Combes JM, Grossmann A, Tchamitchian P (eds) *Wavelets: time-frequency methods and phase space*. Springer, New York, pp 2–20
- Hall FG, Knapp DE, Huemmrich KF (1997) Physically based classification and satellite mapping of biophysical characteristics in the southern boreal forest. *J Geophys Res* 102:29567–29580
- Hendricks-Franssen HJ, Stöckli R, Lehner I, Rotenberg E, Seneviratne SI (2010) Energy balance closure of eddy-covariance data: a multisite analysis for European FLUXNET stations. *Agric For Meteorol* 150:1553–1567
- Heusinkveld BG, Jacobs AFG, Holtslag AAM, Berkowicz SM (2004) Surface energy balance closure in an arid region: role of soil heat flux. *Agric For Meteorol* 122:21–37
- Hiyama T, Strunin MA, Tanaka H, Ohta T (2007) The development of local circulations around the Lena River and their effect on tower-observed energy imbalance. *Hydrol Proc* 21:2038–2048
- Huang J, Lee X, Patton E (2008) A modelling study of flux imbalance and the influence of entrainment in the convective boundary layer. *Boundary-Layer Meteorol* 127:273–292

- Hudgins LE, Mayer ME, Friehe CA (1993) Fourier and wavelet analysis of atmospheric turbulence. In: Meyers E, Roques S (eds) *Progress in wavelet analysis and applications*. Editions Frontiers, Gif-sur-Yvette, pp 491–498
- Inagaki A, Letzel MO, Raasch S, Kanda M (2006) Impact of surface heterogeneity on energy imbalance: a study using LES. *J Meteorol Soc Jpn* 84:187–198
- Ingwersen J, Steffens K, Högy P, Warrach-Sagi K, Zhunusbayeva D, Poltoradnev M, Gäbler R, Wizemann HD, Fangmeier A, Wulfmeyer V, Streck T (2011) Comparison of Noah simulations with eddy covariance and soil water measurements at a winter wheat stand. *Agric For Meteorol* 151:345–355
- Kanda M, Inagaki A, Letzel MO, Raasch S, Watanabe T (2004) LES Study of the energy imbalance problem with eddy covariance fluxes. *Boundary-Layer Meteorol* 110:381–404
- Kochendorfer J, Meyers TP, Frank J, Massman WJ, Heuer MW (2012) How well can we measure the vertical wind speed? Implications for fluxes of energy and mass. *Boundary-Layer Meteorol* 145:383–398
- Kronland-Martinet R, Morlet J, Grossmann A (1987) Analysis of sound patterns through wavelet transforms. *Int J Pattern Recogn* 1:273–302
- Lamaud E, Irvine M (2006) Temperature-humidity dissimilarity and heat-to-water-vapour transport efficiency above and within a pine forest canopy: the role of the Bowen ratio. *Boundary-Layer Meteorol* 120:87–109
- Lee X, Black TA (1993) Atmospheric turbulence within and above a douglas-fir stand. Part II: eddy fluxes of sensible heat and water vapour. *Boundary-Layer Meteorol* 64:369–389
- Lenschow DH, Stankov BB (1986) Length scales in the convective boundary layer. *J Atmos Sci* 43:1198–1209
- Leuning R, van Gorsel E, Massman WJ, Isaac PR (2012) Reflections on the surface energy imbalance problem. *Agric For Meteorol* 156:65–74
- Liebethal C, Huwe B, Foken T (2005) Sensivity analysis for two ground heat flux calculation approaches. *Agric For Meteorol* 132:253–262
- Lothon M, Couvreux F, Donier S, Guichard F, Lacarrère P, Lenschow D, Noilhan J, Saïd F (2007) Impact of coherent eddies on airborne measurements of vertical turbulent fluxes. *Boundary-Layer Meteorol* 124:425–447
- MacPherson JI (1996) NRC Twin Otter operations in BOREAS, (1994) Rep LTR-FR-129. Natl Res Counc Can. Inst for Aerosp Res, Ottawa, 32 pp
- Mahrt L (1998) Flux sampling errors for aircraft and towers. *J Atmos Oceanic Technol* 15:416–429
- Mahrt L (2000) Surface heterogeneity and vertical structure of the boundary layer. *Boundary-Layer Meteorol* 96:33–62
- Maronga B, Raasch S (2013) Large-eddy simulations of surface heterogeneity effects on the convective boundary layer during the LITFASS-2003 experiment. *Boundary-Layer Meteorol* 146:17–44
- Mauder M (2013) A comment on “How well can we measure the vertical wind speed? Implications for fluxes of energy and mass”, by Kochendorfer, et al. *Boundary-Layer Meteorol* 47:329–335
- Mauder M, Foken T (2011) Documentation and instruction manual of the Eddy-Covariance software package TK3. *Arbeitsergebnisse/Universität Bayreuth, Abteilung Mikrometeorologie* - 46. ISSN:1614–8916, 60 pp
- Mauder M, Liebethal C, Goeckede M, Leps JP, Beyrich F, Foken T (2006) Processing and quality control of flux data during LITFASS-2003. *Boundary-Layer Meteorol* 121:67–88
- Mauder M, Jegede OO, Okogbue EC, Wimmer F, Foken T (2007a) Surface energy balance measurements at a tropical site in West Africa during the transition from dry to wet season. *Theor Appl Climatol* 89:171–183
- Mauder M, Desjardins RL, MacPherson I (2007b) Scale analysis of airborne flux measurements over heterogeneous terrain in a boreal ecosystem. *J Geophys Res* 112:D13112
- Mauder M, Oncley S, Vogt R, Weidinger T, Ribeiro L, Bernhofer C, Foken T, Kohsiek W, DeBruin H, Liu H (2007c) The energy balance experiment EBEX-2000. Part II: intercomparison of eddy-covariance sensors and post-field data processing methods. *Boundary-Layer Meteorol* 123:29–54
- Mauder M, Desjardins RL, Pattey E, Worth D (2010) An attempt to close the daytime surface energy balance using spatially-averaged flux measurements. *Boundary-Layer Meteorol* 136:175–191
- Mauder M, Cuntz M, Drüe C, Graf A, Rebmann C, Schmid HP, Schmidt M, Steinbrecher R (2013) A strategy for quality and uncertainty assessment of long-term eddy-covariance measurements. *Agric For Meteorol* 169:122–135
- Moene AF, Schüttemeyer D (2008) The effect of surface heterogeneity on the temperature–humidity correlation and the relative transport efficiency. *Boundary-Layer Meteorol* 129:99–113
- Moeng CH, Sullivan PP (1994) A comparison of shear- and buoyancy-driven planetary boundary layer flows. *J Atmos Sci* 51:999–1022
- Oncley S, Foken T, Vogt R, Kohsiek W, DeBruin H, Bernhofer C, Christen A, van Gorsel E, Grantz D, Feigenwinter C, Lehner I, Liebethal C, Liu H, Mauder M, Pitacco A, Ribeiro L, Weidinger T (2007) The energy balance experiment EBEX-2000. Part I: overview and energy balance. *Boundary-Layer Meteorol* 123:1–28

- Panin GN, Bernhofer Ch (2008) Parametrization of turbulent fluxes over inhomogeneous landscapes. *Izvestiya Atmos Oceanic Phys* 44:701–716
- Panin GN, Tetzlaff G, Raabe A (1998) Inhomogeneity of the land surface and problems in the parameterization of surface fluxes in natural conditions. *Theor Appl Climatol* 60:163–178
- Patton EG, Sullivan PP, Moeng CH (2005) The influence of idealized heterogeneity on wet and dry planetary boundary layers coupled to the land surface. *J Atmos Sci* 62:2078–2097
- Pearson RJ, Oncley SP, Delany AC (1998) A scalar similarity study based on surface layer ozone measurements over cotton during the California Ozone Deposition Experiment. *J Geophys Res* 103:18919–18926
- Raasch S, Harbusch G (2001) An analysis of secondary circulations and their effects caused by small-scale surface inhomogeneities using large-eddy simulation. *Boundary-Layer Meteorol* 101:31–59
- Ruppert J, Thomas C, Foken T (2006) Scalar similarity for relaxed eddy accumulation methods. *Boundary-Layer Meteorol* 120:39–63
- Schmidt H, Schumann U (1989) Coherent structure of the convective boundary layer derived from large-eddy simulations. *J Fluid Mech* 200:511–562
- Segal M, Arritt RW (1992) Nonclassical mesoscale circulations caused by surface sensible heat-flux gradients. *Bull Am Meteorol Soc* 73:1593–1604
- Segal M, Avissar R, McCumber MC, Pielke RA (1988) Evaluation of vegetation effects on the generation and modification of mesoscale circulations. *J Atmos Sci* 45:2268–2293
- Sellers PJ, Hall FG, Kelly RD, Black A, Baldocchi D, Berry J, Ryan M, Ranson KJ, Crill PM, Lettenmaier DP, Margolis H, Cihlar J, Newcomer J, Fitzjarrald D, Jarvis PG, Gower ST, Halliwell D, Williams D, Goodison B, Wickland DE, Guertin FE (1997) BOREAS in 1997: Experiment overview, scientific results, and future directions. *J Geophys Res* 102:28731–28769
- Shen S, Leclerc MY (1995) How large must surface inhomogeneities be before they influence the convective boundary layer structure? A case study. *Q J R Meteorol Soc* 121:1209–1228
- Smith SD (1988) Coefficients for sea-surface wind-stress, heat flux and wind profiles as a function of wind-speed and temperature. *J Geophys Res* 93:15467–15472
- Steinfeld G, Letzel M, Raasch S, Kanda M, Inagaki A (2007) Spatial representativeness of single tower measurements and the imbalance problem with eddy-covariance fluxes: results of a large-eddy simulation study. *Boundary-Layer Meteorol* 123:77–98
- Stoy PC, Katul GG, Siqueira MBS, Juang JY, Novick KA, McCarthy HR, Oishi AC, Uebelherr JM, Kim HS, Oren RAM (2006) Separating the effects of climate and vegetation on evapotranspiration along a successional chronosequence in the southeastern US. *Glob Change Biol* 12:2115–2135
- Stoy PC, Mauder M, Foken T, Marcolla B, Boegh E, Ibrom A, Arain MA, Arneth A, Aurela M, Bernhofer C, Cescatti A, Dellwik E, Duce P, Gianelle D, van Gorsel E, Kiely G, Knohl A, Margolis H, McCaughey H, Merbold L, Montagnani L, Papale D, Reichstein M, Saunders M, Serrano-Ortiz P, Sottocornola M, Spano D, Vaccari F, Varlagin A (2013) A data-driven analysis of energy balance closure across FLUXNET research sites: the role of landscape scale heterogeneity. *Agric For Meteorol* 171–172:137–152
- Strunin MA, Hiyama T (2005) Spectral structure of small-scale turbulent and mesoscale fluxes in the atmospheric boundary layer over a thermally inhomogeneous land surface. *Boundary-Layer Meteorol* 117:479–510
- Stull RB (1988) An introduction to boundary layer meteorology. Kluwer, Dordrecht 666 pp
- Sun J, Lenschow DH, Mahrt L, Crawford TL, Davis KJ, Oncley SP, MacPherson IJ, Wang Q, Dobosy RJ, Desjardins RL (1997) Lake-induced atmospheric circulations during BOREAS. *J Geophys Res* 102:29155–29166
- Taylor PA (1987) Comments and further analysis on effective roughness lengths for use in numerical three-dimensional models. *Boundary-Layer Meteorol* 39:403–418
- Torrence C, Compo GP (1998) A practical guide to wavelet analysis. *Bull Am Meteorol Soc* 79:61–78
- Twine TE, Kustas WP, Norman JM, Cook DR, Houser PR, Meyers TP, Prueger JH, Starks PJ, Wesley ML (2000) Correcting eddy-covariance flux underestimates over a grassland. *Agric For Meteorol* 103:279–300
- Vickers D, Mahrt L (2003) The cospectral gap and turbulent flux calculations. *J Atmos Oceanic Technol* 20:660–672
- von Randow C, Sá LDA, Gannabathula PSSD, Manzi AO, Arlino PRA, Kruijt B (2002) Scale variability of atmospheric surface layer fluxes of energy and carbon over a tropical rain forest in southwest Amazonia 1. Diurnal conditions. *J Geophys Res* 107:8062
- Wieringa J (1993) Representative roughness parameters for homogeneous terrain. *Boundary-Layer Meteorol* 63:323–363
- Wilczak JL, Cancillo ML, King CW (1997) A wind profiler climatology of boundary layer structure above the boreal forest. *J Geophys Res* 102:29083–29100
- Williams AG, Kraus H, Hacker JM (1996) Transport processes in the tropical warm pool boundary layer. Part I: spectral composition of fluxes. *J Atmos Sci* 53:1187–1202

- Wilson K, Goldstein A, Falge E, Aubinet M, Baldocchi D, Berbigier P, Bernhofer C, Ceulemans R, Dolman H, Field C, Grelle A, Ibrom A, Law BE, Kowalski A, Meyers T, Moncrieff J, Monson R, Oechel W, Tenhunen J, Valentini R, Verma S (2002) Energy balance closure at FLUXNET sites. *Agric For Meteorol* 113:223–243
- Zacharias S, Bogen H, Samaniego L, Mauder M, Fuß R, Pütz T, Frenzel M, Schwank M, Baessler C, Butterbach-Bahl K, Bens O, Borg E, Brauer A, Dietrich P, Hajsek I, Helle G, Kiese R, Kunstmann H, Klotz S, Munch JC, Papen H, Priesack E, Schmid HP, Steinbrecher R, Rosenbaum U, Teutsch G, Vereecken H (2011) A network of terrestrial environmental observatories in Germany. *Vadose Zone J* 10:955–973

## Appendix C

Eder F\*, Schmidt M, Damian T, Träumner K, Mauder M (2015a) Meso-scale eddies affect near-surface turbulent exchange: evidence from lidar and tower measurements. *J Appl Meteorol Climatol* 54:189-206, doi: 10.1175/JAMC-D-14-0140.1

©American Meteorological Society. Used with permission.

JANUARY 2015

EDER ET AL.

189

### Mesoscale Eddies Affect Near-Surface Turbulent Exchange: Evidence from Lidar and Tower Measurements

FABIAN EDER

*Institute of Meteorology and Climate Research-Atmospheric Environmental Research (IMK-IFU), Karlsruhe Institute of Technology, Garmisch-Partenkirchen, and Institute of Geography and Geoecology (IfGG), Karlsruhe Institute of Technology, Karlsruhe, Germany*

MARIUS SCHMIDT

*Agrosphere (IBG-3), Jülich Research Centre, Jülich, Germany*

THOMAS DAMIAN AND KATJA TRÄUMNER

*Institute of Meteorology and Climate Research-Troposphere Research (IMK-TRO), Karlsruhe Institute of Technology, Eggenstein-Leopoldshafen, Germany*

MATTHIAS MAUDER

*Institute of Meteorology and Climate Research-Atmospheric Environmental Research (IMK-IFU), Karlsruhe Institute of Technology, Garmisch-Partenkirchen, and Institute of Geography and Geoecology (IfGG), Karlsruhe Institute of Technology, Karlsruhe, Germany*

(Manuscript received 6 June 2014, in final form 9 October 2014)

#### ABSTRACT

The eddy-covariance technique tends to underestimate turbulent heat fluxes, which results in nonclosure of the surface energy balance. This study shows experimental evidence that mesoscale turbulent organized structures, which are inherently not captured by the standard eddy-covariance technique, can affect near-surface turbulent exchange. By using a combined setup of three Doppler wind lidars above a cropland-dominated area in Germany, low-frequency turbulent structures were detected in the surface layer down to a few meters above ground. In addition, data from two micrometeorological stations in the study area were analyzed with respect to energy balance closure. In accordance with several previous studies, the data confirm a strong friction velocity dependence of the energy balance residual. At both stations, the energy balance residual was found to be positively correlated with the vertical moisture gradient in the lower atmospheric boundary layer, but at only one station was it correlated with the temperature gradient. This result indicates that mesoscale transport probably contributes more to the latent heat flux than to the sensible heat flux, but this conclusion depends largely on the measurement site. Moreover, flow distortion due to tower mountings and measurement devices affects the energy balance closure considerably for certain wind directions.

#### 1. Introduction

The eddy-covariance (EC) method (Swinbank 1951) is the most direct measurement technique for quantifying the ecosystem-atmosphere exchange of energy and

*Corresponding author address:* Fabian Eder, Institute of Meteorology and Climate Research-Atmospheric Environmental Research, Karlsruhe Institute of Technology, Kreuzackbahnstraße 19, 82467 Garmisch-Partenkirchen, Germany.  
E-mail: fabian.eder@kit.edu

DOI: 10.1175/JAMC-D-14-0140.1

© 2015 American Meteorological Society

matter on a long-term basis. For this reason, large EC measurement networks have been established (Baldocchi et al. 2001). During the last few decades it became obvious that the EC technique usually does not close the energy balance at the surface—a fact that is known as the energy balance closure problem (Desjardins 1985; Lee and Black 1993; Twine et al. 2000; Hendrickson et al. 2002; Oncley et al. 2007; Foken 2008b; Hendricks-Franssen et al. 2010; Stoy et al. 2013). The available energy for turbulent transport, which is equal to the net radiation flux  $-Q_*$  minus the ground heat flux at the surface  $Q_G$ , is

not totally balanced by the sum of the sensible heat flux  $Q_H$  and the latent heat flux  $Q_E$ :

$$-Q_S^* - Q_G = Q_H + Q_E + Q_R. \quad (1)$$

The energy balance residual  $Q_R$  can amount to more than  $100 \text{ W m}^{-2}$ , depending on measurement site, time of day, and time of year. As an alternative to Eq. (1), Wilson et al. (2002) defined the energy balance ratio  $R$  as the sum of the turbulent fluxes divided by the available energy:

$$R = \frac{Q_H + Q_E}{-Q_S^* - Q_G}. \quad (2)$$

Given that general systematic errors of that extent in the measurement of  $Q_S^*$  (Kohsiek et al. 2007) and  $Q_G$  (Liebethal et al. 2005; Foken 2008b) can be excluded, the energy balance is not closed because the EC method underestimates  $Q_H$  and  $Q_E$ .

Several reasons for the underestimation of turbulent heat fluxes are discussed in the literature. Early studies considered instrumental errors (Laubach et al. 1994; Goulden et al. 1996). Angle-of-attack-dependent errors of nonorthogonal sonic anemometers resulting from flow distortion were recently addressed (Kochendorfer et al. 2012; Nakai and Shimoyama 2012; Mauder 2013; Frank et al. 2013). In addition, the EC technique is based on assumptions of horizontal homogeneity and stationarity that are usually not completely fulfilled under typical field conditions. Therefore, rigorous data screening using a statistical test procedure is a necessary requirement for studying the surface energy balance (Mauder and Foken 2006; Mauder et al. 2013). Moreover, surface heterogeneities within the flux footprint of the measurement (Schmid 1997; Panin et al. 1998) as well as different source areas of the instruments (Culf et al. 2004; Göckede et al. 2008) have to be considered. The above-mentioned issues often cannot sufficiently explain why the turbulent fluxes are generally underestimated at many sites, however. A considerable amount of energy can be stored in the layer between the surface and the location of the measurement devices—for example, in the soil (Heusinkveld et al. 2004; Liebethal et al. 2005) and the plant biomass (Meyers and Hollinger 2004; Lindroth et al. 2010; Kilinc et al. 2012; Emmel et al. 2013). A small amount of energy is also fixed by photosynthesis (Blanken et al. 1997; Schmid et al. 2000; Meyers and Hollinger 2004). Accounting for all storage terms reduces  $Q_R$  significantly, but it is not sufficient for closing the energy balance (Leuning et al. 2012; Stoy et al. 2013).

Another theory is that a considerable amount of  $Q_R$  can be attributed to transport by turbulent structures that are inherently not captured by an EC tower (Mauder et al. 2007; Foken et al. 2011). These could be either

low-frequency motions with time scales that are larger than the averaging time of the EC system (Sakai et al. 2001; Finnigan et al. 2003) or heterogeneity-induced secondary circulations that do not move with the mean wind (Lee and Black 1993; Mahrt 1998; Foken 2008b). These structures induce site-specific horizontal and vertical advection (Staebler and Fitzjarrald 2004; Higgins et al. 2013), which are difficult to capture with tower measurements (Aubinet et al. 2010). In this study, we focus on low-frequency organized structures that fill the entire atmospheric boundary layer (ABL), and, following Kanda et al. (2004), we will call them “turbulent organized structures” (TOS). Large-eddy simulation (LES) studies showed that point measurements, such as the tower-based EC technique, are not able to capture TOS appropriately (Kanda et al. 2004; Inagaki et al. 2006; Steinfeld et al. 2007). Because of the limited grid resolution of current LES model runs, it is still not clear whether these structures reach down into the Prandtl layer or surface layer where flux measurements are usually conducted.

The objective of this study is to show that the TOS extend down to the ground and affect the near-surface exchange. First, the surface energy balances at two EC stations in an agricultural area in the west of Germany are determined. To demonstrate the existence of TOS in the Prandtl layer, data from three synchronously scanning Doppler lidars are analyzed. Because the flux contributions of the TOS cannot be measured directly, we evaluated their role for the vertical exchange of energy indirectly by analyzing the vertical gradients of temperature and moisture in the lower ABL. We assume that TOS are an effective exchange mechanism between the surface layer and the layers farther up in the atmosphere. They can only contribute substantially to the vertical fluxes if there is a pronounced difference in potential temperature and specific moisture between the different layers. During daytime conditions, the air close to the ground is usually warmer and wetter than above, and turbulent fluxes carried by TOS are consequently always positive. In accord with this situation, the neglect of the TOS transport by the EC method results in a systematic underestimation of turbulent heat fluxes, that is, the nonclosure of the surface energy balance. The vertical gradients in the lower ABL were detected with a radiometer and alternatively calculated from surface-layer universal functions. From these data, we attempt to identify parameters that are related to the different magnitudes of nonclosure of the energy balance observed at the sites.

## 2. Measurements and methods

### a. Site description

The measurements were conducted in the Eifel/Lower Rhine Valley Observatory of the Terrestrial

Environmental Observatories (TERENO) network, which is located near Jülich in the west of Germany, close to the borders of Belgium and the Netherlands. The TERENO program is a long-term interdisciplinary research program in Germany that aims to observe the impacts of global change on terrestrial ecosystems at the regional level (Zacharias et al. 2011). The data were collected in the framework of the High Definition Clouds and Precipitation for Advancing Climate Prediction [HD(CP)<sup>2</sup>] project, during the HD(CP)<sup>2</sup> Observational Prototype Experiment (HOPE), which took place in the area in April and May of 2013.

Data from two permanently running EC towers at Selhausen (50.87°N, 6.45°E; 103 m MSL) and Merzenhausen (50.93°N, 6.30°E; 93 m MSL) were used, which are located in the catchment of the Rur river (Fig. 1a). Most of the land in the study area is used for agriculture, mainly sugar beet and winter cereal cultivation (Graf et al. 2010). The regional landscape was originally flat, but it has changed dramatically as a result of the intensive brown-coal surface mining that has occurred there. The replanted spoil heap “Sophienhöhe” (302 m MSL) is the highest topographic elevation in the area and is located approximately 7.5 km north of the EC station at Selhausen and 11 km east of Merzenhausen (Fig. 1a). The two open pit mines that are located 4 km northeast and 6.5 km west of Selhausen are the deepest points in the area.

#### b. Micrometeorological tower measurements

In April and May of 2013, winter wheat was grown on the fields instrumented with EC systems at Selhausen and Merzenhausen. At both sites, all components of the surface energy balance were measured directly: the turbulent fluxes of sensible and latent heat, the net radiation, and the ground heat flux [Eq. (1)].

Model CSAT-3 sonic anemometers (Campbell Scientific, Inc.) were used to measure the three-dimensional wind vector and the sonic temperature and model LI-7500 open-path infrared gas analyzers (Li-Cor, Inc., Biosciences) to measure the absolute humidity at 2 m. The measurement frequency was 20 Hz, and turbulent fluxes of sensible and latent heat were calculated using the “TK3.1” software package (Mauder and Foken 2011). The postprocessing of the field data followed the strategy presented in Mauder et al. (2013) and included the following: a raw-data delay correction that is based on maximizing the initial cross correlations of vertical wind speed with temperature and water vapor concentration, a spike-removal algorithm that is based on median absolute deviation, a planar-fit coordinate rotation (Wilczak et al. 2001), and corrections for high-frequency spectral losses (Moore 1986), the difference between sonic

temperature and air temperature (Schotanus et al. 1983), and density fluctuations (Webb et al. 1980). For postfield quality assurance and quality control (QA/QC), a three-class quality-flagging scheme following that of Mauder et al. (2013) was applied to the 30-min statistics and fluxes. In this study, only data of the highest quality (flag 0) were used, except for the calculation of mean daily energy balance ratios in section 3a, where data of moderate quality (flag 1) were also used.

The net radiation was measured with an NR01 four-component net radiometer (Hukseflux Thermal Sensors B.V.) at Selhausen and with an NR Lite net radiometer (Kipp & Zonen B.V.) at Merzenhausen. The data from the NR Lite were corrected on the basis of side-by-side measurements with an NR01 radiometer at the end of the HOPE campaign. The ground heat flux was determined from three soil heat flux plates (model HFP01SC; Hukseflux), of which one was buried at 3-cm depth and two were placed at 8-cm depth; three Campbell Scientific model TCAV soil temperature sensors at 1-, 5- and 2–6-cm depth; and two Campbell Scientific model CS616 soil moisture sensors at 2.5-cm depth using a calorimetric approach (Liebethal et al. 2005).

#### c. Doppler-lidar wind measurements and dual-Doppler technique

In the area of the Selhausen site, we also measured the spatially resolved turbulent flow field using Doppler lidars. To measure profiles of the vertical wind component above the site, we operated a Doppler wind lidar (Streamline model; HaloPhotonics, Ltd.) approximately 500 m northeast of the micrometeorological tower (Fig. 1b). The Streamline lidar emits a pulsed laser light of 1.5- $\mu\text{m}$  wavelength at a pulse repetition frequency of 15 kHz. To reduce the random error of the velocity estimate, an ensemble average over 15 000 pulses is calculated so that the effective measurement frequency is about 1 Hz. The Streamline lidar achieves a spatial resolution of 18 m. The data from the first five range gates and from range gates with signal-to-noise ratios  $< -17$  dB were not used. The random error, determined from the difference between lag 0 and lag 1 of the autocovariance function (Lenschow and Kristensen 1985; Frehlich 2001), is  $< 0.2 \text{ m s}^{-1}$  for signal-to-noise ratios  $> -17$  dB. The Streamline either pointed vertically upward into the atmosphere to measure profiles of the vertical wind component, or it performed range-height indicator (RHI) scans (Fig. 1b). During the RHI scan, the lidar permanently changed its elevation angle; that is, it moved from 2° elevation to 30° elevation at 2° intervals, but held its azimuth angle at 357°.

In addition, two Doppler lidars (WindTracer model; Lockheed Martin Technologies, Inc.) were used as

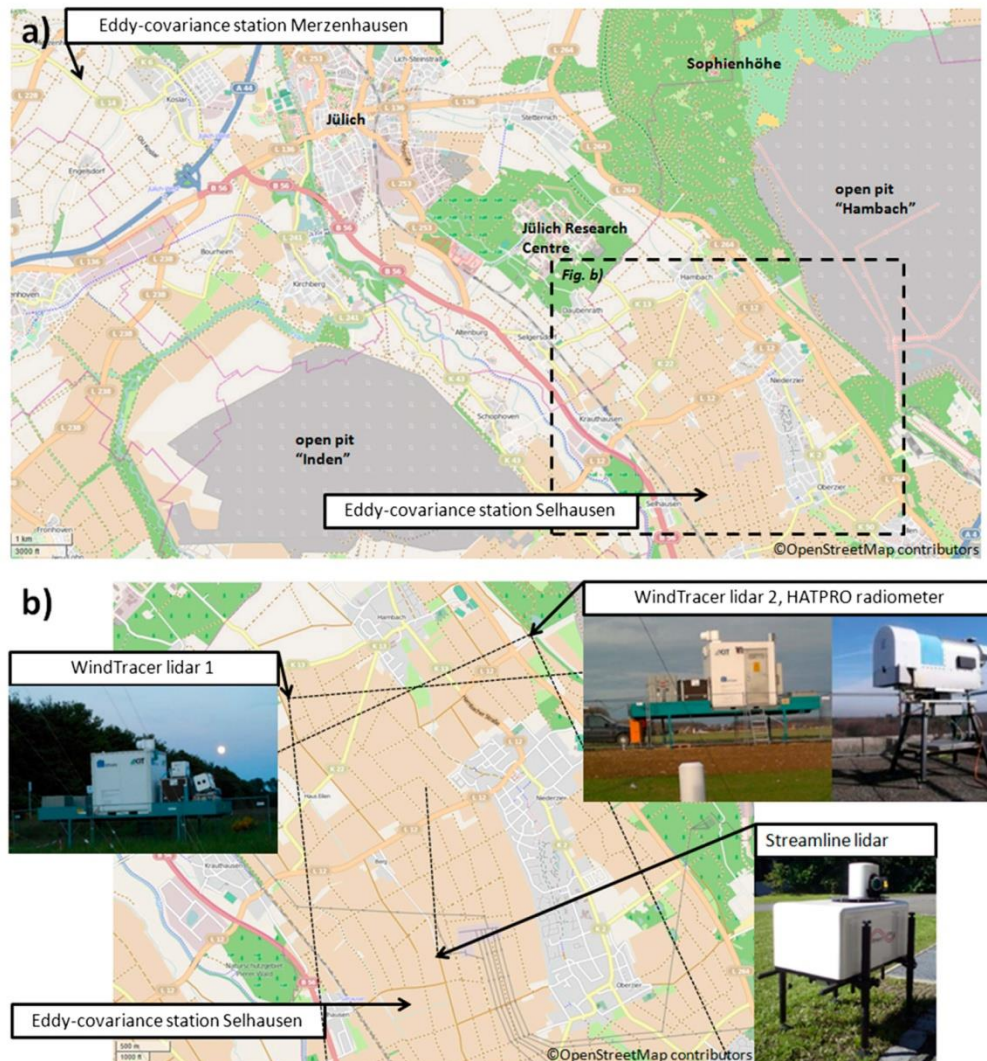


FIG. 1. (a) Overview map (<http://openstreetmap.org>; this map is made available under the Open Database License 1.0: <http://opendatacommons.org/licenses/odbl/1.0/>) of the investigation area indicating the locations of the EC stations at Selhausen and Merzenhausen. (b) Instrument setup for Doppler wind lidar measurements in the Selhausen area: locations of the EC station at Selhausen, the Streamline Doppler lidar, and the WindTracer systems that were operated in dual-Doppler mode. The HATPRO radiometer for the temperature and moisture profiles was located next to the northeastern WindTracer system. The black dashed lines in (b) indicate the borders of the PPI scans of the WindTracer lidars and the orientation of the RHI scans performed by the Streamline lidar.

a coordinated dual-Doppler system that was located approximately 3.5 km north of the Selhausen site (Fig. 1b). Both lidars performed 90°-sector plan-position indicator (PPI) scans (Newsom et al. 2008) at a low elevation. The

system placed in the northeast measured a sector PPI between the azimuth angles of 155° and 245°, whereas the lidar placed in the northwest conducted measurements between the azimuth angles of 84° and 174°. The

elevation for both sector scans differed in a way ( $0.025^\circ$ – $2.025^\circ$ ) that the overlap area was tilted by  $2^\circ$ . In the overlap area of both measurements, the retrieval algorithm (Stawiarski 2014) that was used delivers a 2D horizontal wind field for an area of approximately  $12\text{ km}^2$  with a spatial resolution of about 70 m and a temporal resolution of 12 s. Both lidar systems were synchronized by a control program that ran at a remote operation station. Detailed information on instrumentation, error handling and scan optimization of the applied dual-Doppler technique can be found in Stawiarski et al. (2013). During HOPE, the dual-Doppler technique was also used to detect coherent structures with relatively short time scales in the surface layer (Trümner et al. 2014).

#### d. Determination of vertical gradients

Vertical profiles of potential temperature  $\theta$  and specific humidity  $q$  in the ABL were obtained from a passive microwave radiometer (HATPRO model; RPG Radiometer Physics GmbH) that was located approximately 4 km northeast of the EC system at Selhausen (Fig. 1b). Average vertical profiles from 0 to 10000 m AGL were calculated every 15 min. Here, we used the potential temperature and humidity measurements at 0 and 250 m to determine the differences between the surface layer and outer layer. The outer layer is the main part of the ABL above the surface layer. Additional information on instrument technique and measurement accuracy can be found in Rose et al. (2005), Löhnert et al. (2009), and Löhnert and Maier (2012).

If no profile measurements are available, the local vertical gradients of temperature  $T$  and specific humidity  $q$  can be calculated from surface-layer profile equations (Foken 2008a):

$$\overline{w'T'} = -\frac{\alpha_0 \kappa u_*}{\phi_H(z/L)} \frac{\partial T}{\partial \ln z} \quad \text{and} \quad (3)$$

$$\overline{w'q'} = -\frac{\alpha_{0E} \kappa u_*}{\phi_E(z/L)} \frac{\partial q}{\partial \ln z}, \quad (4)$$

where  $z$  is the aerodynamic measurement height. This approach was tested using the EC data from Selhausen and Merzenhausen. The turbulent fluxes of temperature  $\overline{w'T'}$  and moisture  $\overline{w'q'}$  and the friction velocity  $u_*$  were measured using EC, the coefficients  $\alpha_0$  and  $\alpha_{0E}$  are approximately equal to 1.25, and the von Kármán constant  $\kappa$  is taken to be 0.4. The universal functions of the exchange of temperature  $\phi_H$  and moisture  $\phi_E$  account for the dependence of the turbulent diffusion coefficient on the atmospheric stability parameter  $z/L$ , with  $L$  being the Obukhov length. Thus, the vertical scalar profiles can be derived from

$$T(z) - T(z_{0T}) = \frac{\overline{w'T'}}{\alpha_0 \kappa u_*} \left[ \ln \frac{z}{z_{0T}} - \psi_H \left( \frac{z}{L} \right) \right] \quad \text{and} \quad (5)$$

$$q(z) - q(z_{0E}) = \frac{\overline{w'q'}}{\alpha_{0E} \kappa u_*} \left[ \ln \frac{z}{z_{0E}} - \psi_E \left( \frac{z}{L} \right) \right], \quad (6)$$

where  $z_0$  is surface roughness length and  $z_{0T}$  and  $z_{0E}$  are roughness lengths of temperature and moisture (Foken 2008a). The value of  $z_0$  was set to 0.01 m, which has been suggested for short grass (Wiernga 1993) and should roughly equal the roughness length of winter wheat during spring, and we assumed that  $z_{0T}$  and  $z_{0E}$  were equal to  $0.1z_0$  (Foken 2008a). Here, we used the integral of the universal function for temperature after Businger et al. (1971) and as modified by Högström (1988):

$$\psi_H \left( \frac{z}{L} \right) = 2 \ln \left( \frac{1+y}{2} \right) \quad \text{for} \quad \frac{z}{L} < 0 \quad (7)$$

$$\psi_H \left( \frac{z}{L} \right) = -7.8 \frac{z}{L} \quad \text{for} \quad \frac{z}{L} \geq 0, \quad (8)$$

with

$$y = 0.95 \left( 1 - 11.6 \frac{z}{L} \right)^{1/2}. \quad (9)$$

We assumed that the integral of the universal function for the exchange of moisture  $\psi_E$  is equal to  $\psi_H$ .

#### e. Wavelet spectra

Spectra of the horizontal and vertical wind components were calculated from high-frequency raw data measured by the sonic anemometer and the vertically pointing Streamline lidar. Time series with more than 5% of data missing as a result of unreliable measurements (sections 2b,c) were excluded from the analysis. The remaining gaps in the time series were filled using linear interpolation. We did not apply any coordinate rotation to the measured wind vector. Then, the data from the sonic were block averaged to 1 Hz to reduce the computation time. The block-averaging procedure serves as a low-pass filter that removes all fluctuations with frequencies of greater than 1 Hz, but we focus on low-frequency structures in this study.

The continuous wavelet transform was applied to the data using the Morlet mother wavelet with a frequency parameter of 6 (Torrence and Compo 1998; Mauder et al. 2007). The wavelet coefficients  $W_m(a, b)$  were calculated from the convolution of a time series  $m$  with the mother wavelet  $\Psi$  shifted by  $b$  and scaled by  $a$ . The squaring of the wavelet coefficients yields the wavelet scalogram, and the integration of the scalogram over  $b$  yields the wavelet spectrum (Hudgins et al. 1993).

$$S_m(a) = \frac{\delta j}{a} \frac{\delta t}{C_\delta} \frac{1}{N} \sum_{b=0}^{N-1} |W_m(a, b)|^2, \quad (10)$$

where  $\delta j = 0.25$  is the spacing between the scales of the wavelet transform,  $\delta t$  is the time step of the time series, and  $C_\delta = 0.776$  is a specific constant for the Morlet function (Torrence and Compo 1998). We considered only those wavelet coefficients outside of the “cone of influence” (Torrence and Compo 1998) so that edge effects are negligible. The integral over the total wavelet spectrum is equal to the variance of the time series, and integrating over parts of the spectrum gives the contributions of specific scales. Thus,

$$r_L = \frac{\sum_{a>\tau} S_m(a)}{\sum S_m(a)} \quad (11)$$

is the relative contribution of turbulent structures with time scales larger than  $\tau$ .

Analogous to Eq. (10), the wavelet cross spectrum of two time series  $m$  and  $n$  gives the spectral contributions to the turbulent flux  $\overline{m'n'}$  and is defined as

$$S_{mn}(a) = \frac{\delta j}{a} \frac{\delta t}{C_\delta} \frac{1}{N} \sum_{b=0}^{N-1} W_m(a, b) W_n^*(a, b), \quad (12)$$

with  $W_m(a, b)$  being the wavelet coefficients of time series  $m$  and  $W_n^*(a, b)$  being the complex conjugates of the wavelet coefficients of time series  $n$  (Hudgins et al. 1993).

### 3. Results

#### a. Observed energy balance closure

First, the mean daily surface energy balance ratios at Merzenhausen and Selhausen were calculated from the net radiation and surface heat fluxes according to Eq. (2). We detected slightly higher energy balance ratios ( $0.85 \pm 0.13$ ) at the site in Selhausen and slightly lower values at the Merzenhausen site ( $0.76 \pm 0.11$ ). Both results were in good agreement with those from Schmidt et al. (2012), in which a mean closure of 0.8 was reported for an EC tower at a winter wheat field in Selhausen over a period of 2 yr. In the current study, we found considerable day-to-day variability at both sites.

Second, the 30-min energy balance ratios were calculated using the daytime measurements, and an effect of the mean wind direction on the energy balance closure was found (Figs. 2a,b): at both sites, lower energy balance ratios were measured for northeasterly and easterly winds than for westerly winds. This dependence on wind direction may be explained by heterogeneities

on the landscape scale (Panin and Bernhofer 2008), nonhomogeneous fetch conditions (Panin et al. 1998; Foken 2008b), or flow distortion by the tower and the measurement devices (Högström and Smedman 2004; Nakai et al. 2006; Kochendorfer et al. 2012; Nakai and Shimoyama 2012). We exclude the first explanation, because the most prominent heterogeneity on the landscape scale, the Sophienhöhe hill, lies in different wind sectors for Selhausen (north) and Merzenhausen (east). In addition, the large surface-mining area west of Selhausen did not have any influence on the energy balance closure (Fig. 2a). The horizontal wind speed  $u$  normalized by the friction velocity  $u_*$  showed larger fluctuations in the northeastern and eastern wind sectors at both sites (Figs. 2c,d). This result might suggest the presence of roughness heterogeneities within the flux footprint, but the surface northeast and east of the towers is flat and homogeneous. The third potential explanation is that flow distortion by the tower mountings and measurement devices caused the poor energy balance closure and the differences in  $u/u_*$  for the northeastern and eastern wind directions. This explanation is supported by the systematic, direction-dependent fluctuations of the vertical wind component in that wind sector ( $360^\circ$ – $135^\circ$ ; Figs. 2e,f). The standard QA/QC tests did not detect this flow-distortion problem, although we show in Fig. 2 only data with the best quality flag (section 2b). The exclusion of those days when winds came from the  $360^\circ$ – $135^\circ$  sector leads to slightly higher energy balance ratios (0.88 for Selhausen and 0.80 for Merzenhausen), but the energy balance is still far from being closed completely. Therefore, we investigate in the following sections whether TOS can help to explain the remaining lack of energy balance closure.

#### b. TOS in the surface layer

In this section, we show examples of TOS with time scales of larger than 30 min that extended down to the surface layer at the study site. For this purpose, we used 30-min averages of dual-Doppler lidar data to visualize the horizontal dimensions of the TOS. In addition, the Streamline Doppler wind lidar data gave information about the vertical extent of these structures. First, we focus on two days with high net radiation, different wind regimes, and different energy balance ratios (Fig. 3). The date 7 April represents a day with low wind speeds ( $u = 0$ – $2 \text{ m s}^{-1}$ ) and a relatively low energy balance ratio (0.79 at Selhausen and 0.70 at Merzenhausen), whereas on 16 April higher wind speeds prevailed ( $u = 2$ – $4 \text{ m s}^{-1}$ ) and the energy balance ratio was higher (0.97 at Selhausen and 0.85 at Merzenhausen). The relatively large residuals in the morning hours are most probably due to

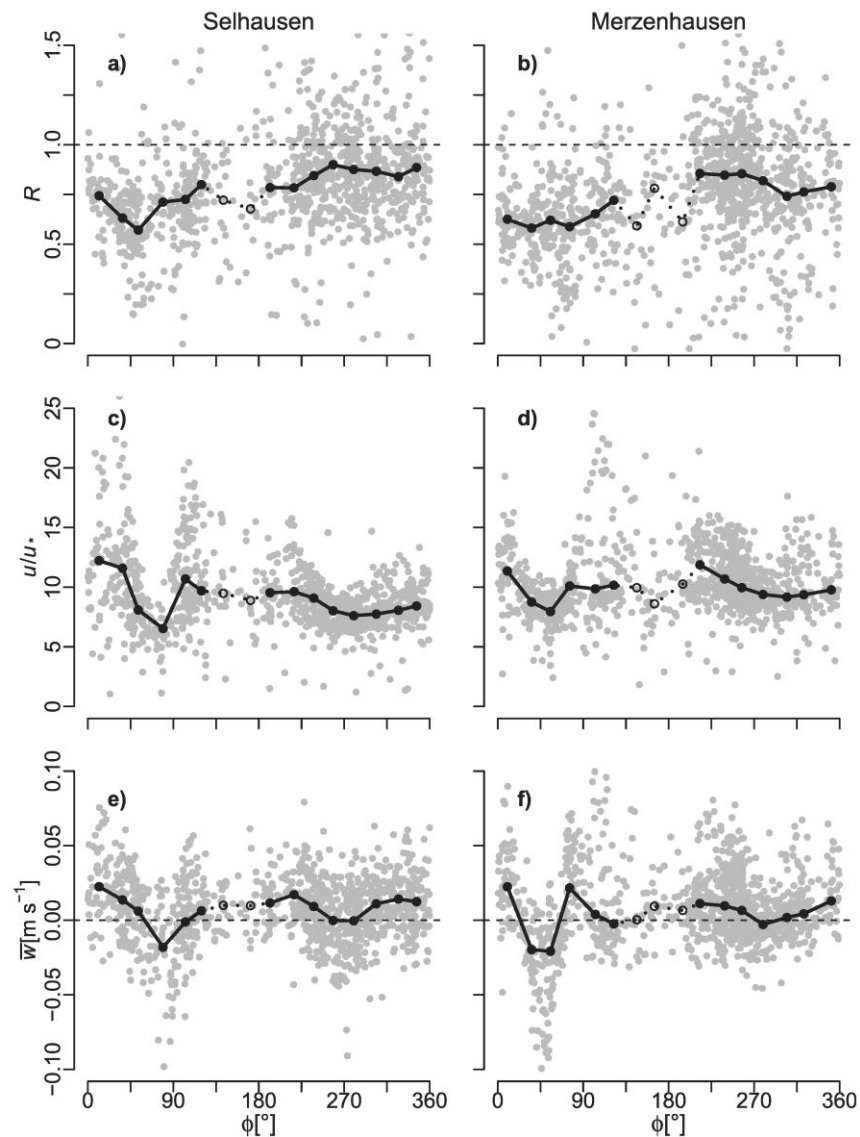


FIG. 2. Dependence of (a),(b) the energy balance ratio  $R$ , (c),(d) the horizontal wind speed normalized by friction velocity  $u/u_*$ , and (e),(f) the mean vertical wind speed  $\bar{w}$  after planar-fit rotation on wind direction  $\phi$  at Selhausen and Merzenhausen. The gray points show all 30-min data with the best quality flag that were measured during daytime ( $-Q_S - Q_G > 20 \text{ W m}^{-2}$ ). The filled black circles and solid lines show the mean values of wind sectors (width of  $22.5^\circ$ ) with at least 30 data points, and the open circles and dotted lines show the mean of the wind sectors with less than 30 data points.

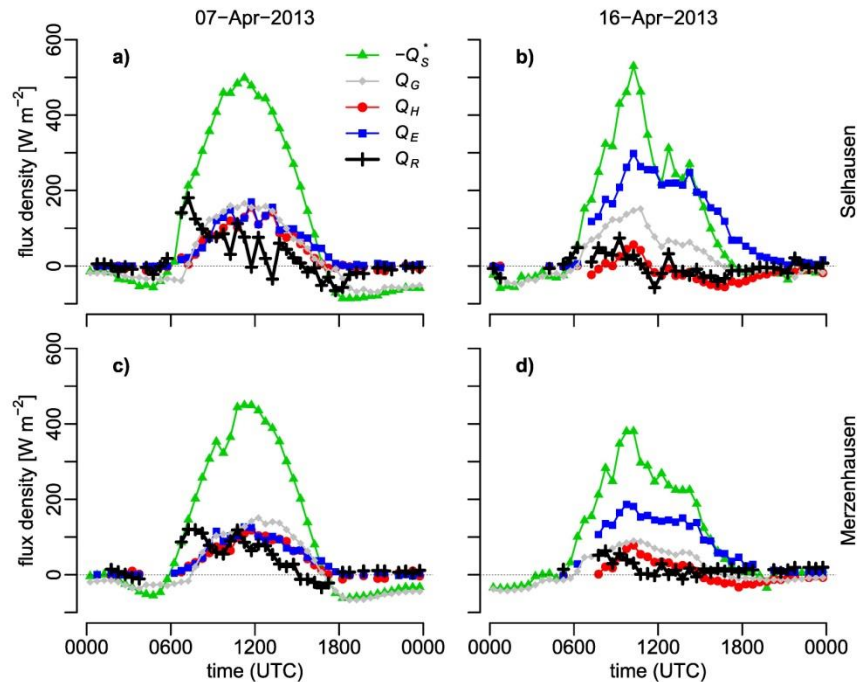


FIG. 3. Net radiation  $Q_S$ , ground heat flux  $Q_G$ , sensible heat flux  $Q_H$ , latent heat flux  $Q_E$ , and residual  $Q_R$  on (a),(c) 7 and (b),(d) 16 Apr 2013, measured at (top) Selhausen and (bottom) Merzenhausen.

the energy storage in the biomass of the winter wheat (Leuning et al. 2012) and the energy that is used to melt the white frost on the surface, for which we did not account.

On both days, we detected TOS in the surface layer. On 7 April (i.e., the low-wind case), cellular structures were identified in the dual-Doppler data around noontime (Fig. 4a) and in the early afternoon. The example in Fig. 4a shows convergence  $-\nabla(uv)$  in the horizontal wind field close to the vertically pointing Streamline lidar. It was calculated from the 2D horizontal wind field ( $u, v$ ):

$$-\nabla(uv) = -\left(\frac{du}{dx} + \frac{dv}{dy}\right), \quad (13)$$

where  $u$  is the zonal wind component,  $v$  is the meridional wind component,  $x$  is the zonal direction, and  $y$  is the meridional direction.

This convergence zone in the surface layer was associated with a quasi-permanent net vertical updraft that extended through the whole ABL for most of the period (Figs. 4b,c). In the case of high background wind (i.e., on 16 April), we did not find cellular structures but we detected parallel bands of higher wind speeds with

low-wind bands between them (Fig. 5a). In the vertically pointing lidar, we detected structures with short time scales (Fig. 5b) and a small mean vertical wind component (Fig. 5c). In the entire dual-Doppler dataset, we found clear cellular structures only on 7 April. In the 30-min-averaged horizontal wind fields, we usually found bands of different wind speeds that are aligned parallel to the mean wind direction. This could be surface-layer streaks (Cantwell 1981; Robinson 1991; Moeng and Sullivan 1994), but streaks are high-frequency structures with spatial dimensions of several hundreds of meters (Newsom et al. 2008; Träumner et al. 2014) that should vanish when calculating a 30-min average. Therefore, we argue that we detected traces of large TOS that probably fill in the whole ABL and reach down into the surface layer because their spanwise extent is on the order of the boundary layer depth and their longitudinal extent is larger than the dual-Doppler lidar's field of view.

To investigate how deep the TOS can penetrate into the surface layer, we performed additional RHI scans with the Streamline wind lidar. An RHI scan describes a series of measurements at different elevation angles and constant azimuth angle. For example, the data from

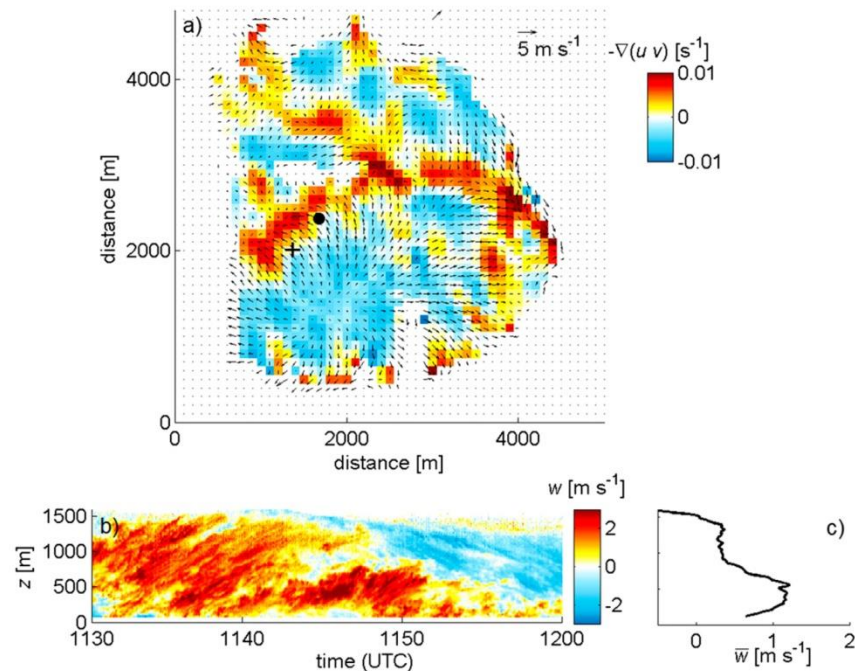


FIG. 4. (a) The 30-min average (1130–1200 UTC 7 Apr 2013) of the horizontal flow field around Selhausen measured with the dual-Doppler technique, located on a slightly tilted overlap area at 20–120 m AGL. The arrows show the horizontal wind vector, the colors show convergences and divergences in the flow field, the black dot indicates the location of the Streamline lidar, and the black plus sign shows the location of the EC station at Selhausen. (b) The vertical wind component  $w$  measured with the Streamline wind lidar during the 30-min period. (c) The vertical profile of the 30-min average of  $w$  measured with the Streamline lidar.

1030 to 1100 UTC 17 April ( $u \approx 1 \text{ m s}^{-1}$ ) show a mixture of cell-like structures and parallel bands in the horizontal wind field with convergence at a distance of 1000–1500 m from the Streamline lidar and divergence at a distance of 300–1000 m in the direction of the RHI scan (Fig. 6a). In the RHI scan we found that at the same time and at the same distances from the lidar the radial velocities changed their sign, which indicates convergence and divergence. These convergence and divergence zones reached down to the lowest measurement points above the ground ( $\sim 15 \text{ m AGL}$ ). On 28 April, we found even stronger convergence in the RHI scans (Fig. 6c), but no dual-Doppler data were available for that time period. Thus, we reason that TOS that fill the entire ABL can penetrate deep into the Prandtl layer (Figs. 6b,c).

Since TOS can reach close to the surface, they should also affect the data of the micrometeorological tower. To prove that, we calculated wavelet spectra from the daily time series of the  $u$  and  $w$  components measured with the sonic anemometer at the Selhausen site (Fig. 7).

In addition, we determined the  $w$  spectra in the outer layer using the data from the vertically pointing Streamline wind lidar. The  $w$  spectra in the surface layer show some low-frequency contribution ( $f < 1/1800 \text{ Hz}$ ) on 7 April that is due to the convective coherent structures but not on 16 April, and the overall low-frequency contribution to the surface-layer  $w$  spectra is weak. The outer-layer ( $z \geq 100 \text{ m}$ )  $w$  spectra and surface-layer  $u$  spectra show a significant low-frequency part, and they have similar spectral shapes. This result suggests that the TOS measured with the dual-Doppler technique (Figs. 4, 5a, and 6a) affect the horizontal wind component in the surface layer and consequently can cause horizontal advection and horizontal flux divergences that are not considered in the standard EC approach (Finnigan et al. 2003).

Another interesting feature is that on 7 April the surface-layer  $u$  spectrum and the outer-layer  $w$  spectra were shifted to lower frequencies, which could explain the poorer energy balance closure on that day. For this

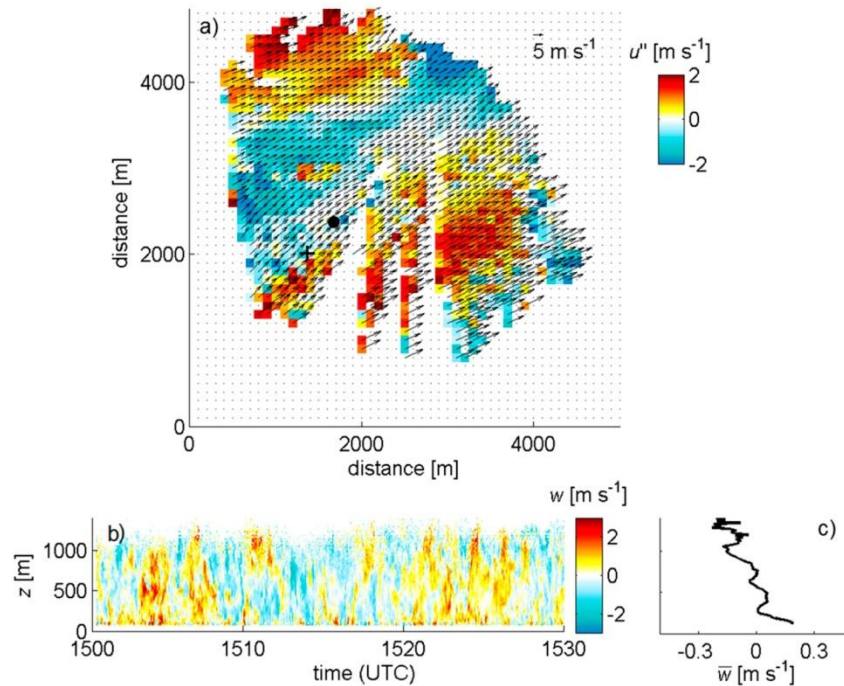


FIG. 5. The horizontal flow field and vertical wind component around Selhausen at 1500–1530 UTC 7 Apr 2013. This layout is identical to that in Fig. 4 except for the color scale in (a), which now indicates the spatial deviations  $u'$  from the space–time-averaged horizontal wind speed.

reason, we calculated the relative low-frequency contribution to the daily  $u$  spectra using Eq. (11). We did not find an appreciable correlation between the low-frequency part of the  $u$  spectrum and the energy balance ratio (linear model; coefficient of determination  $R^2 = 0.05$ ), which suggests that considering the strengths of TOS alone is not sufficient for explaining the unclosed energy balance. In addition, the vertical scalar gradients need to be taken into account, which is done in the following section.

*c. Relation of friction velocity and vertical gradients to the energy balance residual*

As explained in section 1, a considerable vertical gradient in temperature and/or humidity is necessary in order that TOS can contribute to the near-surface energy exchange. In other words, the magnitude of the energy balance residual should correlate with the vertical gradient of temperature and humidity in the lower part of the ABL. For this purpose, we determined the temperature and moisture difference between the surface layer and a height of 250 m AGL using the profiles from the

HATPRO microwave radiometer. Then, we performed a linear-regression analysis between the mean daily energy balance residual and the corresponding mean vertical gradients, by considering only the daytime values (0800–1700 UTC). We excluded days on which the mean wind direction was within the  $360^\circ$ – $135^\circ$  sector (section 3a). In a second step, we also excluded days with less than 50% data availability, mainly as a result of rain events and poor data quality according to the applied QA/QC scheme (section 2b).

The regression analysis between various atmospheric parameters and the mean daily energy balance residual at the Selhausen site revealed a negative correlation between  $Q_R$  and the friction velocity measured with the sonic anemometer (Fig. 8a), with  $R^2 = 0.23$ . With respect to the vertical gradients, there was no correlation with temperature (Fig. 8b) but there was a correlation with atmospheric moisture (Fig. 8c), with  $R^2 = 0.36$ . This result means that large energy balance residuals predominantly occurred during periods with large vertical moisture differences in the lower ABL. The coefficients of determination become even larger ( $R^2 = 0.32$  for

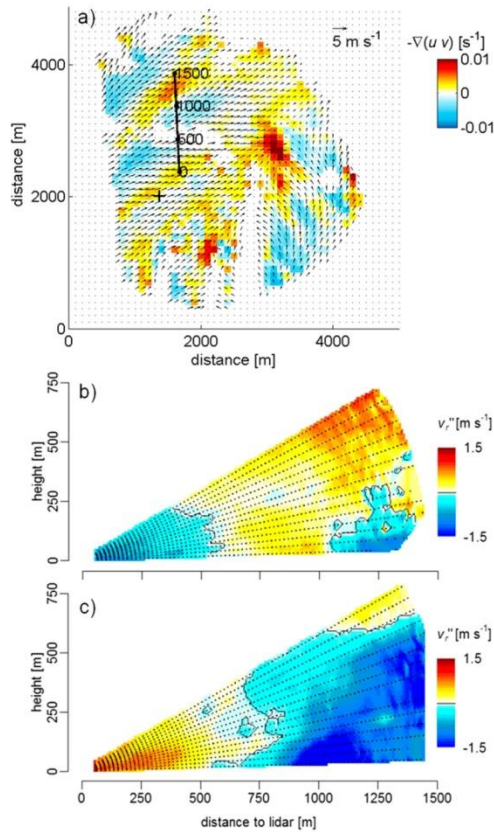


FIG. 6. (a) The 30-min average (1030–1100 UTC 17 Apr 2013) of the horizontal flow field around Selhausen (layout similar to that in Fig. 4a); the solid black line shows the orientation of the RHI scan of the Streamline lidar. (b) The synchronous 30-min average of the radial velocity deviation from space–time-averaged wind  $v_r''$ , measured with the Streamline lidar that performed RHI scans between 0° and 30° elevation and at 357° azimuth angle. (c) The 30-min average of  $v_r''$  at 1230–1300 UTC 28 Apr 2013.

$u_*$  and 0.50 for the moisture gradient) if we exclude the outlier in Figs. 8a–c (marked with a circle). The multiple linear regression of the energy balance residual against  $u_*$  and the moisture gradient, that is,

$$Q_R = c_0 + c_1 \frac{1}{u_*} + c_2 \lambda \frac{\Delta q}{\Delta z}, \quad (14)$$

has an  $R^2$  of 0.40 (all days) and 0.60 (without the outlier), with  $c_0 = -44.09 \text{ W m}^{-2}$ ,  $c_1 = 8.38 \text{ kg m s}^{-4}$ , and  $c_2 = 3.69 \text{ kg m}^{-1} \text{ s}^{-1}$  being regression coefficients (without the outlier) and  $\lambda$  being the heat of vaporization.

As an alternative to the HATPRO profiles, we calculated the vertical gradients between the surface and the eddy-tower measurement height from the universal functions following Eqs. (5)–(9). Again,  $Q_R$  correlates with the vertical moisture gradient ( $R^2 = 0.33$ ) but not with the vertical temperature gradient (Figs. 9a,b). The multivariate regression of  $Q_R$  against  $u_*$  and the moisture gradient yields an  $R^2$  of 0.42 (all days) and 0.52 (without the outlier), with  $c_0 = -33.61 \text{ W m}^{-2}$ ,  $c_1 = 11.75 \text{ kg m s}^{-4}$ , and  $c_2 = 2.90 \times 10^{-3} \text{ kg m}^{-1} \text{ s}^{-1}$  (without the outlier).

When the regression analysis was repeated for the Merzenhausen site, only very weak correlations were found between the vertical scalar gradients determined from the HATPRO radiometer and the mean daytime  $Q_R$  at Merzenhausen, with  $R^2$  values of 0.13 for the temperature gradient and 0.03 for the moisture gradient (data not shown). The gradients determined from the radiometer were probably not representative for the Merzenhausen site because of the larger distance of approximately 12.5 km between the locations of the HATPRO device and the EC station (Fig. 1). We calculated the vertical gradients from the universal functions applied to the local tower measurement, and we found a correlation between  $Q_R$  and the temperature ( $R^2 = 0.35$ ) as well as the moisture gradient ( $R^2 = 0.38$ ), whereas the correlation with  $u_*$  is weak ( $R^2 = 0.11$ ; Fig. 10). The multiple linear model

$$Q_R = c_0 + c_1 c_p \frac{\Delta T}{\Delta z} + c_2 \lambda \frac{\Delta q}{\Delta z} \quad (15)$$

has an  $R^2$  value of 0.46, with  $c_p$  being the specific heat capacity of air at constant pressure and  $c_0 = -3.63 \text{ W m}^{-2}$ ,  $c_1 = 11.45 \times 10^{-3} \text{ kg m}^{-1} \text{ s}^{-1}$ , and  $c_2 = 5.26 \times 10^{-3} \text{ kg m}^{-1} \text{ s}^{-1}$ . At the Merzenhausen site, the inclusion of  $u_*$  does not improve the model performance significantly. In summary, the friction velocity, the temperature gradient, and the moisture gradient can help to explain large energy balance residuals on a daily basis, but not all three parameters were equally relevant for the two sites analyzed in this study.

#### 4. Discussion

In this study, we tested the hypothesis that TOS are a major cause for the unclosed energy balance. On 7 April, the dual-Doppler data showed cellular structures (Fig. 4a), whereas we usually detected parallel bands with different wind speeds as, for example, on 16 April (Fig. 5a), in the horizontal wind field of the surface layer. The cellular structures indicate the presence of convective cells, or Bénard cells (Ahlers et al. 2009), which are a typical feature in LES studies of the buoyancy-driven

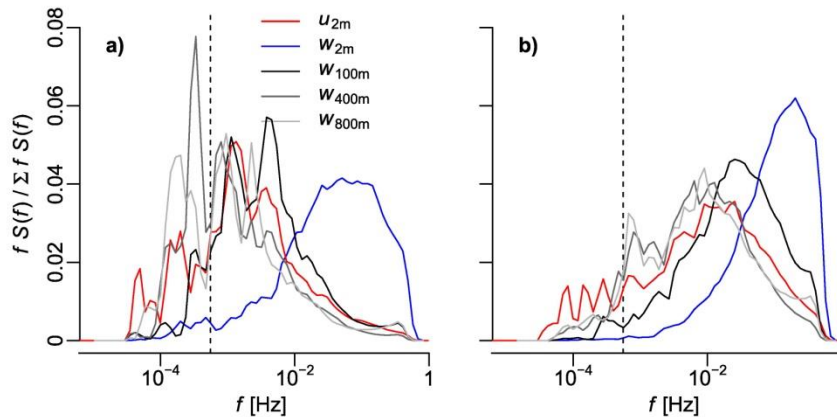


FIG. 7. Wavelet spectra of horizontal ( $u$ ) and vertical ( $w$ ) wind components measured at Selhausen on (a) 7 and (b) 16 Apr 2013. The measurements at 2 m AGL were conducted with a CSAT-3 sonic anemometer, and the measurements at 100, 400, and 800 m were taken with the Streamline Doppler wind lidar; the vertical dashed line indicates  $f = 1/1800$  Hz (i.e., a period of 30 min).

ABL (Schmidt and Schumann 1989; Kanda et al. 2004; Huang et al. 2008). Those convective cells have been described as “spoke patterns” (Schmidt and Schumann 1989); that is, they form a network of narrow convergence lines with strong updrafts aloft and wider circular downdraft regions. The data from the vertically pointing lidar indicate that the updraft regions are located above the convergence lines and that these updrafts reach far

up into the atmosphere (Fig. 4b). According to LES studies, the surface-layer convective cells merge into large buoyancy-driven updrafts that fill the entire ABL (Schmidt and Schumann 1989; Moeng and Sullivan 1994). Such large-scale turbulent structures were suspected to be responsible for the saw-blade pattern of the energy balance residual (Blanken et al. 1997) that we observed at Selhausen on 7 April (Fig. 3a); if such large structures are

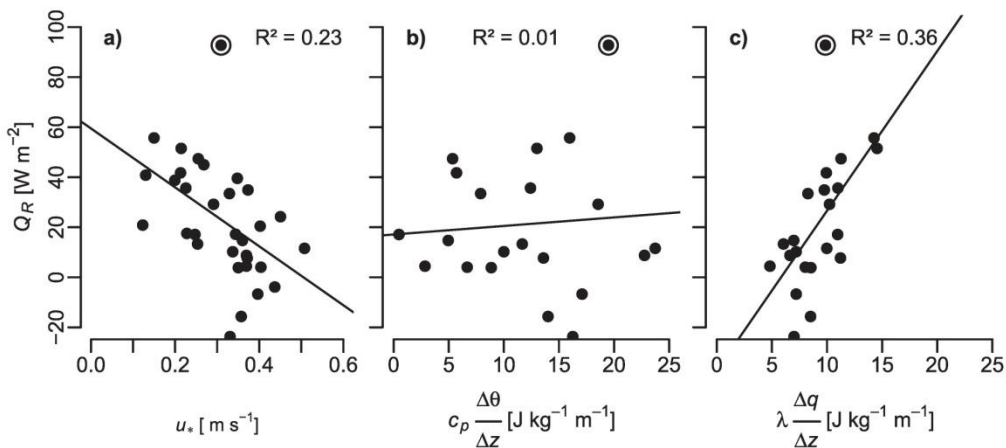


FIG. 8. Linear regression analysis between the daily averages of the energy balance residual  $Q_R$  at Selhausen and (a) friction velocity  $u_*$ , (b) the vertical gradient of potential temperature  $\Delta\theta/\Delta z$  multiplied by  $c_p$ , and (c) specific humidity  $\Delta q/\Delta z$  multiplied by  $\lambda$ , determined from the HATPRO profiles (0–250 m AGL). Days with a mean wind direction from  $0^\circ$  to  $135^\circ$  and less than 50% data availability were excluded from the analysis. The specific heat capacity of air at constant pressure  $c_p$  and the heat of vaporization  $\lambda$  were needed to convert to energy units. For each data point, we used only the daytime data measured between 0800 and 1700 UTC. The circle denotes an outlier (see text).

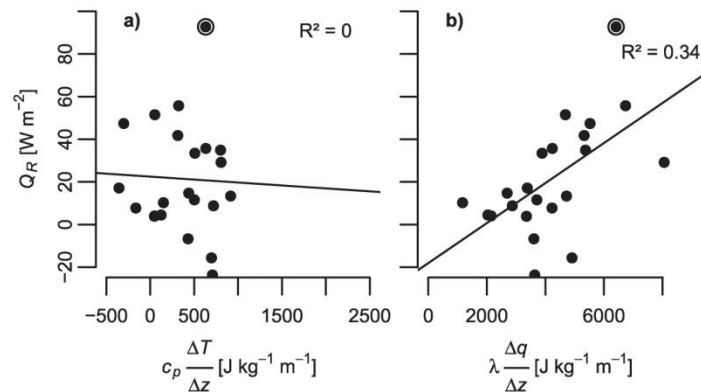


FIG. 9. Linear regression analysis between the daily averages of the energy balance residual  $Q_R$  at Selhausen and (a) the vertical gradient of temperature  $\Delta T/\Delta z$  multiplied by  $c_p$  and (b) the specific humidity  $\Delta q/\Delta z$  multiplied by  $\lambda$ , determined from the universal functions (0–2 m). Days with a mean wind direction from  $0^\circ$  to  $135^\circ$  and less than 50% data availability were excluded from the analysis. Only the daytime data measured between 0800 and 1700 UTC are used.

(are not) properly sampled by the EC measurement, that is, the cell does (does not) advect past the tower within the 30-min averaging interval, the energy balance residual is smaller (larger). Pure convective cells were only detected with the dual-Doppler technique for several hours, however, when the mean wind speed was low enough and buoyancy was high. The horizontal wind field in the surface layer was usually dominated by

parallel bands with different wind speeds (Figs. 5a and 6a) that could be traces of horizontal rolls (Etling and Brown 1993; Moeng and Sullivan 1994) or secondary circulations that are induced by upstream surface heterogeneities (Maronga and Raasch 2013). We found evidence that, if the background wind is high enough, there is strong mechanical mixing in the surface layer and the majority of the energy-transporting eddies are

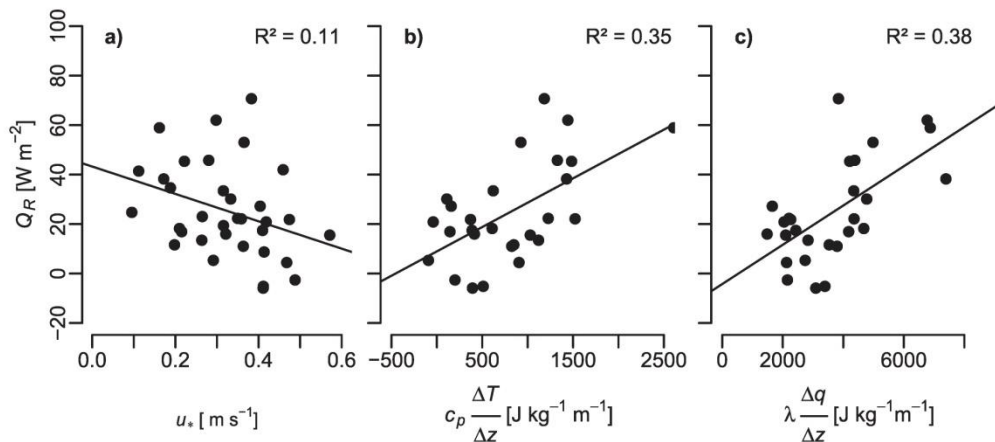


FIG. 10. Linear regression analysis between the daily averages of the energy balance residual  $Q_R$  at Merzenhausen and (a) the friction velocity  $u_*$ , (b) the vertical gradient of temperature  $\Delta T/\Delta z$  multiplied by  $c_p$ , and (c) the specific humidity  $\Delta q/\Delta z$  multiplied by  $\lambda$ , determined from the universal functions (0–2 m). Days with a mean wind direction from  $0^\circ$  to  $135^\circ$  and less than 50% data availability were excluded from the analysis. Only the daytime data measured between 0800 and 1700 UTC were used.

captured by the EC measurement (Fig. 5b). For this reason, the energy balance residual is negatively correlated with the friction velocity (Fig. 8a). This dependence is well known and suggests that a high intensity of mechanically induced turbulence improves the energy balance closure (Blanken et al. 1997; Wilson et al. 2002; Barr et al. 2006; Hendricks-Franssen et al. 2010; Stoy et al. 2013; Anderson and Wang 2014).

The RHI scans that were performed with the Streamline lidar on 17 and 28 April confirm that the TOS can reach almost down to the surface, since we still found strong convergence in the horizontal wind at 15 m AGL (Figs. 6b,c). The dual-Doppler data and the data from the Streamline lidar also suggest that TOS only affect the  $u$  component in the surface layer and the  $w$  component in the outer layer, which is confirmed by the wavelet spectra (Fig. 7). For this reason, TOS do not contribute much to the cospectra of  $w$  and  $T$  and  $w$  and  $q$  in the surface layer. This is the concept of the ogive test (Desjardins et al. 1989), which was suggested to quantify low-frequency losses of EC data (Foken et al. 1995, 2012; Charuchittipan et al. 2014). The ogive is the cumulative integral of the cospectrum starting with the highest frequencies and calculating up to a wavelength of several hours. We applied this test using the wavelet cross spectra [Eq. (12)], but it did not indicate any significant low-frequency vertical flux contribution on 7 April (data not shown), presumably because the  $w$  component was not affected and the structures were not moving with the mean wind. Our data suggest that the “missing” energy is represented rather in the horizontal fluxes.

Because the TOS affect the horizontal wind component in the surface layer, we tested whether the nonclosure of the energy balance can be related to the low-frequency part of the  $u$  spectrum, but this approach was not successful because of the extreme nonstationarity of this time series. For doing spectral analysis on time series data, we need stationary conditions over many hours, a condition that was not fulfilled in the field because of the diurnal cycle, veering wind directions, and variable weather conditions. Therefore, we conclude that using point measurements alone is not sufficient to quantify the contribution of low-frequency motions to the surface energy fluxes, in particular if secondary circulations are not carried along with the mean wind. We did demonstrate that ground-based remote sensing instruments can help to detect large-scale TOS that are difficult to capture with meteorological towers.

The Doppler lidar data alone do not allow one to discern whether the observed TOS contribute to the near-surface exchange, that is, whether they are “active” turbulent motions (Townsend 1976). If we take into account the

vertical gradients of temperature and moisture in the ABL, however, we can evaluate indirectly whether the TOS affect the vertical exchange of energy. At both sites, Selhausen and Merzenhausen, we found a correlation between the mean daytime energy balance residual and the moisture gradient, but a correlation was found with the gradient of potential temperature only at Merzenhausen (Figs. 8b,c, 9, and 10b,c). At Selhausen, the energy balance residual was larger when the differences in specific humidity between the surface layer and the outer layer were larger. In accord with this, the TOS may have contributed more to the latent heat flux than to the sensible heat flux at Selhausen. In other words, for adjusting the energy balance closure, a larger fraction of the residual energy should be assigned to the latent heat flux. This contradicts the cospectral similarity approach (Blanken et al. 1997; Twine et al. 2000), which says that  $Q_R$  should be distributed among  $Q_H$  and  $Q_E$  according to the measured Bowen ratio. Data from aircraft measurements over the boreal forest in Canada (Eder et al. 2014) and lysimeter measurements in the Alpine region (Wohlfahrt et al. 2010) also suggest that a majority of the energy balance residual should be added to the latent heat flux. The results from the Merzenhausen site (Figs. 10b, c), however, suggest that the TOS may contribute similarly to the fluxes of sensible heat and latent heat, which supports the approach to close the energy balance by conserving the Bowen ratio (Blanken et al. 1997; Twine et al. 2000). Therefore, we cannot give a definite recommendation on how to correct the unclosed energy balance, but the partitioning of the mesoscale flux seems to be highly dependent on the measurement site.

For calculating the vertical gradients, we recommend the use of profile measurements of  $\theta$  and  $q$  (Fig. 8). If the profiles are not available, as was the case for the Merzenhausen site, the application of profile equations seems to be a good alternative (Figs. 9 and 10). Because these gradients are derived from biased EC fluxes estimates, however, we tested whether the magnitude of the EC fluxes alone is sufficient to explain the energy balance residual (data not shown). If so, a systematic instrumental bias could also be a major cause of the unclosed energy balance, but the correlations were much weaker ( $R^2 < 0.18$ ) than those in Figs. 9 and 10. This gives us confidence that calculating the vertical gradients of  $T$  and  $q$  is a convenient approach for showing that the EC method does not capture the flux contributions of TOS.

In addition, we have shown that some part of the nonclosure of the energy balance can be explained by flow-distortion effects (section 3a). The 30-min averages of the vertical wind component show a strong dependence on

wind direction for the northeastern wind sector (Figs. 3e,f). The EC systems were arranged in such a way that there is no flow distortion for the main wind direction. That is, the sonic anemometer is facing to the southwest, and the tower mountings and the measurement devices are located in the northeastern wind sector, where they deflect the wind field. This may result in a decorrelation of the vertical wind and the scalars, that is, in lower flux estimates. We accordingly calculated a lower energy balance ratio for the northeastern and eastern wind sectors at both EC towers (Figs. 3a,b). It is important to note that the automated QA/QC routine that was applied to the data did not detect this effect, because the measured mean vertical wind component lay below the preset threshold of  $0.1 \text{ m s}^{-1}$  and the measured integral turbulence characteristics deviated by less than 30% from the modeled ones (Mauder and Foken 2011). Therefore, an influence of anemometer backwind deficiencies, tower mountings, and nearby instruments on the EC fluxes has to be taken into consideration for the northeastern sector, even after filtering out unreliable data using the QA/QC routine. We strongly recommend checking the processed data, especially  $\bar{w}$  and  $u|u_g$ , for such effects. Because it is not clear whether the design of the anemometer or the instrumental setup is the main source of disturbance, future research on this topic would be desirable.

In summary, we showed that a large fraction of the observed variability in the energy balance residual can be explained by the friction velocity and the vertical gradients of temperature and moisture (section 3c), after excluding data from wind sectors that are affected by flow distortion and after excluding measurement days with insufficient data availability. Therefore, Eqs. (14) and (15) might serve as a first step to develop a parameterization for the energy balance residual. The remaining variability results most likely from 1) the neglect of energy storage terms, which were relevant during the first days of the investigation period (i.e., at the beginning of April 2013), and 2) the random measurement error that is due to the stochastic nature of turbulence, instrumental noise, and the changing footprint of the measurement (Mauder et al. 2013).

## 5. Conclusions

We proved with field measurements that TOS with time scales of larger than 30 min can extend deep into the surface layer, and we have confirmed the dependence of the energy balance closure on friction velocity. The latter result suggests that the closure improves with enhanced mechanical mixing and increased propagation speed of the coherent structures. The vertical humidity gradient in

the lower ABL also helped to explain the observed variability of  $Q_R$ , whereas the vertical temperature gradient was only relevant for one of the two sites under investigation. This finding indicates that the energy balance at the EC towers lacks closure because TOS affect the near-surface exchange. Besides TOS, there are also heterogeneity-induced mesoscale secondary circulations that are fixed in space (Lee and Black 1993; Mahrt 1998; Foken 2008b), which cannot be captured by point measurements alone. Although we did not detect them with the dual-Doppler lidar in this study area, we expect them to play a significant role in ecosystem–atmosphere exchange in complex terrain—for example, sites in mountainous areas (Brötz et al. 2014), sites close to land–water boundaries (Higgins et al. 2013), or roughness heterogeneities such as forest edges (Eder et al. 2013).

Our study also shows that point measurements are not an adequate tool for quantifying the flux contribution of TOS, because these features are three-dimensional. Ground-based remote sensing measurements give more insight into the spatial structure of the surface layer, and we were able to visualize TOS in the surface layer, but their flux contributions can only be calculated if we also know the temperature and moisture field with a high temporal and spatial resolution. Because these requirements cannot be fulfilled with current field experiments, only intensive modeling studies can help. An LES model allows for conducting virtual measurements under well-defined environmental conditions, but the investigation of near-surface exchange requires a very fine grid resolution to prevent wall effects and to resolve atmospheric turbulence instead of parameterizing it in the surface layer.

*Acknowledgments.* The authors thank the KITcube team—in particular, Andreas Wieser and Bianca Adler—for their assistance with the lidar and HATPRO measurements. We acknowledge field support by Alexander Graf, Martina Klein, and Daniel Dolfus of the Transregional collaborative research center (SFB/TR) 32 “Patterns in Soil–Vegetation–Atmosphere Systems: Monitoring, Modelling, and Data Assimilation” funded by the Deutsche Forschungsgesellschaft (DFG). We thank Baltasar Trancón y Widemann for providing the wavelet routine. The data acquisition for this study was conducted in the framework of the “High definition clouds and precipitation for advancing climate prediction” (HDCP<sup>2</sup>) research initiative, funded by the German Federal Ministry of Education and Research (BMBF). A large part of this work was conducted within the Helmholtz Young Investigator Group “Capturing all relevant scales of biosphere–atmosphere exchange—the enigmatic energy balance closure problem,” which

is funded by the Helmholtz-Association through the President's Initiative and Networking Fund and by KIT.

## REFERENCES

- Ahlers, G., S. Grossmann, and D. Lohse, 2009: Heat transfer and large scale dynamics in turbulent Rayleigh-Bénard convection. *Rev. Mod. Phys.*, **81**, 503–537, doi:10.1103/RevModPhys.81.503.
- Anderson, R. G., and D. Wang, 2014: Energy budget closure observed in paired eddy covariance towers with increased and continuous daily turbulence. *Agric. For. Meteorol.*, **184**, 204–209, doi:10.1016/j.agrformet.2013.09.012.
- Aubinet, M., and Coauthors, 2010: Direct advection measurements do not help to solve the night-time CO<sub>2</sub> closure problem: Evidence from three different forests. *Agric. For. Meteorol.*, **150**, 655–664, doi:10.1016/j.agrformet.2010.01.016.
- Baldocchi, D., and Coauthors, 2001: FLUXNET: A new tool to study the temporal and spatial variability of ecosystem-scale carbon dioxide, water vapor, and energy flux densities. *Bull. Amer. Meteor. Soc.*, **82**, 2415–2434, doi:10.1175/1520-0477(2001)082<2415:FANTTS>2.3.CO;2.
- Barr, A. G., K. Morgenstern, T. A. Black, J. H. McCaughey, and Z. Nescic, 2006: Surface energy balance closure by the eddy-covariance method above three boreal forest stands and implications for the measurement of the CO<sub>2</sub> flux. *Agric. For. Meteorol.*, **140**, 322–337, doi:10.1016/j.agrformet.2006.08.007.
- Blanken, P. D., and Coauthors, 1997: Energy balance and canopy conductance of a boreal aspen forest: Partitioning overstory and understory components. *J. Geophys. Res.*, **102**, 28 915–28 927, doi:10.1029/97JD00193.
- Brötz, B., R. Eigenmann, A. Dörnbrack, T. Foken, and V. Wirth, 2014: Early-morning flow transition in a valley in low-mountain terrain under clear-sky conditions. *Bound.-Layer Meteorol.*, **152**, 45–63, doi:10.1007/s10546-014-9921-7.
- Businger, J. A., J. C. Wyngaard, Y. Izumi, and E. F. Bradley, 1971: Flux-profile relationships in the atmospheric surface layer. *J. Atmos. Sci.*, **28**, 181–189, doi:10.1175/1520-0469(1971)028<0181:FPRITA>2.0.CO;2.
- Cantwell, B. J., 1981: Organized motion in turbulent flow. *Annu. Rev. Fluid Mech.*, **13**, 457–515, doi:10.1146/annurev.fl.13.010181.002325.
- Charuchitipan, D., W. Babel, M. Mauder, J. P. Leps, and T. Foken, 2014: Extension of the averaging time in eddy-covariance measurements and its effect on the energy balance closure. *Bound.-Layer Meteorol.*, **152**, 303–327, doi:10.1007/s10546-014-9922-6.
- Culf, A. D., T. Foken, and J. H. C. Gash, 2004: The energy balance closure problem. *Vegetation, Water, Humans and the Climate: A New Perspective on an Interactive System*, P. Kabat et al., Eds., Springer, 159–166.
- Desjardins, R. L., 1985: Carbon dioxide budget of maize. *Agric. For. Meteorol.*, **36**, 29–41, doi:10.1016/0168-1923(85)90063-2.
- , J. I. MacPherson, P. H. Schuepp, and F. Karanja, 1989: An evaluation of aircraft flux measurements of CO<sub>2</sub>, water vapor and sensible heat. *Bound.-Layer Meteorol.*, **47**, 55–69, doi:10.1007/BF00122322.
- Eder, F., A. Serafimovich, and T. Foken, 2013: Coherent structures at a forest edge: Properties, coupling and impact of secondary circulations. *Bound.-Layer Meteorol.*, **148**, 285–308, doi:10.1007/s10546-013-9815-0.
- , F. De Roo, K. Kohnert, R. Desjardins, H. P. Schmid, and M. Mauder, 2014: Evaluation of two energy balance closure parameterizations. *Bound.-Layer Meteorol.*, **151**, 195–219, doi:10.1007/s10546-013-9904-0.
- Emmel, C., E. Paul-Limoges, T. A. Black, and A. Christen, 2013: Vertical distribution of radiation and energy balance partitioning within and above a lodgepole pine stand recovering from a recent insect attack. *Bound.-Layer Meteorol.*, **149**, 133–163, doi:10.1007/s10546-013-9844-8.
- Etling, D., and R. A. Brown, 1993: Roll vortices in the planetary boundary layer: A review. *Bound.-Layer Meteorol.*, **65**, 215–248, doi:10.1007/BF00705527.
- Finnigan, J. J., R. Clement, Y. Malhi, R. Leuning, and H. A. Cleugh, 2003: A re-evaluation of long-term flux measurement techniques. Part I: Averaging and coordinate rotation. *Bound.-Layer Meteorol.*, **107**, 1–48, doi:10.1023/A:1021554900225.
- Foken, T., 2008a: *Micrometeorology*. Springer, 308 pp.
- , 2008b: The energy balance closure problem: An overview. *Ecol. Appl.*, **18**, 1351–1367, doi:10.1890/06-0922.1.
- , R. Dlugi, and G. Kramm, 1995: On the determination of dry deposition and emission of gaseous compounds at the biosphere-atmosphere interface. *Meteor. Z.*, **4**, 91–118.
- , M. Aubinet, J. J. Finnigan, M. Y. Leclerc, M. Mauder, and K. T. Paw U, 2011: Results of a panel discussion about the energy balance closure correction for trace gases. *Bull. Amer. Meteor. Soc.*, **92**, ES13–ES18, doi:10.1175/2011BAMS3130.1.
- , R. Leuning, S. R. Oncley, M. Mauder, and M. Aubinet, 2012: Corrections and data quality control. *Eddy Covariance: A Practical Guide to Measurement and Data Analysis*, M. Aubinet, T. Vesala, and D. Papale, Eds., Springer, 85–131.
- Frank, J. M., W. J. Massman, and B. E. Ewers, 2013: Underestimates of sensible heat flux due to vertical velocity measurement errors in non-orthogonal sonic anemometers. *Agric. For. Meteorol.*, **171–172**, 72–81, doi:10.1016/j.agrformet.2012.11.005.
- Frehlich, R., 2001: Estimation of velocity error for Doppler lidar measurements. *J. Atmos. Oceanic Technol.*, **18**, 1628–1639, doi:10.1175/1520-0426(2001)018<1628:EOVEFD>2.0.CO;2.
- Göckede, M., and Coauthors, 2008: Quality control of CarboEurope flux data—Part 1: Coupling footprint analyses with flux data quality assessment to evaluate sites in forest ecosystems. *Biogeosciences*, **5**, 433–450, doi:10.5194/bg-5-433-2008.
- Goulden, M. L., J. W. Munger, S. M. Fan, B. C. Daube, and S. C. Wofsy, 1996: Measurements of carbon sequestration by long-term eddy covariance: Methods and a critical evaluation of accuracy. *Global Change Biol.*, **2**, 169–182, doi:10.1111/j.1365-2486.1996.tb00070.x.
- Graf, A., and Coauthors, 2010: Boundedness of turbulent temperature probability distributions, and their relation to the vertical profile in the convective boundary layer. *Bound.-Layer Meteorol.*, **134**, 459–486, doi:10.1007/s10546-009-9444-9.
- Hendricks-Franssen, H. J., R. Stöckli, I. Lehner, E. Rotenberg, and S. I. Seneviratne, 2010: Energy balance closure of eddy-covariance data: A multisite analysis for European FLUXNET stations. *Agric. For. Meteorol.*, **150**, 1553–1567, doi:10.1016/j.agrformet.2010.08.005.
- Heusinkveld, B. G., A. F. G. Jacobs, A. A. M. Holtslag, and S. M. Berkowicz, 2004: Surface energy balance closure in an arid region: Role of soil heat flux. *Agric. For. Meteorol.*, **122**, 21–37, doi:10.1016/j.agrformet.2003.09.005.
- Higgins, C. W., E. Pardyak, M. Froidevaux, V. Simeonov, and M. B. Parlange, 2013: Measured and estimated water vapor advection in the atmospheric surface layer. *J. Hydrometeorol.*, **14**, 1966–1972, doi:10.1175/JHM-D-12-0166.1.
- Högström, U., 1988: Non-dimensional wind and temperature profiles in the atmospheric surface layer: A re-evaluation. *Bound.-Layer Meteorol.*, **42**, 55–78, doi:10.1007/BF00119875.

- , and A. S. Smedman, 2004: Accuracy of sonic anemometers: Laminar wind-tunnel calibrations compared to atmospheric in situ calibrations against a reference instrument. *Bound.-Layer Meteor.*, **111**, 33–54, doi:10.1023/B:BOUN.0000011000.05248.47.
- Huang, J., X. Lee, and E. Patton, 2008: A modelling study of flux imbalance and the influence of entrainment in the convective boundary layer. *Bound.-Layer Meteor.*, **127**, 273–292, doi:10.1007/s10546-007-9254-x.
- Hudgins, L. E., M. E. Mayer, and C. A. Friehe, 1993: Fourier and wavelet analysis of atmospheric turbulence. *Progress in Wavelet Analysis and Applications*, E. Meyers and S. Roques, Eds., Editions Frontiers, 491–498.
- Inagaki, A., M. O. Letzel, S. Raasch, and M. Kanda, 2006: Impact of surface heterogeneity on energy imbalance: A study using LES. *J. Meteor. Soc. Japan*, **84**, 187–198, doi:10.2151/jmsj.84.187.
- Kanda, M., A. Inagaki, M. O. Letzel, S. Raasch, and T. Watanabe, 2004: LES study of the energy imbalance problem with eddy covariance fluxes. *Bound.-Layer Meteor.*, **110**, 381–404, doi:10.1023/B:BOUN.0000007225.45548.7a.
- Kilinc, M., J. Beringer, L. B. Hutley, V. Haverd, and N. Tapper, 2012: An analysis of the surface energy budget above the world's tallest angiosperm forest. *Agric. For. Meteorol.*, **166–167**, 23–31, doi:10.1016/j.agrformet.2012.05.014.
- Kochendorfer, J., T. P. Meyers, J. Frank, W. J. Massman, and M. W. Heuer, 2012: How well can we measure the vertical wind speed? Implications for fluxes of energy and mass. *Bound.-Layer Meteor.*, **145**, 383–398, doi:10.1007/s10546-012-9738-1.
- Kohsiek, W., C. Liebenthal, T. Foken, R. Vogt, S. P. Oncley, Ch. Bernhofer, and H. A. R. Debruin, 2007: The Energy Balance Experiment EBEX-2000. Part III: Behaviour and quality of the radiation measurements. *Bound.-Layer Meteor.*, **123**, 55–75, doi:10.1007/s10546-006-9135-8.
- Laubach, J., M. Raschendorfer, H. Kreilein, and G. Gravenhorst, 1994: Determination of heat and water vapour fluxes above a spruce forest by eddy correlation. *Agric. For. Meteorol.*, **71**, 373–401, doi:10.1016/0168-1923(94)90021-3.
- Lee, X., and T. A. Black, 1993: Atmospheric turbulence within and above a Douglas-fir stand. Part II: Eddy fluxes of sensible heat and water vapour. *Bound.-Layer Meteor.*, **64**, 369–389, doi:10.1007/BF00711706.
- Lenschow, D. H., and L. Kristensen, 1985: Uncorrelated noise in turbulence measurements. *J. Atmos. Oceanic Technol.*, **2**, 68–81, doi:10.1175/1520-0426(1985)002<0068:UNITM>2.0.CO;2.
- Leuning, R., E. van Gorsel, W. J. Massman, and P. R. Isaac, 2012: Reflections on the surface energy imbalance problem. *Agric. For. Meteorol.*, **156**, 65–74, doi:10.1016/j.agrformet.2011.12.002.
- Liebenthal, C., B. Huwe, and T. Foken, 2005: Sensitivity analysis for two ground heat flux calculation approaches. *Agric. For. Meteorol.*, **132**, 253–262, doi:10.1016/j.agrformet.2005.08.001.
- Lindroth, A., M. Mölder, and F. Lagergren, 2010: Heat storage in forest biomass improves energy balance closure. *Biogeosciences*, **7**, 301–313, doi:10.5194/bg-7-301-2010.
- Löhnert, U., and O. Maier, 2012: Operational profiling of temperature using ground-based microwave radiometry at Payerne: Prospects and challenges. *Atmos. Meas. Tech.*, **5**, 1121–1134, doi:10.5194/amt-5-1121-2012.
- , D. D. Turner, and S. Crewell, 2009: Ground-based temperature and humidity profiling using spectral infrared and microwave observations. Part I: Simulated retrieval performance in clear-sky conditions. *J. Appl. Meteor. Climatol.*, **48**, 1017–1032, doi:10.1175/2008JAMC2060.1.
- Mahrt, L., 1998: Flux sampling errors for aircraft and towers. *J. Atmos. Oceanic Technol.*, **15**, 416–429, doi:10.1175/1520-0426(1998)015<0416:FSEFAA>2.0.CO;2.
- Maronga, B., and S. Raasch, 2013: Large-eddy simulations of surface heterogeneity effects on the convective boundary layer during the LITFASS-2003 experiment. *Bound.-Layer Meteor.*, **146**, 17–44, doi:10.1007/s10546-012-9748-z.
- Mauder, M., 2013: A comment on “How well can we measure the vertical wind speed? Implications for fluxes of energy and mass” by Kochendorfer et al. *Bound.-Layer Meteor.*, **147**, 329–335, doi:10.1007/s10546-012-9794-6.
- , and T. Foken, 2006: Impact of post-field data processing on eddy covariance flux estimates and energy balance closure. *Meteor. Z.*, **15**, 597–609, doi:10.1127/0941-2948/2006/0167.
- , and —, 2011: Documentation and instruction manual of the eddy-covariance software package TK3. University of Bayreuth Dept. of Micrometeorology Rep. 46, 60 pp.
- , R. L. Desjardins, and I. MacPherson, 2007: Scale analysis of airborne flux measurements over heterogeneous terrain in a boreal ecosystem. *J. Geophys. Res.*, **112**, D13112, doi:10.1029/2006JD008133.
- , M. Cuntz, C. Drüe, A. Graf, C. Rebmann, H. P. Schmid, M. Schmidt, and R. Steinbrecher, 2013: A strategy for quality and uncertainty assessment of long-term eddy-covariance measurements. *Agric. For. Meteorol.*, **169**, 122–135, doi:10.1016/j.agrformet.2012.09.006.
- Meyers, T. P., and S. E. Hollinger, 2004: An assessment of storage terms in the surface energy balance of maize and soybean. *Agric. For. Meteorol.*, **125**, 105–115, doi:10.1016/j.agrformet.2004.03.001.
- Moeng, C. H., and P. P. Sullivan, 1994: A comparison of shear- and buoyancy-driven planetary boundary layer flows. *J. Atmos. Sci.*, **51**, 999–1022, doi:10.1175/1520-0469(1994)051<0999:ACOSAB>2.0.CO;2.
- Moore, C. J., 1986: Frequency response corrections for eddy correlation systems. *Bound.-Layer Meteor.*, **37**, 17–35, doi:10.1007/BF00122754.
- Nakai, T., and K. Shimoyama, 2012: Ultrasonic anemometer angle of attack errors under turbulent conditions. *Agric. For. Meteorol.*, **162–163**, 14–26, doi:10.1016/j.agrformet.2012.04.004.
- , M. K. Van der Molen, J. H. C. Gash, and Y. Kodama, 2006: Correction of sonic anemometer angle of attack errors. *Agric. For. Meteorol.*, **136**, 19–30, doi:10.1016/j.agrformet.2006.01.006.
- Newsom, R. K., R. Calhoun, D. Ligon, and J. Allwine, 2008: Linearly organized turbulence structures observed over a suburban area by dual-Doppler lidar. *Bound.-Layer Meteor.*, **127**, 111–130, doi:10.1007/s10546-007-9243-0.
- Oncley, S., and Coauthors, 2007: The Energy Balance Experiment EBEX-2000. Part I: Overview and energy balance. *Bound.-Layer Meteor.*, **123**, 1–28, doi:10.1007/s10546-007-9161-1.
- Panin, G. N., and Ch. Bernhofer, 2008: Parametrization of turbulent fluxes over inhomogeneous landscapes. *Izv. Atmos. Ocean. Phys.*, **44**, 701–716, doi:10.1134/S0001433808060030.
- , G. Tetzlaff, and A. Raabe, 1998: Inhomogeneity of the land surface and problems in the parameterization of surface fluxes in natural conditions. *Theor. Appl. Climatol.*, **60**, 163–178, doi:10.1007/s007040050041.
- Robinson, S. K., 1991: Coherent motions in the turbulent boundary layer. *Annu. Rev. Fluid Mech.*, **23**, 601–639, doi:10.1146/annurev.fl.23.010191.003125.
- Rose, T., S. Crewell, U. Löhnert, and C. Simmer, 2005: A network suitable microwave radiometer for operational monitoring of the cloudy atmosphere. *Atmos. Res.*, **75**, 183–200, doi:10.1016/j.atmosres.2004.12.005.

- Sakai, R. K., D. R. Fitzjarrald, and K. E. Moore, 2001: Importance of low-frequency contributions to eddy fluxes observed over rough surfaces. *J. Appl. Meteor.*, **40**, 2178–2192, doi:10.1175/1520-0450(2001)040<2178:IOLFCT>2.0.CO;2.
- Schmid, H. P., 1997: Experimental design for flux measurements: Matching scales of observations and fluxes. *Agric. For. Meteorol.*, **87**, 179–200, doi:10.1016/S0168-1923(97)00011-7.
- , C. S. B. Grimmond, F. Cropley, B. Offerle, and H. B. Su, 2000: Measurements of CO<sub>2</sub> and energy fluxes over a mixed hardwood forest in the mid-western United States. *Agric. For. Meteorol.*, **103**, 357–374, doi:10.1016/S0168-1923(00)00140-4.
- Schmidt, H., and U. Schumann, 1989: Coherent structure of the convective boundary layer derived from large-eddy simulations. *J. Fluid Mech.*, **200**, 511–562, doi:10.1017/S0022112089000753.
- Schmidt, M., T. G. Reichenau, P. Fiener, and K. Schneider, 2012: The carbon budget of a winter wheat field: An eddy covariance analysis of seasonal and inter-annual variability. *Agric. For. Meteorol.*, **165**, 114–126, doi:10.1016/j.agrformet.2012.05.012.
- Schotanus, P., F. T. M. Nieuwstadt, and H. A. R. de Bruin, 1983: Temperature measurement with a sonic anemometer and its application to heat and moisture fluxes. *Bound.-Layer Meteorol.*, **26**, 81–93, doi:10.1007/BF00164332.
- Staebler, R. M., and D. R. Fitzjarrald, 2004: Observing subcanopy CO<sub>2</sub> advection. *Agric. For. Meteorol.*, **122**, 139–156, doi:10.1016/j.agrformet.2003.09.011.
- Stawiariski, C., 2014: Optimizing dual-Doppler lidar measurements of surface layer coherent structures with large-eddy simulations. Ph.D. thesis, Karlsruhe Institute of Technology, 197 pp. [Available online at <http://digbib.ubka.uni-karlsruhe.de/volltexte/1000039726>.]
- , K. Trümmer, C. Knigge, and R. Calhoun, 2013: Scopes and challenges of dual-Doppler lidar wind measurements—An error analysis. *J. Atmos. Oceanic Technol.*, **30**, 2044–2062, doi:10.1175/JTECH-D-12-00244.1.
- Steinfeld, G., M. Letzel, S. Raasch, M. Kanda, and A. Inagaki, 2007: Spatial representativeness of single tower measurements and the imbalance problem with eddy-covariance fluxes: Results of a large-eddy simulation study. *Bound.-Layer Meteorol.*, **123**, 77–98, doi:10.1007/s10546-006-9133-x.
- Stoy, P. C., and Coauthors, 2013: A data-driven analysis of energy balance closure across FLUXNET research sites: The role of landscape scale heterogeneity. *Agric. For. Meteorol.*, **171–172**, 137–152, doi:10.1016/j.agrformet.2012.11.004.
- Swinbank, W. C., 1951: The measurement of vertical transfer of heat and water vapor by eddies in the lower atmosphere. *J. Meteorol.*, **8**, 135–145, doi:10.1175/1520-0469(1951)008<0135:TMOVTO>2.0.CO;2.
- Torrence, C., and G. P. Compo, 1998: A practical guide to wavelet analysis. *Bull. Amer. Meteor. Soc.*, **79**, 61–78, doi:10.1175/1520-0477(1998)079<0061:APGTWA>2.0.CO;2.
- Townsend, A. A., 1976: *The Structure of Turbulent Shear Flow*. Cambridge University Press, 429 pp.
- Trümmer, K., T. Damian, C. Stawiariski, and A. Wieser, 2014: Turbulent structures and coherence in the atmospheric surface layer. *Bound.-Layer Meteorol.*, doi:10.1007/s10546-014-9967-6, in press.
- Twine, T. E., and Coauthors, 2000: Correcting eddy-covariance flux underestimates over a grassland. *Agric. For. Meteorol.*, **103**, 279–300, doi:10.1016/S0168-1923(00)00123-4.
- Webb, E. K., G. I. Pearman, and R. Leuning, 1980: Correction of flux measurements for density effects due to heat and water vapour transfer. *Quart. J. Roy. Meteor. Soc.*, **106**, 85–100, doi:10.1002/qj.49710644707.
- Wiernga, J., 1993: Representative roughness parameters for homogeneous terrain. *Bound.-Layer Meteorol.*, **63**, 323–363, doi:10.1007/BF00705357.
- Wilczak, J., S. Oncley, and S. Stage, 2001: Sonic anemometer tilt correction algorithms. *Bound.-Layer Meteorol.*, **99**, 127–150, doi:10.1023/A:1018966204465.
- Wilson, K., and Coauthors, 2002: Energy balance closure at FLUXNET sites. *Agric. For. Meteorol.*, **113**, 223–243, doi:10.1016/S0168-1923(02)00109-0.
- Wohlfahrt, G., C. Irschick, B. Thalinger, L. Hörtnagl, N. Obojes, and A. Hammerle, 2010: Insights from independent evapotranspiration estimates for closing the energy balance: A grassland study. *Vadose Zone J.*, **9**, 1025–1033, doi:10.2136/vzj2009.0158.
- Zacharias, S., and Coauthors, 2011: A network of terrestrial environmental observatories in Germany. *Vadose Zone J.*, **10**, 955–973, doi:10.2136/vzj2010.0139.

## Appendix D

Eder F, De Roo F, Rotenberg E, Yakir D, Schmid HP, Mauder M (2015b) Secondary circulations at a solitary forest surrounded by semi-arid shrubland and their impact on eddy-covariance measurements. *Agric For Meteorol* 211:115-127

© Elsevier. Used with permission

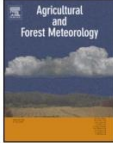
Agricultural and Forest Meteorology 211 (2015) 115–127



Contents lists available at [ScienceDirect](#)

## Agricultural and Forest Meteorology

journal homepage: [www.elsevier.com/locate/agrformet](http://www.elsevier.com/locate/agrformet)



## Secondary circulations at a solitary forest surrounded by semi-arid shrubland and their impact on eddy-covariance measurements



Fabian Eder<sup>a,b,\*</sup>, Frederik De Roo<sup>a</sup>, Eyal Rotenberg<sup>c</sup>, Dan Yakir<sup>c</sup>, Hans Peter Schmid<sup>a</sup>, Matthias Mauder<sup>a,b</sup>

<sup>a</sup> Institute of Meteorology and Climate Research, Atmospheric Environmental Research (IMK-IFU), Karlsruhe Institute of Technology (KIT), Kreuzackbahnstrasse 19, 82467 Garmisch-Partenkirchen, Germany

<sup>b</sup> Institute of Geography and Geoecology (IGG), Karlsruhe Institute of Technology (KIT), Kaiserstraße 12, 76131 Karlsruhe, Germany

<sup>c</sup> Department of Earth and Planetary Sciences (EPS), The Weizmann Institute of Science, Rehovot 76100, Israel

### ARTICLE INFO

#### Article history:

Received 4 December 2014

Received in revised form 26 May 2015

Accepted 1 June 2015

#### Keywords:

Eddy covariance  
Large-eddy simulation  
Lidar  
Ogive analysis  
Secondary circulation

### ABSTRACT

The Yatir forest in Israel is a solitary forest at the dry timberline that is surrounded by semi-arid shrubland. Due to its low albedo and its high surface roughness, the forest has a strong impact on the surface energy budget, and is supposed to induce a secondary circulation, which was assessed using eddy-covariance (EC) and Doppler lidar measurements and large-eddy simulation (LES). The buoyancy fluxes were 220–290 W m<sup>-2</sup> higher above the forest, and the scale of the forest relative to the boundary-layer height is ideal for generating a secondary circulation, as confirmed by a LES run without background wind. However, usually a relatively high background wind (6 m s<sup>-1</sup>) prevails at the site. Thus, with the Doppler lidar a persistent updraft above the forest was detected only on 5 of the 16 measurement days. Nevertheless, the secondary circulation and convective coherent structures caused low-frequency flux contributions in the mixed-layer *w* spectra, the surface layer *u* and *w* spectra and in the surface-layer momentum fluxes. According to the ogive functions from the tower data and a control volume approach using the LES, such low-frequency contributions with timescales >30 min were a major reason the non-closure of the energy balance at the desert site. In the roughness sublayer above the forest, these large structures were broken up into smaller eddies and the energy balance was closed.

© 2015 Elsevier B.V. All rights reserved.

### 1. Introduction

The convective atmospheric boundary layer is conceptually divided into a surface layer and a mixed layer or outer layer (Driedonks and Tennekes, 1984). The turbulence of the homogeneous surface layer under stationary convective conditions obeys Monin–Obukhov similarity theory. In addition, large convective coherent structures that scale with the height of the atmospheric boundary layer influence the horizontal wind component (Kaimal, 1978; Højstrup, 1981). They are often called ‘inactive motions’ because according to Townsend (1961) and Bradshaw (1967) they are imprints of large turbulent fluctuations originating from the outer layer and do not contribute to shear stress. The convective coherent structures are thermals (Wilczak and Tillman, 1980; Williams and Hacker, 1993), open cells (Kropfli and Hildebrand, 1980; Träumner et al., 2014) or, in case of background wind, as horizontal rolls (Etling and Brown, 1993; Drobinski et al., 1998; Maronga and Raasch, 2013) and typically have horizontal length scales of 1.5 times the boundary-layer height (Kaimal et al., 1976; Caughey and Palmer, 1979; Liu et al., 2011). However, homogeneous field conditions can rarely be met in reality, which complicates the application of universal scaling rules and the interpretation of boundary-layer measurements. Differences in surface roughness, temperature or moisture are supposed to create internal boundary layers (Garratt, 1990; Strunin et al., 2004), to induce advection on the surface-layer or boundary-layer scale (Raupach and Finnigan, 1995; Higgins et al., 2013) and, if the differences in surface properties are strong enough and if the surface patches are large enough, to induce secondary circulations (Mahfouf et al., 1987; Dalu and Pielke, 1993; Courault et al., 2007; van Heerwaarden and Vilà-Guerau de Arellano, 2008; Garcia-Carreras et al., 2010; Sührling and Raasch, 2013; Dixon et al., 2013; Kang and Lenschow, 2014; van Heerwaarden et al., 2014).

\* Corresponding author at: Institute of Meteorology and Climate Research, Atmospheric Environmental Research, Karlsruhe Institute of Technology, Kreuzackbahnstrasse 19, 82467 Garmisch-Partenkirchen, Germany. Tel.: +49 8821 183 137; fax: +49 8821 73573.

E-mail address: [fabian.eder@kit.edu](mailto:fabian.eder@kit.edu) (F. Eder).

<http://dx.doi.org/10.1016/j.agrformet.2015.06.001>  
0168-1923/© 2015 Elsevier B.V. All rights reserved.

Large-scale boundary-layer structures also have an effect on surface flux measurements conducted with the eddy covariance technique (Foken, 2008; Foken et al., 2011). The eddy-covariance (EC) method is very attractive for determining land-atmosphere exchange of energy and trace gases, since it does not disturb the ecosystem under investigation and the flux measurement operates on the ecosystem scale, i.e. it is representative of a larger area (Schmid, 1994; Baldocchi, 2003). However, this method generally does not close the energy balance at the earth's surface, which is called the energy balance closure problem (Foken, 2008). Accordingly, the energy balance ratio  $R$ , which is the sum of sensible heat flux  $Q_H$  and latent heat flux  $Q_E$  divided by net radiation  $-Q_S^*$  minus the ground heat flux  $Q_G$ ,

$$R = \frac{Q_H + Q_E}{-Q_S^* - Q_G}, \quad (1)$$

is usually smaller than unity. Multi-site analyses across different ecosystems have shown that energy balance ratios usually range between 0.7 and 0.9 (Wilson et al., 2002; Hendricks-Franssen et al., 2010; Stoy et al., 2013).

A potential reason for this is the non-consideration of fluxes carried by (i) turbulent structures with timescales larger than the averaging time of the EC system (Sakai et al., 2001; Turnipseed et al., 2002; Foken et al., 2006; Charuchittipan et al., 2014) or by (ii) secondary circulations that are bound to surface heterogeneities and do not move in space (Lee and Black, 1993; Mahrt, 1998; Hiyama et al., 2007). There are indications that the non-closure of the energy balance is related to the heterogeneity of the surrounding landscape (Mauder et al., 2007a; Panin and Bernhofer, 2008; Stoy et al., 2013), but experimental evidence that secondary circulations are an important transport mechanism in the surface layer is still lacking.

In this study, we aim to investigate the structure of the convective boundary layer above a well-defined surface heterogeneity. The Yatir forest in Israel is a planted pine forest with a scale of approximately 6–10 km, located in a semi-arid region at the dry timberline at the northern border of the Negev desert. Due to its low albedo and its increased surface roughness as compared to the semi-arid desert, the forest generates higher turbulent heat fluxes

than the adjacent desert (Rotenberg and Yakir, 2011). We hypothesize that the resulting spatial differences in surface buoyancy flux,

$$Q_B = Q_H \left( 1 + 0.61T \frac{c_p Q_E}{\lambda Q_H} \right), \quad (2)$$

where  $T$  is the temperature,  $c_p$  is specific heat of air at constant pressure and  $\lambda$  is the heat of vaporization (Schoanus et al., 1983; Charuchittipan et al., 2014), should drive a secondary circulation between the forest and the desert. For this reason, it will be investigated whether Yatir forest is large enough and whether the surface heat flux differences are strong enough to modify the convective boundary-layer dynamics and to induce a secondary circulation. Scaling approaches, ground-based remote sensing measurements, high-frequency 3d-wind measurements and large-eddy simulation (LES) will be used for this study. In particular, the role of secondary circulations for the measured surface energy balances at the forest and the desert site will be investigated. It is intended to provide evidence why the turbulent heat fluxes are likely to be underestimated by the EC method. For this purpose, wind spectra and ogive functions will be calculated and the LES model will be used to identify the missing flux components by considering the flux budget equation of virtual control volumes.

## 2. Methods

### 2.1. Research site

The measurements (Fig. 1) were taken at Yatir pine forest (31°20'43.1"N, 35°3'6.7"E, 660 m a.s.l.) and in the nearby semi-arid shrub land (31°19'6.5"N, 34°58'54.84"E, 461 m a.s.l.). The site lies in the transition zone between the Mediterranean climate and the semi-arid climate. The mean annual precipitation is 285 mm with a distinct dry summer period. The measurement campaign lasted from 21 August to 11 September 2013. As such, it took place more than 6 months after the last rain event in the area.

The Yatir forest is dominated by *Pinus halpensis* trees of 11 m height that were planted mostly from 1964 to 1969 and cover an area of about 2800 ha (Grünzweig et al., 2003; Rotenberg and Yakir, 2011). The surrounding area has been under grazing for at least several decades and is sparsely covered with shrubs and herbaceous annuals and perennials. Since the measurements were conducted at the end of the dry season, the major part of the semi-arid shrub-

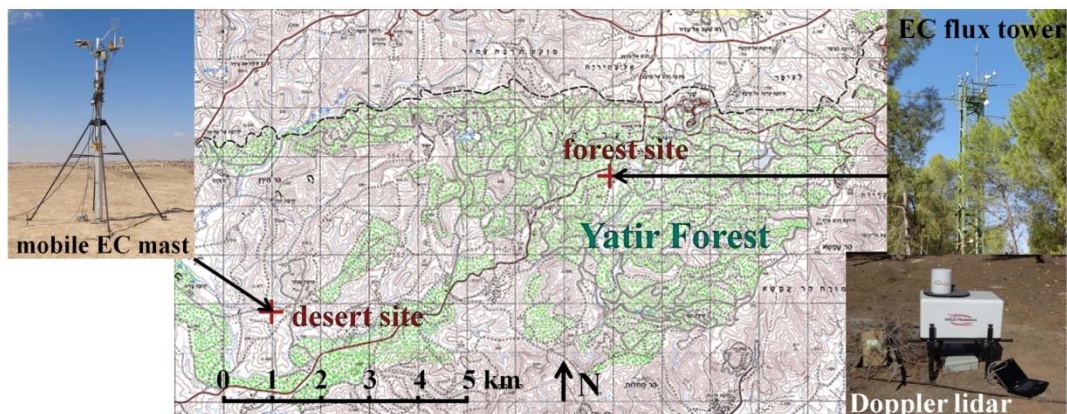


Fig. 1. Topographic map of the Yatir forest showing the locations of the measurement devices at the desert site and the forest site. Please note that there is no forest south and west of the desert site at present.

land was free of vegetation. For this reason, we will call the site that was located there a “desert” for simplicity.

The atmospheric boundary layer in the region is known to be influenced by cyclical large-scale synoptic weather variations (Dayan et al., 1988). The weather conditions during summer are dominated by the “Persian trough”, a surface low-pressure trough that extends from the Asian monsoon region through the Persian Gulf to the Aegean Sea (Ziv et al., 2004). It is responsible for the persistent north-westerly flow from the eastern Mediterranean to Israel, known as the Etesian winds. The Persian trough is capped by a subtropical anticyclone centred over North Africa and the Middle East, and the strength of that anticyclonic flow determines the depth of the trough and the mean boundary-layer depth in the region (Dayan et al., 2002). Furthermore, the boundary-layer development is also affected by the diurnal sea-breeze cycle. During daytime, a sea breeze from the Mediterranean Sea that acts like a weak cold front penetrates inland (Dayan et al., 1988; Dayan and Rodnizki, 1999). It is associated with a reduced boundary-layer depth (Levi et al., 2011).

## 2.2. Eddy-covariance and radiation measurements

In order to assess the energy balance and the turbulent heat fluxes at the forest site and the desert site, EC and radiation measurements were conducted. At the forest, data from the FLUXNET station “Yatir” (IL-Yat) were used (Fig. 1). A R3-50 sonic anemometer (Gill Instruments, UK) measured the wind vector and the sonic temperature, a LI-7000 gas analyzer (Licor Biogeosciences, USA) the water vapour and carbon dioxide concentration, two CM21 pyranometers (Kipp & Zonen, The Netherlands) the short-wave up- and down-welling radiation and two PIR pyrgeometers (Eppley lab, USA) the long-wave up- and down-welling radiation. The sonic and the inlet of the gas analyzer were mounted at a height of 19 m a.g.l., i.e. 8 m above the top of the forest canopy, the radiation sensors at 5 m above the top of the forest (Rotenberg and Yakir, 2011). The data were stored on a CR1000 data logger (Campbell Scientific, USA). In the desert, a small meteorological mast was operated (Fig. 1) that was equipped with a R3-100 sonic anemometer (Gill Instruments, UK), a LI-7200 gas analyzer (Licor Biogeosciences, USA), two CMP21 pyranometers (Kipp & Zonen, The Netherlands), two CGR4 pyrgeometers (Kipp & Zonen, The Netherlands) and a CR3000 data logger (Campbell Scientific, USA). The measurement height was 6 m a.g.l.

At both systems, the measurement frequency was 20 Hz. The post-field data processing according to Mauder et al. (2013) included a raw data delay correction based on the maximization of the cross-correlation, a spike removal based on median absolute deviation, a double rotation of the wind vector and corrections for the high-frequency spectral loss (Moore, 1986), the difference between sonic temperature and air temperature (Schotanus et al., 1983) and density fluctuations (Webb et al., 1980). The calculations were done with the software package TK3.11 (Mauder and Foken, 2011). For quality assurance and quality control (QA/QC), a three-class quality flagging scheme according to Mauder et al. (2013) was applied to the 30-min turbulent statistics and fluxes. In this study, data of moderate (flag 1) and highest quality (flag 0) were used.

## 2.3. Doppler lidar measurements

In addition to the micrometeorological measurements, a scanning Doppler wind lidar (Streamline, HaloPhotonics Ltd., U.K.) was operated next to the meteorological tower at the forest site (Fig. 1). It emits a pulsed laser light of 1.5  $\mu\text{m}$  wavelength at a pulse repetition frequency of 15 kHz and averages over 15000 pulses, i.e. its effective measurement frequency is approximately 1 Hz. The Doppler lidar determines the wind component along the optical

axis, the radial velocity, from the Doppler shift of the emitted laser pulse due to the movement of atmospheric particles relative to the device. During the measurement campaign, the Doppler lidar mainly pointed vertically upward into the atmosphere to measure profiles of the vertical wind component with a vertical resolution of 30 m. Every 30 min, a velocity azimuth display scan (Browning and Wexler, 1968) with 16 points was performed in order to measure the horizontal wind profile. Data from the lowest 60 m and data with poor quality, i.e. signal-to-noise ratios  $< -17$  dB, were discarded. For signal-to-noise ratios  $> -17$  dB, the measurement precision is better than  $0.2 \text{ m s}^{-1}$ , which was determined from the difference between lags 0 and 1 of the auto-covariance function (Lenschow and Kristensen, 1985; Frehlich, 2001). Moreover, the boundary-layer height  $z_i$  was determined from the maximum negative gradient in the backscatter intensity profile (Emeis et al., 2008).

## 2.4. Fourier and wavelet analysis

Fourier and wavelet analysis were performed in order to determine the mixed-layer and surface-layer velocity spectra using the 20-Hz sonic anemometer data of  $u$ ,  $v$  and  $w$ , and the 1-Hz Doppler lidar data of  $w$ , where  $u$  represents the along-wind,  $v$  the crosswind, and  $w$  the vertical wind component. At first, unreliable data were removed from the time series: lidar data with low signal-to-noise ratios (Section 2.3) and sonic data that were beyond the consistency limits (Mauder et al., 2013) or that were spikes according to median absolute deviation method. Time series from which more than 5% of the data had to be rejected were excluded from the analysis. The gaps were filled by means of linear interpolation and the high-frequency sonic data were rotated into the mean wind direction, i.e.  $\bar{v} = 0$ .

The Fourier transform was applied to the time series data in order to perform an ogive test, that was introduced by Desjardins et al. (1989) and applied to micrometeorological tower measurements by Foken et al. (1995) to test whether all low-frequency contributions are captured. This requires calculating the Fourier co-spectrum  $Co_{mn}$  of two time series  $m$  and  $n$  given as

$$Co_{mn}(f) = \Re(F_m^*(f)F_n(f)), \quad (3)$$

where  $F_m$  and  $F_n$  are the complex coefficients of the fast Fourier transforms of  $m$  and  $n$ ,  $f$  denotes the frequency, the asterisk denotes the complex conjugate and  $\Re$  indicates taking the real part (Stull, 1988). The ogive function  $og$  is the cumulative integral of the co-spectrum starting from the highest frequency  $f_{\max}$  (Foken et al., 2006),

$$og(f_0) = \int_{f_{\max}}^{f_0} Co_{mn}(f) df. \quad (4)$$

If the ogive function already converges for frequencies  $f_0 < 1/1800$  Hz, all turbulent motions are captured within 30 min, which was the averaging interval of the EC method.

The wavelet transform was applied to calculate the wind velocity spectra, because it resolves the time series in frequency and time domain and is also able to capture turbulent motions that do not pass by the measurement device regularly in time. The sonic data were block-averaged to 1 Hz in order to reduce the computation time. A continuous wavelet transform was applied using the Morlet mother wavelet with a frequency parameter of 6 (Torrence and Compo, 1998; Mauder et al., 2007b). The convolution of a time series  $m$  with the mother wavelet  $\Psi$  shifted by  $b$  and scaled by  $a$  gives the wavelet coefficients  $W_m(a, b)$ . The wavelet spectrum  $S_m(a)$

**Table 1**  
Overview of the LES configuration.

Surface heat flux ( $\text{K m s}^{-1}$ )	0.4 (forest); 0.16 (desert)
Roughness length (m)	2.0 (forest), 0.01 (desert)
Background wind ( $\text{m s}^{-1}$ )	0; 6
Initial boundary layer height (m)	1200
Number of grid points (-)	1200 × 1200 × 120
Domain size (m)	24000 × 24000 × 2400
Size of the forest rectangle (m)	10000 (lateral) × 6000 (longitudinal)
Time step (s)	1.8
Spatial resolution (m)	20
Simulation duration (h)	6

is obtained after squaring the wavelet coefficients and integrating over  $b$  (Hudgins et al., 1993),

$$S_m(a) = \frac{\delta j}{a} \frac{\delta t}{C_\delta} \frac{1}{N} \sum_{b=0}^{N-1} |W_m(a, b)|^2, \quad (5)$$

where  $\delta j = 0.25$  is the spacing between the scales of the wavelet transform,  $\delta t$  is the time step of the time series, and  $C_\delta = 0.776$  is a specific constant for the Morlet function (Torrence and Compo, 1998). In order to prevent edge effects, only those wavelet coefficients outside of the cone of influence were considered (Torrence and Compo, 1998). The integral over the wavelet spectrum is equal to the variance of the time series and integrating over parts of the spectrum gives the contributions of specific scales. Accordingly,

$$r_L = \frac{\sum_{a>\tau} S_m(a)}{\sum S_m(a)} \quad (6)$$

is the relative contribution of turbulent structures with time scales larger than  $\tau$ .

2.5. Large-eddy simulation

The LES model PALM v3.9 (Maronga et al., 2015) was used to evaluate the influence of the desert–forest system on the boundary-layer structure under idealized conditions (Table 1). The shape of the Yatir forest was approximated by a rectangular triangle. The difference between forest and desert was encoded in different surface fluxes and roughness lengths. We did not include an additional plant canopy layer for the forest, since we are primarily interested in the boundary-layer structure and circulations above the forest and desert. Also, we only ran dry simulations, because the humidity was practically negligible during the days of the measurement campaign. Another idealization was that the simulations took place in flat terrain, although in reality the terrain around the Yatir forest consists of moderate hills and it slowly rises for 200 m from the desert measurement station to that within the forest (Section 2.1). This idealization allowed us to disentangle the influence of surface parameters on the boundary layer structure from that by the topography.

In the horizontal, periodic boundary conditions were applied. The size of the domain was sufficiently large such that the forest did not interact with its periodic copies. At the upper boundary, the vertical velocity and the perturbation pressure were zero. At the lower boundary, the standard Prandtl layer parameterization of PALM was applied, using Monin–Obukhov similarity theory within the first grid cell. The simulations were initialized with a constant potential temperature of 305 K up to 1200 m, above which there was a capping inversion of 0.01  $\text{K m}^{-1}$ . We focused on two different cases: a simulation with zero background wind, and another with 6.0  $\text{m s}^{-1}$  background wind from the northwest, i.e. 315°, that is representative for the conditions during the measurement campaign. For detailed information on the LES model including the

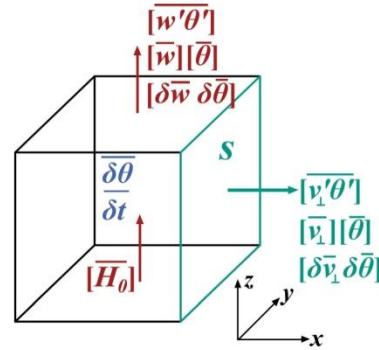


**Fig. 2.** Scheme describing control volume and corresponding flux components for the sensible heat flux. The flux through the lower face of the cube is the prescribed surface heat flux. Through each other face  $s$  of the cube, sensible heat is transported by the turbulent fluxes  $[\overline{v_\perp' \theta'}]$ , advection  $[\overline{w'} \theta']$  and dispersive fluxes  $[\overline{\delta v_\perp \delta \theta}]$ , where  $v_\perp$  is the velocity vector perpendicular to the corresponding face. For the upper face of the control volume,  $v_\perp$  is replaced by  $w$ , and  $[\overline{w' \theta'}]$  represents the EC flux at the top of the control volume. In addition potential temperature can be stored in the control volume over time, i.e.  $\frac{\partial \theta}{\partial t} \neq 0$ . The notation is according to the text.

boundary conditions, sub-grid and Prandtl layer parameterization, we refer to Maronga et al. (2015).

2.6. Control volume approach

In the LES model, the velocity vector field and the scalar fields are output at the spatial and temporal resolutions specified in Table 1. This offers the opportunity to set up a virtual cubic control volume (Fig. 2) around the measurement locations at the forest centre and in the desert and to calculate the complete flux budget equation for the sensible heat flux (Finnigan et al., 2003). Spatiotemporally averaging the equation for the potential temperature of PALM (Maronga et al., 2015) over the cubic control volume and over 30 min yields the budget equation

$$[\overline{H_0}] = [\overline{w' \theta'}] + \sum_s [\overline{v_\perp' \theta'}]_s + [\overline{w'} \theta'] + \sum_s [\overline{v_\perp \delta \theta}]_s + [\overline{\delta w \delta \theta}] + \sum_s [\overline{\delta_s v_\perp \delta_s \theta}]_s + \iiint \frac{\partial \theta}{\partial t} dx dy dz, \quad (7)$$

where  $H_0$  denotes prescribed surface heat flux,  $x$ ,  $y$  and  $z$  the Cartesian coordinates,  $w$  the wind component in  $z$  direction,  $\theta$  the potential temperature,  $v_\perp$  the velocity vector perpendicular to any lateral face  $s$  of the cube in the  $xz$ - or  $yz$ -plane. The angular brackets indicate the spatial average over the respective face of the cube, the  $\delta$  corresponding spatial fluctuations, the overbars temporal averages, the primes the temporal fluctuations. The term on the left-hand side of Eq. (7) is the 'true' surface heat flux, the terms of the right-hand side denote the EC flux at the top of the control volume, the horizontal flux divergence, the vertical and horizontal advection, the vertical and horizontal dispersive fluxes (Belcher et al., 2012) and the storage of  $\theta$  within the control volume. The parameterized sub-grid fluxes were added to the virtual EC flux and horizontal turbulent fluxes. For the present study, the side length of the cubic control volumes was chosen as 5 grid points and they were located at the forest centre and at the approximate location of the ceilometer in the desert.

**Table 2**  
Daytime (5–15 UTC) surface-layer parameters at the desert site and the forest site.

Date	$u_{\text{desert}}$ [m s <sup>-1</sup> ]	$u_{\text{forest}}$ [m s <sup>-1</sup> ]	$z/L_{\text{desert}}$ [-]	$z/L_{\text{forest}}$ [-]	$Bo_{\text{desert}}$ [-]	$Bo_{\text{forest}}$ [-]	$Q_{B,\text{desert}}$ [W m <sup>-2</sup> ]	$Q_{B,\text{forest}}$ [W m <sup>-2</sup> ]
22 August 2013	0.26	–	–2.17	–	11.1	–	140.1	–
23 August 2013	0.24	0.78	–0.91	–0.11	8.4	12.7	158.3	409.8
24 August 2013	0.27	0.75	–0.51	–0.10	9.7	15.8	158.6	278.3
25 August 2013	0.24	0.66	–0.97	–0.18	10.0	9.4	179.1	362.1
26 August 2013	0.28	0.76	–1.25	–0.37	21.9	10.5	169.2	415.4
27 August 2013	0.26	0.81	–0.76	–0.10	8.6	7.4	179.9	418.2
28 August 2013	0.21	0.78	–2.49	–0.11	3.7	24.7	157.5	438.8
29 August 2013	0.23	0.69	–1.25	–0.21	7.3	7.1	163.1	419.1
30 August 2013	–	0.72	–	–0.70	–	15.6	–	406.0
31 August 2013	–	0.65	–	–0.26	–	17.1	–	334.8
01 September 2013	0.24	–	–1.39	–	7.0	–	207.1	–
02 September 2013	0.23	–	–1.88	–	9.5	–	161.5	–
03 September 2013	0.22	0.70	–0.98	–0.20	7.4	15.9	156.2	415.6
04 September 2013	0.25	0.76	–0.70	–0.10	6.8	11.7	159.4	343.7
05 September 2013	0.26	0.87	–0.65	–0.09	7.7	–	163.9	–
06 September 2013	0.28	0.70	–1.07	–0.23	13.3	43.5	149.5	380.7
07 September 2013	0.26	0.74	–4.00	–0.17	12.0	14.7	182.5	443.2
08 September 2013	–	0.65	–	–0.17	–	9.5	–	399.2
09 September 2013	–	0.71	–	–0.20	–	16.1	–	400.5
10 September 2013	–	0.72	–	–0.28	–	10.6	–	342.9

$u$ : friction velocity;  $z$ : measurement height;  $L$ : Obukhov length;  $Bo$ : Bowen ratio;  $Q_B$ : surface buoyancy flux.

**Table 3**  
Daytime (5–15 UTC) boundary-layer parameters.

Date	$z_i$ [m]	$U$ [m s <sup>-1</sup> ]	$\phi$ [°]	$w_{\text{desert}}$ [m s <sup>-1</sup> ]	$w_{\text{forest}}$ [m s <sup>-1</sup> ]	$L_{\text{rau}}$ [m]
22 August 2013	1220	6.99	296	1.78	–	3830
23 August 2013	1000	7.05	310	1.72	2.20	2700
24 August 2013	1210	8.31	286	1.76	2.05	3360
25 August 2013	1160	5.61	311	1.83	2.20	2170
26 August 2013	1030	6.25	330	1.91	2.26	2450
27 August 2013	1010	6.84	345	1.75	2.19	2290
28 August 2013	790	5.87	329	1.53	2.10	2180
29 August 2013	780	6.68	310	1.63	2.01	1930
30 August 2013	–	5.55	337	–	2.05	–
31 August 2013	–	4.77	297	–	2.01	–
01 September 2013	900	5.25	286	1.71	–	–
02 September 2013	800	5.28	303	1.64	–	–
03 September 2013	820	5.91	325	1.68	2.17	1980
04 September 2013	930	6.67	285	1.68	1.96	2580
05 Sept 2013	–	6.74	312	1.70	2.43	–
09 Sept 2013	980	5.49	316	–	2.13	–
10 Sept 2013	1420	6.19	348	–	2.20	–

$z_i$ : boundary-layer height above the forest,  $U$ : mean wind speed at 200–500 m a.g.l.,  $\phi$ : mean wind direction at 200–500 m a.g.l.,  $w$ : convective velocity scale,  $L_{\text{rau}}$ : convective length scale according to Raupach and Finnigan (1995).

### 3. Results and discussion

#### 3.1. Surface turbulent heat fluxes and energy balance closure

The average daily cycles of net radiation and surface turbulent heat fluxes at both sites (Fig. 3) illustrate the extremely dry conditions in the area with a mean daytime Bowen-ratio of 8.4 at the desert site and 12.5 at the forest site. The results are in accordance with long-term measurements of Rotenberg and Yakir (2011) at the Yatir forest, who found Bowen-ratios larger than 10 and sensible heat fluxes up to 926 W m<sup>-2</sup> during summer. Fig. 3 also shows the increased sensible heat flux above the forest, for which several explanations can be found:

- Due to its low albedo (12.5%) as compared to the desert (33.7%), the forest reflects less shortwave radiation, e.g. about 200 W m<sup>-2</sup> less around noontime. In addition, the long-wave upwelling radiation at the forest is lower by about 100 W m<sup>-2</sup>. This sur-

plus of energy is mainly put into  $Q_H$  because of the extremely dry conditions.

- The high surface roughness length of the forest increases friction, which leads to an increased turbulence intensity above the forest site. As a result, the friction velocity at the forest site is about 3 times larger than at the desert site (Table 2). This increased turbulence intensity above the forest facilitates the vertical transfer of heat (Juang et al., 2007) which is known as the canopy convective effect (Rotenberg and Yakir, 2010, 2011).

Regarding the surface energy balance,  $Q_G$  was not measured, although it probably has a large amplitude, especially at the desert site (Heusinkveld et al., 2004). However, on a daily basis, and especially over a longer period,  $Q_G$  should be zero on average, because the energy that is stored in the soil during the day is released during the evening and the night. Leuning et al. (2012) confirmed that the ratios of  $(Q_H + Q_E)/(-Q_S^*)$  and  $(Q_H + Q_E)/(-Q_S^* - Q_G)$  on a daily time scale are equivalent. Accordingly, the average energy balance

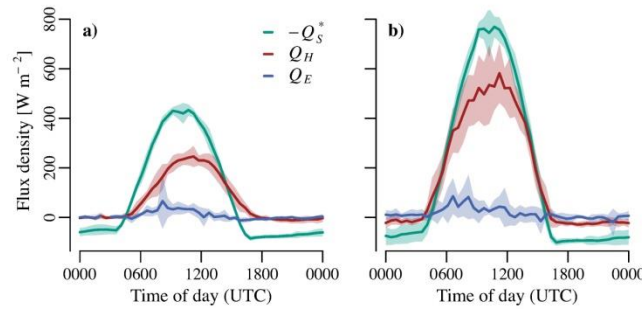


**Fig. 3.** Average net radiation  $-Q_s^*$ , sensible heat flux  $Q_H$  and latent heat flux  $Q_E$  at (a) the desert site and (b) the forest site between 22 August and 11 September 2013. The shaded areas indicate the standard deviation.

closure at both sites was calculated by integrating  $-Q_s^*$ ,  $Q_H$  and  $Q_E$  over the whole measurement campaign, and the energy balance was found to be not closed at the desert site ( $R = 0.81$ ) whilst it was closed at the forest site ( $R = 1.00$ ). Under the assumption that under these extremely dry conditions only  $Q_H$  and not  $Q_E$  is considerably underestimated, we could correct for this systematic error at the desert site by adding the complete ‘missing’ energy ( $0.19 Q_s^*$ ) to  $Q_H$ . This would increase the sensible heat flux above the desert by 20%.

Consequently, there is a difference in surface buoyancy  $Q_B$  (Eq. (2), Table 2) between forest and desert of about  $270\text{--}340\text{ W m}^{-2}$  during daytime, or of about  $220\text{--}290\text{ W m}^{-2}$  if we account for the underestimation of  $Q_H$  at the desert site. If the forest is large enough (Section 3.2), this might induce a secondary circulation (Section 3.3) that could affect in turn the measurements of the turbulent heat fluxes (Section 3.4).

### 3.2. Boundary-layer convective scaling

For generating secondary circulations, surface patches must be large enough to induce advection at the boundary-layer scale. In the convective boundary-layer, large eddies exchange air between the surface and boundary-layer top within a time scale of  $z_i/w_*$ , which is usually a few tens of minutes. Accordingly, the surface heterogeneity should be larger than the distance  $L_{\text{Rau}}$  that the flow travels during this mixing time scale (Raupach and Finnigan, 1995),

$$L_{\text{Rau}} = C_{\text{Rau}} \frac{U z_i}{w_*}, \quad (8)$$

where  $U$  is the mean wind speed of the well-mixed bulk of the convective boundary layer, which was determined from the wind profile of the Doppler lidar between 200 m and 500 m a.g.l. (Table 3), and  $C_{\text{Rau}} = 0.8$  (Mahrt, 2000) is a non-dimensional coefficient. The blending height concept (Mahrt, 2000) is an alternative method for estimating the minimum size of surface heterogeneities. However, this approach was not applicable for the convective boundary layer at the Yatir site, since it only considers vertical mixing due to shear-induced turbulence.

$L_{\text{Rau}}$  was calculated using the daytime averages of  $U$ ,  $z_i$  and  $w_*$  (Table 3). For most measurement days, it was found that the size of surface heterogeneities should be at least around 2–2.5 km. On 22 August and 24 August,  $L_{\text{Rau}}$  was  $>3$  km due to the relatively deep boundary layers on 22 August and 24 August and the relatively high wind speed on 24 August. The shape of the Yatir forest is approximately a triangle, with a size of 10 km in East–West direction and 6 km in North–South direction. Accordingly, it should be always large enough to generate secondary circulations. Furthermore, since the mean daytime boundary-layer height above the

forest was about 800–1400 m (Table 3) with maximum values of about 2000 m around noontime, the forest also fulfils the prerequisites by Patton et al. (2005) who found that heterogeneities with a size of around 4–9 times the boundary-layer height are most effective in generating secondary circulations. Recently, van Heerwaarden et al. (2014) stressed that the optimum ratio of heterogeneity size to boundary-layer height increases with increasing heat flux amplitude.

### 3.3. Secondary circulation above the forest

The surface buoyancy flux above Yatir forest is  $\sim 220\text{--}290\text{ W m}^{-2}$  larger than in the desert (Section 3.1) and that the forest is large enough to cause boundary-layer scale advection (Section 3.2). Accordingly, a secondary circulation might develop in that area, which was tested by means of LES and analyzing the wind measurements of the Doppler lidar and the sonic anemometers.

As described in Section 2.5, two different LES runs were performed, one with zero background wind and one with a background wind of  $6\text{ m s}^{-1}$  from 315° that is representative of the typical meteorological conditions during the measurement campaign (Table 3). The boundary-layer height was initialized with 1200 m (Section 2.5) and grew up to about 1500 m after 3 h of simulation. Thus, ratio of heterogeneity scale to boundary-layer height was about 5–7. The forest was encoded as an isolated patch with a larger surface heat flux that covered about 5% of the model domain and exhibited a 2.3 times higher surface buoyancy flux than the domain average that is almost equal to the desert buoyancy flux. For such heat-flux amplitudes, van Heerwaarden et al. (2014) confirmed the suggested ideal ratio of heterogeneity scale to boundary-layer height by Patton et al. (2005) of 4–9. For the zero-wind case (Fig. 4a,c), a strong updraft above the forest was found after 3 h of simulation with vertical wind speeds  $>3\text{ m s}^{-1}$  at the forest centre. The desert area showed hexagonal patterns that are typical for open cell convection (Schmidt and Schumann, 1989; Träumner et al., 2014). However, it seems that updrafts  $>2\text{ m s}^{-1}$  were suppressed within a distance of  $<5$  km from the forest border (Fig. 4c). Accordingly, at low wind speeds, the forest is able to induce meso-scale circulations similar to those which were detected with aircrafts above lakes in the boreal forest (Sun et al., 1997), above patches with different surface moisture in the Sahel region (Taylor et al., 2007; Garcia-Carreras et al., 2010) and the Great Plains, USA (Kang et al., 2007), or above irrigated agricultural land in arid regions (Mahrt et al., 1994; Wulfmeyer et al., 2014).

For the LES run with background wind (Fig. 4b,d), only a weak net updraft was found above the forest (Fig. 4b). The whole simulation domain was dominated by bands of up- and downdrafts

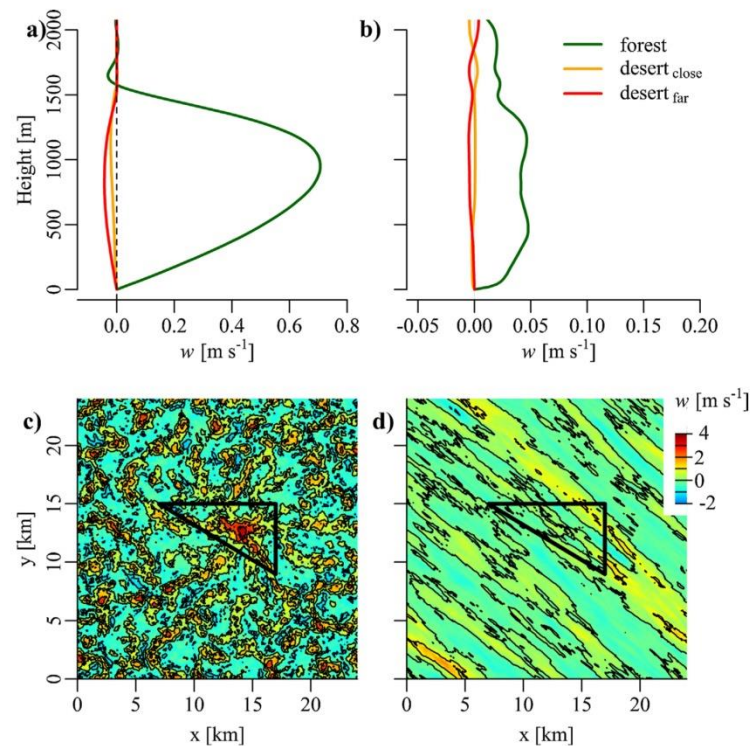


**Fig. 4.** The vertical wind component  $w$  from the LES runs without (a,c) and with geostrophic wind (b,d) after 3 h of simulation; panels (a) and (b) show the spatially-averaged profiles above the forest, above those parts of the desert that are within a distance of 10 km from the forest centre ( $\text{desert}_{\text{close}}$ ) and above those parts of the desert further away from the forest ( $\text{desert}_{\text{far}}$ ); panels (c) and (d) show an horizontal cross-section of 30-min averages of  $w$  at a height of approximately 0.6 z; the tick black lines in (c) and (d) show the location of the forest, i.e. the area with the increased surface heat flux.

with absolute vertical wind speeds mostly  $<1 \text{ m s}^{-1}$  (Fig. 4d) that could be traces of horizontal roll convection (Etling and Brown, 1993). There were slightly stronger updrafts ( $\bar{w} > 1 \text{ m s}^{-1}$ ) downwind of the forest, but all in all, the large-eddy-simulation did not provide clear evidence for a strong stationary secondary circulation between forest and desert under these wind conditions. This is in accordance with aircraft measurements of Dixon et al. (2013), who found that heterogeneity-induced circulations only existed up to background wind speeds of about  $5 \text{ m s}^{-1}$  (Dixon et al., 2013), and a LES study of Kang and Lenschow (2014), where background wind inhibited the formation of a heterogeneity-induced secondary circulation.

Then, the vertical wind velocity profiles above the forest measured with the Doppler lidar were analyzed in order to test whether they confirm the findings from the LES. According to the modelling results, the secondary circulation should be visible as a persistent vertical updraft above the forest. A persistent updraft was considered as (i) a mean vertical wind velocity  $>0.5 \text{ m s}^{-1}$  for (ii) at least a 3-h period and (iii) extending  $>500 \text{ m}$  in height. Persistent updrafts were found on 5 days during the measurement campaign (22 August, 30 August, 31 August, 1 September, 10 September) above the forest, although the mean horizontal wind speed ( $U$ ) was relatively high ( $4.8\text{--}7.0 \text{ m s}^{-1}$ ) on those days (Table 3). An example of a strong persistent updraft on 10 September is shown in Fig. 5a. Interestingly, relatively low wind speeds ( $<3 \text{ m s}^{-1}$ ) and low friction

velocities ( $<0.5 \text{ m s}^{-1}$ ) were measured at the forest tower during that event (Fig. 5b,c), which presumably allowed the development of a well-shaped secondary circulation. However, all these events occurred before 12 h UTC, i.e. before the onset of the sea breeze (Section 2.1) that usually arrives at the measurement site during the early afternoon hours. The sea breeze circulation is associated with higher wind speeds. The development of a distinct secondary circulation is weakened and the persistent updraft moves downwind of the forest (Fig. 4d).

In addition, it was tested whether such a secondary circulation becomes apparent as significant low-frequency contributions at atmospheric wind spectra. For this reason, wavelet spectra (Section 2.4) from the sonic anemometer data and the  $w$  time series of the vertically pointing Doppler lidar were investigated for time scales  $>30 \text{ min}$ . Here, we show examples from 25 August and from 27 August. We found low-frequency contributions to the  $w$  spectra in the entire mixed layer (Fig. 6a,d) and especially in the  $u$  and  $v$  spectra above the desert site (Fig. 6b,e). These low-frequency contributions could be either caused by a stationary secondary circulation between forest and desert that do not obey mixed-layer scaling (Kang, 2009), or by buoyancy-driven convective coherent structures that obey mixed-layer scaling (Kaimal et al., 1976; Kaimal, 1978; Højstrup, 1981; McNaughton, 2004). The measured spectra were also compared with the spectral model of Højstrup (1981) that explicitly considers the low-frequency contributions

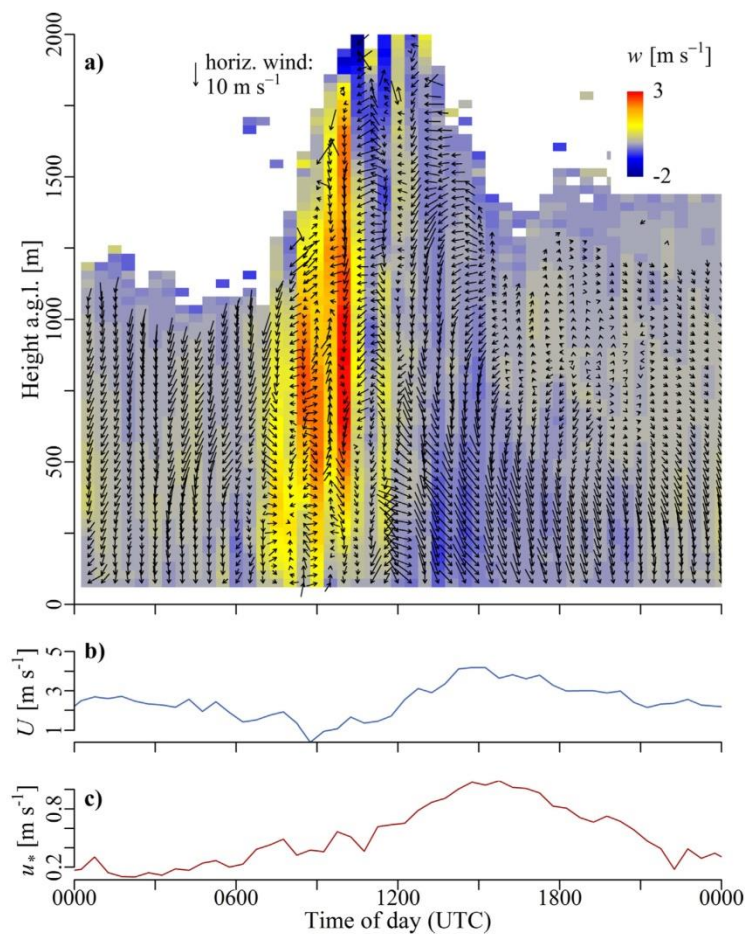


**Fig. 5.** Doppler lidar measurements of the wind field above the Yatir forest on 10 September 2013 (a); the arrows show the horizontal wind speed and wind direction, the colours indicate 30-min averages of the vertical wind component  $w$ ; panels (b) and (c) show the horizontal wind speed  $U$  and the friction velocity  $u_*$  measured with the sonic anemometer above the forest canopy.

of convective coherent structures to the surface-layer horizontal wind components. The data from the forest site show a good agreement with the model of Højstrup (1981), but the measured low-frequency contributions at the desert site were larger than predicted by the model, especially on 25 August. These additional contributions may originate from secondary circulations induced by the forest-desert heterogeneity, even though the Doppler lidar

did not show a mean vertical updraft above the forest on those days. Above the forest, the  $u$  and  $v$  spectra were shifted to higher frequencies, because in the roughness sublayer the convective coherent structures were less dominant and probably broken up into smaller organized structures (Raupach et al., 1996; Finnigan, 2000). Accordingly, the spectral ratios  $r_L$  (Eq. (6)) of the  $u$  and  $v$  spectra above the forest are significantly smaller than above the desert (Table 4). The

**Table 4**

Mean values of low-frequency contribution (time scales > 30 min)  $r_L$  to spectra of wind components above desert and forest for the whole measurement campaign.

Wind component	Instrument	Height a.g.l.	$r_L$ (desert)	$r_L$ (forest)
$u$	R3-50 sonic anemometer	6(19) <sup>a</sup> m	0.31 ± 0.08	0.11 ± 0.04
$v$	R3-50 sonic anemometer	6(19) <sup>a</sup> m	0.29 ± 0.07	0.12 ± 0.03
$w$	R3-50 sonic anemometer	6(19) <sup>a</sup> m	0.02 ± 0.01	0.01 ± 0.003
$w$	Streamline lidar	100 m	–	0.11 ± 0.07
$w$	Streamline lidar	400 m	–	0.13 ± 0.04
$w$	Streamline lidar	800 m	–	0.16 ± 0.08

<sup>a</sup> Measurement height of sonic anemometers was 6 m at the desert site and 19 m at the forest site.

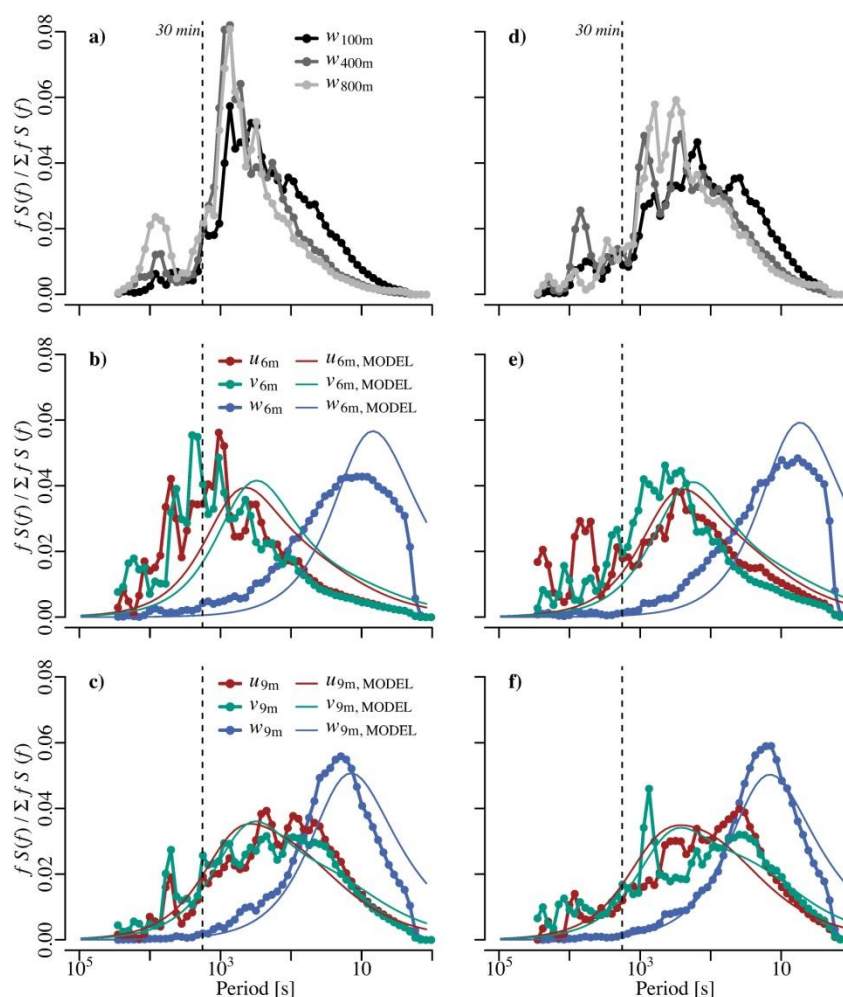


**Fig. 6.** Normalized wavelet spectra of the three wind components  $u$ ,  $v$  and  $w$  using the data from (a to c) 25 August and (d to f) 27 August 2014. The mixed-layer  $w$  spectra (a,d) were determined from the Streamline data, the surface-layer spectra above (d,e) the desert and (c,f) the forest from the sonic anemometer measurements. The surface-layer spectra were compared with the spectral model of Højstrup (1981). The vertical dashed line indicates a period of 30 min which was the averaging time for the EC measurements.

$w$  spectra from the surface layer did not show any significant low-frequency contribution (Table 3, Fig. 6) which is in accordance with the spectral model. To sum up, we found significant low-frequency contributions, especially in the surface-layer  $u$  and  $v$  spectra that are most likely caused by convective coherent structures, and, to a lesser extent, also by a stationary secondary circulation between the forest and the desert.

#### 3.4. Implications for flux measurements and energy balance closure

As presented in the previous section, convective coherent structures and secondary circulations induce low-frequency con-

tributions to the surface-layer horizontal wind spectra with time scales larger than the averaging time of the EC systems. The low-frequency contributions above the desert site were larger than above the forest site at the respective measurement levels of the EC systems (Table 4). Hence, the energy balance at the desert site was not closed, while it was closed at the forest site (Section 3.1).

This relation suggests that the averaging time of 30 min is not sufficient to capture all atmospheric motions contributing to surface-atmosphere exchange. In order to verify this assumption, ogive functions for the desert site and the forest site were calculated (Section 2.4). Here, the ogives were calculated using the daytime measurements between 7 and 15 UTC for the momentum

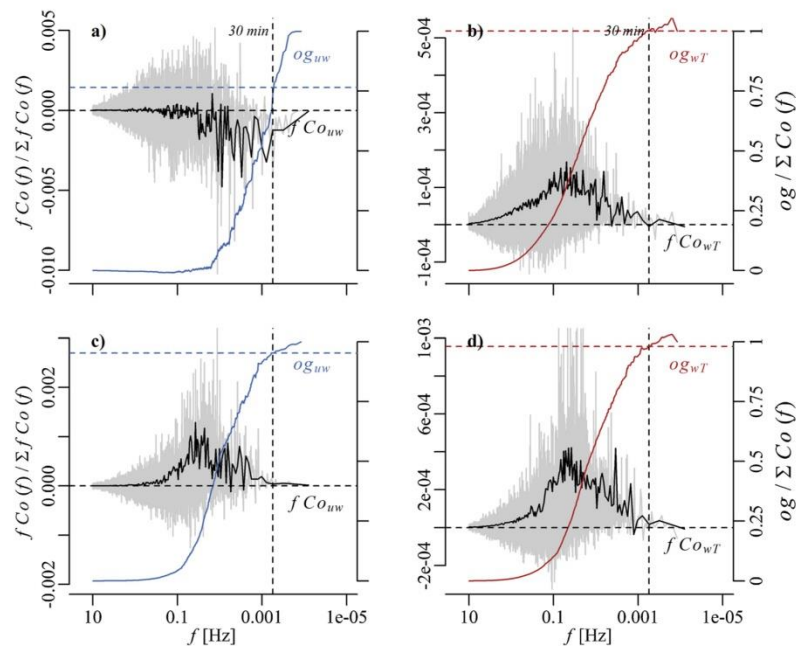


**Fig. 7.** Fourier co-spectra and ogive functions normalized by the co-spectrum for momentum flux (a,c) and sensible heat flux (b,d) at the desert site (a,b) and the forest site (c,d) on 25 August 2013. For this analysis only periods up to 3 h were considered. The grey line indicates the original co-spectrum, the black line the smoothed co-spectrum, the solid coloured lines the normalized ogive function, and the horizontal dashed line the respective value of the ogive function at a period of 30 min.

flux following Foken et al. (2006) and for the sensible heat flux, by considering all frequencies up to a period of 3 h. Fig. 7 shows examples of co-spectra and ogive functions for 25 August, and these results are representative for the whole measurement campaign. For the momentum flux at the desert site, the ogive function was not convergent within 30 min, but it was convergent at the forest site. For the sensible heat flux, both ogives were convergent within 30 min. Thus, the ogive test does not indicate any significant low-frequency contribution to the sensible heat flux. However, this is not surprising since the surface-layer  $w$  spectra did not show any low-frequency contributions (Section 3.3, Fig. 6). In the surface layer, the horizontal wind components are affected by the secondary circulation and the convective coherent structures. For this reason, the ogive function of the momentum flux at the desert site does not converge and we expect that the horizontal sensible heat fluxes  $u\overline{T'}$  and  $v\overline{T'}$  are similarly affected by the secondary circulations. In other words, we expect that the low-frequency circulations at the desert site cause advection and horizontal flux divergence (Finnigan et al., 2003; Foken et al., 2010, 2011), but the calculation of the co-spectra of  $u$  and  $T$  and of  $v$  and  $T$  did not provide any meaningful result. Moreover, a stationary secondary circulation between the forest and the desert with a lifetime >3 h could not be captured with this approach that is based on a point measurement.

Our results are different from the results of Heusinkveld et al. (2004) from measurements in the nearby Negev desert. They did not find any significant low-frequency contributions to the fluxes and they were able to close the energy balance. However, Heusinkveld et al. (2004) conducted their measurements further

inside the desert, and far away from any pronounced surface heterogeneity like the Yatir forest. Thus, at their site, secondary circulations were probably not relevant. No significant low-frequency contributions affected the surface-layer measurements and consequently, the energy balance was closed.

Furthermore, LES offers the possibility to calculate the complete flux budget (Finnigan et al., 2003), following the control volume approach presented in Section 2.6. This was done for one control volume above the desert site (Fig. 8a) and one above the forest site (Fig. 8b) using the model run with a background wind of  $6 \text{ m s}^{-1}$ . The LES reproduces that, above the forest, the sensible heat flux estimate using the EC method is identical to the surface sensible heat flux, i.e. the turbulent fluxes are not underestimated and the energy balance should be closed. At the desert site, the virtual EC flux underestimates the surface sensible heat flux by 30%. This underestimation at the desert site is due to net advection of sensible heat out of the control volume. The forest site is also subject to a net advection of sensible heat into its control volume, but this is compensated by the horizontal flux divergence. However, it should be noted that no canopy layer and thus to roughness sublayer was represented in the LES model and the top of the control volumes was at 100 m a.g.l. due to the coarse grid resolution. Nevertheless, this approach successfully reproduces that the EC method tends to systematically underestimate the surface heat fluxes at the desert site, but not at the forest site, and that advection is a major reason. This advection is caused by turbulent structures with timescales larger than 30 min that become apparent as low-frequency contributions to the horizontal wind spectra in the surface layer (Fig. 6) and to the surface-layer momentum flux (Fig. 7).

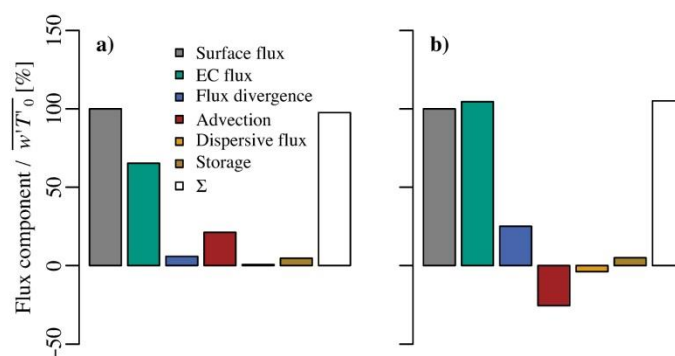


Fig. 8. Components of the sensible heat flux budget normalized by the prescribed surface flux determined from the LES control volume method for the desert site (a) and the forest site (b) for a background wind of  $6 \text{ m s}^{-1}$ ; the  $\Sigma$  indicates the sum of the EC flux, flux divergence, advection, dispersive flux and storage components.

#### 4. Conclusions

Due to its isolated location, the Yatir forest represents a pronounced surface heterogeneity that is an ideal natural laboratory for investigating secondary circulations and its affect on micrometeorological measurements under constant fair weather conditions. Because of its low albedo and its increased surface roughness, the forest creates higher turbulent heat fluxes which results in horizontal surface buoyancy flux differences of  $220\text{--}290 \text{ W m}^{-2}$ . Moreover, the forest has dimensions of about 5 times the usual boundary-layer height, which is ideal for inducing a strong secondary circulation (Patton et al., 2005). Moreover, it is larger than the convective length scale of Raupach and Finnigan (1995) and is thus able to modify the complete overlying atmospheric boundary layer.

The LES run without background wind confirmed the development of a secondary circulation that becomes apparent as a strong persistent updraft above the forest. However, in the Doppler lidar measurements, such persistent vertical updrafts were only found on 5 of 16 measurements days, during hours with relatively low wind speeds. The LES confirmed that, with a common background flow of  $6 \text{ m s}^{-1}$ , the vertical velocity field is dominated by convective coherent structures that are not related to the surface heterogeneity. The weak updraft downwind of the forest could not be captured with a single Doppler lidar located at the forest centre.

Secondary circulations and convective coherent structures are responsible for the underestimation of the turbulent fluxes by 19% at the desert site. The associated low-frequency contributions with timescales  $>30 \text{ min}$  cannot be captured with the standard EC method. The ogive test indicated low-frequency contributions to co-spectrum of  $u$  and  $w$ , but not to the co-spectrum  $w$  and  $T$ . Our data suggest that the 'missing' energy is mainly contained in advection and the horizontal fluxes and not in the low frequencies of the vertical turbulent fluxes. Analyzing the complete flux budget of a virtual control volume in the LES model confirmed that the low-frequency structures cause considerable advection at the desert site that is responsible for the non-closure of the energy balance. Above the forest, the surface-layer spectra are shifted to higher frequencies, all ogive functions converge within 30 min, and the energy balance is closed, presumably because the large eddies are broken up into smaller structures in the roughness sublayer of the forest.

Thus, it could be shown that differences in landuse do not only have a strong effect on the local energy budget, but also affect the structure of the overlying boundary layer. The afforestation efforts in the Yatir area probably also modify the local boundary-layer height, the cloud formation and the regional weather and climate.

Furthermore, secondary circulations are not restricted to special sites like the Yatir forest. Such effects could occur in every landscape that is characterized by sufficiently large surface patches that have different surface buoyancy fluxes, e.g. due to differences in surface moisture, different agricultural crops or in urban areas. For investigating the effects of landuse on boundary-layer properties, a careful selection of the measurement location is required. We recommend performing a simple numerical simulation in advance of the campaign for this purpose. Moreover, an integrated approach using surface flux measurements, ground-based remote sensing measurements and numerical simulation gives the best insights into the processes at work.

#### Acknowledgements

The authors would like to thank the staff from the Department of Earth and Planetary Sciences of the Weizmann Institute of Science for the assistance during the field campaign. This work was conducted within the Helmholtz Young Investigator Group "Capturing all relevant scales of biosphere-atmosphere exchange – the enigmatic energy balance closure problem", which is funded by the Helmholtz-Association through the President's Initiative and Networking Fund, and by KIT.

#### References

- Baldocchi, D.D., 2003. Assessing the eddy covariance technique for evaluating carbon dioxide exchange rates of ecosystems: past, present and future. *Glob. Change Biol.* 9, 479–492.
- Belcher, S.E., Harman, I.N., Finnigan, J.J., 2012. The wind in the willows: flows in forest canopies in complex terrain. *Annu. Rev. Fluid Mech.* 44, 479–504.
- Bradshaw, P., 1967. 'Inactive' motion and pressure fluctuations in turbulent boundary layers. *J. Fluid Mech.* 30, 241–258.
- Browning, K.A., Wexler, R., 1968. The determination of kinematic properties of a wind field using Doppler radar. *J. Appl. Meteorol.* 7, 105–113.
- Caughey, S.J., Palmer, S.G., 1979. Some aspects of turbulence structure through the depth of the convective boundary layer. *Q.J.R. Meteorol. Soc.* 105, 811–827.
- Charuchittipan, D., Babel, W., Mauder, M., Leps, J.P., Foken, T., 2014. Extension of the averaging time in eddy-covariance measurements and its effect on the energy balance closure. *Bound. Layer Meteorol.* 152, 303–327.
- Courault, D., Drobinski, P., Brunet, Y., Lacarrere, P., Talbot, C., 2007. Impact of surface heterogeneity on a buoyancy-driven convective boundary layer in light winds. *Bound. Layer Meteorol.* 124, 383–403.
- Dalu, G.A., Pielke, R.A., 1993. Vertical heat fluxes generated by mesoscale atmospheric flow induced by thermal inhomogeneities in the PBL. *J. Atmos. Sci.* 50, 919–926.
- Dayan, U., Shenav, R., Graber, M., 1988. The spatial and temporal behavior of the mixed layer in Israel. *J. Appl. Meteorol.* 27, 1382–1394.
- Dayan, U., Rodnizki, J., 1999. The temporal behavior of the atmospheric boundary layer in Israel. *J. Appl. Meteorol.* 38, 830–836.

- Desjardins, R.L., MacPherson, J.I., Schuepp, P.H., Karanja, F., 1989. An evaluation of aircraft flux measurements of CO<sub>2</sub>, water vapor and sensible heat. *Bound. Layer Meteorol.* 47, 55–69.
- Dixon, N.S., Parker, D.J., Taylor, C.M., Garcia-Carreras, L., Harris, P.P., Marsham, J.H., Polcher, J., Woolley, A., 2013. The effect of background wind on mesoscale circulations above variable soil moisture in the Sahel. *Q.J.R. Meteorol. Soc.* 139, 1009–1024.
- Driedonks, A.G.M., Tennekes, H., 1984. Entrainment effects in the well-mixed atmospheric boundary layer. *Bound. Layer Meteorol.* 30, 75–105.
- Drobinski, P., Brown, R., Flamant, P., Pelon, J., 1998. Evidence of organized large eddies by ground-based Doppler lidar, sonic anemometer and sodar. *Bound. Layer Meteorol.* 88, 343–361.
- Emeis, S., Schäfer, K., Münkel, C., 2008. Surface-based remote sensing of the mixing-layer height – a review. *Meteorol. Z.* 17, 621–630.
- Etling, D., Brown, R.A., 1993. Roll vortices in the planetary boundary layer: a review. *Bound. Layer Meteorol.* 65, 215–248.
- Finnigan, J.J., Clement, R., Malhi, Y., Leuning, R., Cleugh, H.A., 2003. A re-evaluation of long-term flux measurement techniques part I: averaging and coordinate rotation. *Bound. Layer Meteorol.* 107, 1–48.
- Finnigan, J., 2000. Turbulence in plant canopies. *Annu. Rev. Fluid Mech.* 32, 519–571.
- Foken, T., Dlugi, R., Kramm, G., 1995. On the determination of dry deposition and emission of gaseous compounds at the biosphere-atmosphere interface. *Meteorol. Z.* 4, 91–118.
- Foken, T., Wimmer, F., Mauder, M., Thomas, C., Liebethal, C., 2006. Some aspects of the energy balance closure problem. *Atmos. Chem. Phys.* 6, 4395–4402.
- Foken, T., 2008. The energy balance closure problem: an overview. *Ecol. Appl.* 18, 1351–1367.
- Foken, T., Aubinet, M., Finnigan, J.J., Leclerc, M.Y., Mauder, M., Paw, U.K.T., 2011. Results of a panel discussion about the energy balance closure correction for trace gases. *Bull. Am. Meteorol. Soc.* 92, ES13–ES18.
- Foken, T., Mauder, M., Liebethal, C., Wimmer, F., Beyrich, F., Leps, J.P., Raasch, S., DeBruin, H., Meijninger, W., Bange, J., 2010. Energy balance closure for the LITFASS-2003 experiment. *Theor. Appl. Climatol.* 101, 149–160.
- Frehlich, R., 2001. Estimation of velocity error for Doppler lidar measurements. *J. Atmos. Oceanic Technol.* 18, 1628–1639.
- Garcia-Carreras, L., Parker, D.J., Taylor, C.M., Reeves, C.E., Murphy, J.G., 2010. Impact of mesoscale vegetation heterogeneities on the dynamical and thermodynamic properties of the planetary boundary layer. *J. Geophys. Res.* Atmos. 115, D03102.
- Garratt, J.R., 1990. The internal boundary layer – a review. *Bound. Layer Meteorol.* 50, 171–203.
- Grünzweig, J.M., Lin, T., Rotenberg, E., Schwartz, A., Yakir, D., 2003. Carbon sequestration in arid-land forest. *Glob. Change Biol.* 9, 791–799.
- Hendricks-Franssen, H.J., Stöckli, R., Lehner, I., Rotenberg, E., Seneviratne, S.I., 2010. Energy balance closure of eddy-covariance data: a multisite analysis for European FLUXNET stations. *Agric. For. Meteorol.* 150, 1553–1567.
- Heusinkveld, B.G., Jacobs, A.F.G., Holtslag, A.A.M., Berkowicz, S.M., 2004. Surface energy balance closure in an arid region: role of soil heat flux. *Agric. For. Meteorol.* 122, 21–37.
- Higgins, C.W., Pardyjak, E., Froidevaux, M., Simeonov, V., Parlange, M.B., 2013. Measured and estimated water vapor advection in the atmospheric surface layer. *J. Hydrometeorol.* 14, 1966–1972.
- Hiyama, T., Strunin, M.A., Tanaka, H., Ohta, T., 2007. The development of local circulations around the Lena river and their effect on tower-observed energy imbalance. *Hydrol. Process.* 21, 2038–2048.
- Højstrup, J., 1981. A simple model for the adjustment of velocity spectra in unstable conditions downstream of an abrupt change in roughness and heat flux. *Bound. Layer Meteorol.* 21, 341–356.
- Hudgins, L.E., Mayer, M.E., Fricke, C.A., 1993. Fourier and wavelet analysis of atmospheric turbulence. In: Meyers, E., Roques, S. (Eds.), *Progress in Wavelet Analysis and Applications*. Editions Frontiers, Gif-sur-Yvette, France, pp. 491–498.
- Juang, J.Y., Katul, G., Siqueira, M., Stoy, P., Novick, K., 2007. Separating the effects of albedo from eco-physiological changes on surface temperature along a successional chronosequence in the southeastern United States. *Geophys. Res. Lett.* 34, L21408.
- Kaimal, J.C., 1978. Horizontal velocity spectra in an unstable surface layer. *J. Atmos. Sci.* 35, 18–24.
- Kaimal, J.C., Wyngaard, J.C., Haugen, D.A., Coté, O.R., Izumi, Y., Caughey, S.J., Readings, C.J., 1976. Turbulence structure in the convective boundary layer. *J. Atmos. Sci.* 33, 2152–2169.
- Kang, S.L., Lenschow, D.H., 2014. Temporal evolution of low-level winds induced by two-dimensional mesoscale surface heat-flux heterogeneity. *Bound. Layer Meteorol.* 151, 501–529.
- Kang, S.-L., 2009. Temporal oscillations in the convective boundary layer forced by mesoscale surface heat-flux variations. *Bound. Layer Meteorol.* 132, 59–81.
- Kang, S.-L., Davis, K.J., LeMone, M., 2007. Observations of the ABL structures over a heterogeneous land surface during IHOP-2002. *J. Hydrometeorol.* 8, 221–244.
- Kropfli, R.A., Hildebrand, P.H., 1980. Three-dimensional wind measurements in the optically clear planetary boundary layer with dual-Doppler radar. *Radio Sci.* 15, 283–296.
- Lee, X., Black, T.A., 1993. Atmospheric turbulence within and above a douglas-fir stand. Part II: eddy fluxes of sensible heat and water vapour. *Bound. Layer Meteorol.* 64, 369–389.
- Lenschow, D.H., Kristensen, L., 1985. Uncorrelated noise in turbulence measurements. *J. Atmos. Oceanic Technol.* 2, 68–81.
- Leuning, R., van Gorsel, E., Massman, W.J., Isaac, P.R., 2012. Reflections on the surface energy imbalance problem. *Agric. For. Meteorol.* 156, 65–74.
- Levi, Y., Shilo, E., Setter, I., 2011. Climatology of a summer coastal boundary layer with 1290-MHz wind profiler radar and a WRF simulation. *J. Appl. Meteorol. Climatol.* 50, 1815–1826.
- Liu, G., Sun, J., Yin, L., 2011. Turbulence characteristics of the shear-free convective boundary layer driven by heterogeneous surface heating. *Bound. Layer Meteorol.* 140, 57–71.
- Mahfouf, J.F., Richard, E., Mascart, P., 1987. The influence of soil and vegetation on the development of mesoscale circulations. *J. Clim. Appl. Meteorol.* 26, 1483–1495.
- Mahrt, L., 1998. Flux sampling errors for aircraft and towers. *J. Atmos. Oceanic Technol.* 15, 416–429.
- Mahrt, L., 2000. Surface heterogeneity and vertical structure of the boundary layer. *Bound. Layer Meteorol.* 96, 33–62.
- Mahrt, L., Sun, J., Vickers, D., MacPherson, J.I., Pederson, J.R., Desjardins, R.L., 1994. Observations of fluxes and inland breezes over a heterogeneous surface. *J. Atmos. Sci.* 51, 2484–2499.
- Maronga, B., Gryschka, M., Heinze, R., Hoffmann, F., Kanani-Sühring, F., Keck, M., Ketelsen, K., Letzel, M.O., Sühring, M., Raasch, S., 2015. The parallelized large-eddy simulation model (PALM) version 4.0 for atmospheric and oceanic flows: model formulation recent developments, and future perspectives. *Geosci. Model Dev. Discuss.* 8, 1539–1637.
- Maronga, B., Raasch, S., 2013. Large-eddy simulations of surface heterogeneity effects on the convective boundary layer during the LITFASS-2003 experiment. *Bound. Layer Meteorol.* 146, 17–44.
- Mauder, M., Jegede, O.O., Okogbue, E.C., Wimmer, F., Foken, T., 2007a. Surface energy balance measurements at a tropical site in West Africa during the transition from dry to wet season. *Theor. Appl. Climatol.* 89, 171–183.
- Mauder, M., Desjardins, R.L., MacPherson, I., 2007b. Scale analysis of airborne flux measurements over heterogeneous terrain in a boreal ecosystem. *J. Geophys. Res.* 112, D13112.
- Mauder, M., Cuntz, M., Drüe, C., Graf, A., Rebmann, C., Schmid, H.P., Schmidt, M., Steinbrecher, R., 2013. A strategy for quality and uncertainty assessment of long-term eddy-covariance measurements. *Agric. For. Meteorol.* 169, 122–135.
- Mauder, M., Foken, T., 2011. Documentation and Instruction Manual of the Eddy-Covariance Software Package TK3. University of Bayreuth, Department of Micrometeorology, Arbeitsergebnisse 46, Bayreuth, Germany.
- McNaughton, K.G., 2004. Turbulence structure of the unstable atmospheric surface layer and transition to the outer layer. *Bound. Layer Meteorol.* 112, 199–221.
- Moore, C.J., 1986. Frequency response corrections for eddy correlation systems. *Bound. Layer Meteorol.* 37, 17–35.
- Panin, G.N., Bernhofer, Ch., 2008. Parametrization of turbulent fluxes over inhomogeneous landscapes. *Izv. Atmos. Oceanic Phys.* 44, 701–716.
- Patton, E.G., Sullivan, P.P., Moeng, C.H., 2005. The influence of idealized heterogeneity on wet and dry planetary boundary layers coupled to the land surface. *J. Atmos. Sci.* 62, 2078–2097.
- Raupach, M.R., Finnigan, J.J., 1995. Scale issues in boundary-layer meteorology: surface energy balances in heterogeneous terrain. *Hydrol. Process.* 9, 589–612.
- Raupach, M.R., Finnigan, J.J., Brunet, Y., 1996. Coherent eddies and turbulence in vegetation canopies: the mixing-layer analogy. *Bound. Layer Meteorol.* 78, 351–382.
- Rotenberg, E., Yakir, D., 2010. Contribution of semi-arid forests to the climate system. *Science* 327, 451–454.
- Rotenberg, E., Yakir, D., 2011. Distinct patterns of changes in surface energy budget associated with forestation in the semiarid region. *Glob. Change Biol.* 17, 1536–1548.
- Sakai, R.K., Fitzjarrald, D.R., Moore, K.E., 2001. Importance of low-frequency contributions to eddy fluxes observed over rough surfaces. *J. Appl. Meteorol.* 40, 2178–2192.
- Schmid, H.P., 1994. Source areas for scalars and scalar fluxes. *Bound. Layer Meteorol.* 67, 293–318.
- Schmidt, H., Schumann, U., 1989. Coherent structure of the convective boundary layer derived from large-eddy simulations. *J. Fluid Mech.* 200, 511–562.
- Schotanus, P., Nieuwstadt, F.T.M., de Bruin, H.A.R., 1983. Temperature measurement with a sonic anemometer and its application to heat and moisture fluxes. *Bound. Layer Meteorol.* 26, 81–93.
- Stoy, P.C., Mauder, M., Foken, T., Marcolla, B., Boegh, E., Ibróm, A., Arain, M.A., Arneth, A., Aurela, M., Bernhofer, C., Cescaati, A., Dellwik, E., Duce, P., Gianelle, D., van Gorsel, E., Kiely, G., Knohl, A., Margolis, H., McCaughey, H., Merbold, L., Montagnani, L., Papale, D., Reichstein, M., Saunders, M., Serrano-Ortiz, P., Sottocornola, M., Spano, D., Vaccari, F., Varlagin, A., 2013. A data-driven analysis of energy balance closure across fluxnet research sites: the role of landscape scale heterogeneity. *Agric. For. Meteorol.* 171–172, 137–152.
- Strunin, M.A., Hiyama, T., Asanuma, J., Ohta, T., 2004. Aircraft observations of the development of thermal internal boundary layers and scaling of the convective boundary layer over non-homogeneous land surfaces. *Bound. Layer Meteorol.* 111, 491–522.
- Stull, R.B., 1988. *An Introduction to Boundary Layer Meteorology*. Kluwer Academic Publishers, Dordrecht.
- Sühring, M., Raasch, S., 2003. Heterogeneity-induced heat flux patterns in the convective boundary layer: can they be detected from observations and is there a blending height? A large-eddy simulation study for the LITFASS-2003 experiment. *Bound. Layer Meteorol.* 148, 309–331.

- Sun, J., Lenschow, D.H., Mahrt, L., Crawford, T.L., Davis, K.J., Oncley, S.P., MacPherson, I.J., Wang, Q., Dobosy, R.J., Desjardins, R.L., 1997. Lake-induced atmospheric circulations during boreas. *J. Geophys. Res.* 102, 29155–29166.
- Taylor, C.M., Parker, D.J., Harris, P.P., 2007. An observational case study of mesoscale atmospheric circulations induced by soil moisture. *Geophys. Res. Lett.* 34, L15801.
- Torrence, C., Compo, G.P., 1998. A practical guide to wavelet analysis. *Bull. Am. Meteorol. Soc.* 79, 61–78.
- Townsend, A.A., 1961. Equilibrium layers and wall turbulence. *J. Fluid Mech.* 11, 97–120.
- Träumner, K., Damian, T., Stawiarski, C., Wieser, A., 2014. Turbulent structures and coherence in the atmospheric surface layer. *Bound. Layer Meteorol.* 154, 1–25.
- Turnipseed, A.A., Blanken, P.D., Anderson, D.E., Monson, R.K., 2002. Energy budget above a high-elevation subalpine forest in complex topography. *Agric. For. Meteorol.* 110, 177–201.
- van Heerwaarden, C.C., Mellado, J.P., De Lozar, A., 2014. Scaling laws for the heterogeneously heated free convective boundary layer. *J. Atmos. Sci.* 71, 3975–4000.
- van Heerwaarden, C.C., Vilà-Guerau de Arellano, J., 2008. Relative humidity as an indicator for cloud formation over heterogeneous land surfaces. *J. Atmos. Sci.* 65, 3263–3277.
- Webb, E.K., Pearman, G.I., Leuning, R., 1980. Correction of flux measurements for density effects due to heat and water vapour transfer. *Q.J.R. Meteorol. Soc.* 106, 85–100.
- Wilczak, J.M., Tillman, J.E., 1980. The three-dimensional structure of convection in the atmospheric surface layer. *J. Atmos. Sci.* 37, 2424–2443.
- Williams, A.G., Hacker, J.M., 1993. Interactions between coherent eddies in the lower convective boundary layer. *Bound. Layer Meteorol.* 64, 55–74.
- Wilson, K., Goldstein, A., Falge, E., Aubinet, M., Baldocchi, D., Berbigier, P., Bernhofer, C., Ceulemans, R., Dolman, H., Field, C., Grelle, A., Ibrom, A., Law, B.E., Kowalski, A., Meyers, T., Moncrieff, J., Monson, R., Oechel, W., Tenhunen, J., Valentini, R., Verma, S., 2002. Energy balance closure at FLUXNET sites. *Agric. For. Meteorol.* 113, 223–243.
- Wulfmeyer, V., Branch, O., Warrach-Sagi, K., Bauer, H.S., Schmitz, T., Becker, K., 2014. The impact of plantations on weather and climate in coastal desert regions. *J. Appl. Meteorol. Climatol.* 53, 1143–1169.
- Ziv, B., Saaroni, H., Alpert, P., 2004. The factors governing the summer regime of the eastern mediterranean. *Int. J. Climatol.* 24, 1859–1871.